

Air Force Institute of Technology

AFIT Scholar

Theses and Dissertations

Student Graduate Works

12-1997

Reduced Computational Cost, Totally Symmetric Angular Quadrature Sets for Discrete Ordinates Radiation Transport

Joseph M. Oder

Follow this and additional works at: <https://scholar.afit.edu/etd>



Part of the [Nuclear Commons](#)

Recommended Citation

Oder, Joseph M., "Reduced Computational Cost, Totally Symmetric Angular Quadrature Sets for Discrete Ordinates Radiation Transport" (1997). *Theses and Dissertations*. 5728.

<https://scholar.afit.edu/etd/5728>

This Thesis is brought to you for free and open access by the Student Graduate Works at AFIT Scholar. It has been accepted for inclusion in Theses and Dissertations by an authorized administrator of AFIT Scholar. For more information, please contact richard.mansfield@afit.edu.



REDUCED COMPUTATIONAL COST,
TOTALLY SYMMETRIC
ANGULAR QUADTRATURE SETS FOR
DISCRETE ORDINATES RADIATION TRANSPORT

THESIS

Joseph M. Oder, Captain, USAF
AFIT/GAP/ENP/97D-07

DISTRIBUTION STATEMENT A

Approved for public release;
Distribution Unlimited

DEPARTMENT OF THE AIR FORCE
AIR UNIVERSITY
AIR FORCE INSTITUTE OF TECHNOLOGY

DTIC QUALITY INSPECTED 3

Wright-Patterson Air Force Base, Ohio

19980120 124

AFIT/GAP/ENP/97D-07

REDUCED COMPUTATIONAL COST,
TOTALLY SYMMETRIC
ANGULAR QUADTRATURE SETS FOR
DISCRETE ORDINATES RADIATION TRANSPORT

THESIS

Joseph M. Oder, Captain, USAF
AFIT/GAP/ENP/97D-07

DTIC QUALITY INSPECTED 3

Approved for public release; distribution unlimited

AFIT/GAP/ENP/97D-07

REDUCED COMPUTATIONAL COST, TOTALLY SYMMETRIC
ANGULAR QUADRATURE SETS FOR
DISCRETE ORDINATES RADIATION TRANSPORT

THESIS

Presented to the Faculty of the School of Engineering
of the Air Force Institute of Technology
Air University
Air Education and Training Command
In Partial Fulfillment of the Requirements for the
Degree of Master of Science

Joseph M. Oder, B.S., M.S.

Captain, USAF

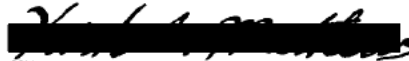
November 1997

Approved for public release; distribution unlimited


REDUCED COMPUTATIONAL COST,
TOTALLY-SYMMETRIC
ANGULAR QUADRATURE SETS FOR
DISCRETE ORDINATES RADIATION TRANSPORT

Joseph M. Oder, B.S., M.S.
Captain, USAF


Approved:


Kirk A. Mathews (Chairman)

1 Dec 1997
date


William P. Baker

24 Nov 97
date


Jeffrey B. Martin

24 Nov '97
date

Acknowledgments

I would like to thank all those individuals who made the completion of this work possible. The members of my committee, whose knowledge and guidance provided the foundation of this work, are principal among these. My advisor, Dr. Kirk Mathews is a recognized expert in the field of transport theory and the originator of the methodology behind the ideas presented here. His patience or prodding at the appropriate times allowed me to gain the knowledge I needed while keeping on a limited time line. Maj. Jeffery Martin provided a practical and military prospective, ensuring I did not wander far afield during my research. Dr William Baker's mathematical knowledge ensured a solid theoretical foundation.

I would also like to thank Capt. Rod Miller who took valuable time away from his doctoral research to provide benchmark Monte Carlo solutions to the problems presented here, providing FORTRAN routines to reduce my data into usable formats, and running my quadrature sets on the transport code he is developing. His assistance in introducing me into the obscure world of the UNIX operating system and setting up of the program packages needed for this work was invaluable.

It is of course necessary to recognize the Air Force Institute of Technology and especially the Department of Physics for giving my the opportunity to attend this institute and providing the equipment I needed for my research.

Lastly I must thank my wife Laura whose patience and willingness to take on the majority of the responsibility involved in raising our new daughter Caitlin, allowed me the time necessary and the secure family basis I needed to keep me motivated.

Table of Contents

Acknowledgments	ii
List of Figures	vi
List of Tables.....	xi
Abstract	xiii
I. Introduction	I-1
Background.....	I-1
Motivation	I-2
The Boltzmann Transport Equation	I-3
Statement of the Problem	I-11
Scope	I-11
General Approach and Sequence of Presentation.....	I-12
II. Theory.....	II-1
Angular Discretization.....	II-3
Spatial Discretization	II-8
Consequences of Discretization	II-9
III. Method	III-1
Zero Components.....	III-1
Quadrature Derivation	III-3
IV. Results.....	IV-1
Problem Definition	IV-4

Test Problem One – Cube Source in Cube Shield.....	IV-5
Tetrahedral Mesh	IV-6
Parallelepiped Mesh.....	IV-22
Test Problem Two – Spherical Source in Spherical Shield	IV-30
Tetrahedral Mesh	IV-30
Parallelepiped Mesh.....	IV-45
V. Conclusion	V-1
Recommendations for further research.....	V-2
VI. Bibliography.....	VI-1
Appendix A.....	A-1
Appendix B.....	B-1
Appendix C.....	C-1
Vita.....	Vita-1

List of Figures

FIGURE I-1: DIRECTION COSINES	I-4
FIGURE II-1: PARTICLE ENTERING FROM DIRECTION $\hat{\Omega}$, SCATTERING INTO DIRECTION $\hat{\Omega}'$	II-2
FIGURE III-1: UNIT SPHERE AND PRINCIPAL OCTANT SHOWING QUADRATURE BASE SET CASES AND DESIGNATORS	III-4
FIGURE III-2: $\mu \leftrightarrow \xi$ EXCHANGE OPERATION	III-4
FIGURE III-3: $\mu \leftrightarrow \eta$ EXCHANGE OPERATION	III-5
FIGURE III-4: COMPLETE PRINCIPAL OCTANT AFTER $\xi \leftrightarrow \eta$ EXCHANGE OPERATION.....	III-5
FIGURE III-5: EXAMPLE MQ ₅ QUADRATURE LAYOUT	III-15
FIGURE III-6 :SPHERICAL HARMONICS, $Y_l^m(\theta, \phi)$	III-19
FIGURE III-7: MQ _{3A} QUADRATURE LAYOUT.....	III-20
FIGURE III-8: MQ _{7A} QUADRATURE LAYOUT	III-21
FIGURE IV-1: GEOMETRY FOR THE CUBE IN CUBE PROBLEM.....	IV-4
FIGURE IV-2: GEOMETRY FOR THE SPHERE IN SPHERE PROBLEM	IV-5
FIGURE IV-3: TETRAHEDRAL MESHES USED IN TEST PROBLEM ONE	IV-6
FIGURE IV-4: CONTOUR PLOT OF THE SURFACE AVERAGE SCALAR FLUX, CUBE PROBLEM, COARSE TETRAHEDRAL MESH	IV-8
FIGURE IV-5: CONTOUR PLOT OF SURFACE AVERAGE SCALAR, CUBE PROBLEM, FINE TETRAHEDRAL MESH	IV-9

FIGURE IV-6: SURFACE AVERAGE SCALAR FLUX, CUBE PROBLEM, COARSE TETRAHEDRAL MESH.....	IV-10
FIGURE IV-7: SURFACE AVERAGE SCALAR FLUX, CUBE PROBLEM, FINE TETRAHEDRAL MESH.....	IV-11
FIGURE IV-8: NET CURRENT THROUGH THE SURFACE, CUBE PROBLEM, COARSE TETRAHEDRAL MESH.....	IV-11
FIGURE IV-9: NET CURRENT THROUGH THE SURFACE, CUBE PROBLEM, FINE TETRAHEDRAL MESH.....	IV-12
FIGURE IV-10: VOLUME AVERAGE SCALAR FLUX, SHIELD REGION, CUBE PROBLEM COARSE TETRAHEDRAL MESH	IV-14
FIGURE IV-11 VOLUME AVERAGE SCALAR FLUX, SHIELD REGION, CUBE PROBLEM, FINE TETRAHEDRAL MESH.....	IV-15
FIGURE IV-12: VOLUME AVERAGE SCALAR FLUX, SOURCE REGION, CUBE PROBLEM, COARSE TETRAHEDRAL MESH	IV-15
FIGURE IV-13: VOLUME AVERAGE SCALAR FLUX, SOURCE REGION, FINE CUBE	IV-16
FIGURE IV-14: COMPUTATIONAL EFFICIENCY, SURFACE FLUX, CUBE PROBLEM, COARSE TETRAHEDRAL MESH	IV-19
FIGURE IV-15: COMPUTATIONAL EFFICIENCY, SURFACE FLUX, CUBE PROBLEM, FINE TETRAHEDRAL MESH	IV-19
FIGURE IV-16: COMPUTATIONAL EFFICIENCY, SURFACE CURRENT, CUBE PROBLEM COARSE TETRAHEDRAL MESH	IV-20

FIGURE IV-17: COMPUTATIONAL EFFICIENCY, SURFACE CURRENT, CUBE PROBLEM FINE TETRAHEDRAL MESH	IV-20
FIGURE IV-18: COMPUTATIONAL EFFICIENCY, VOLUME AVERAGE SCALAR FLUX, CUBE PROBLEM COARSE TETRAHEDRAL MESH	IV-21
FIGURE IV-19: COMPUTATIONAL EFFICIENCY, VOLUME AVERAGE SCALAR FLUX, CUBE PROBLEM FINE TETRAHEDRAL MESH	IV-21
FIGURE 20: CONTOUR PLOT OF SCALAR FLUX IN THE $Z = .125\text{CM}$ PLANE, CUBE PROBLEM, PARALLELEPIPED MESH	IV-23
FIGURE IV-21: SCALAR FLUX AT CUBE SURFACE.....	IV-24
FIGURE IV-22 :VOLUME AVERAGE SCALAR FLUX, CUBE PROBLEM, PARALLELEPIPED MESH	IV-28
FIGURE IV-23: NET CURRENT THROUGH THE SURFACE, CUBE PROBLEM, PARALLELEPIPED MESH	IV-28
FIGURE IV-24: USER TIME VS. RELATIVE ERROR IN VOLUME AVERAGE SCALAR FLUX, CUBE PROBLEM, PARALLELEPIPED MESH.....	IV-29
FIGURE IV-25: USER TIME VS. RELATIVE ERROR IN NET CURRENT THROUGH THE SURFACE, CUBE PROBLEM, PARALLELEPIPED MESH.....	IV-29
FIGURE IV-26: TETRAHEDRAL MESH STRUCTURES USED IN PROBLEM 2.....	IV-31
FIGURE IV-27: SOURCE REGION FOR SPHERE PROBLEM, COARSE MESH.....	IV-32
FIGURE IV-28: CONTOUR PLOT OF SURFACE AVERAGE SCALAR FLUX, SPHERE PROBLEM, COARSE TETRAHEDRAL MESH	IV-34

FIGURE IV-29: CONTOUR PLOT OF SURFACE AVERAGE SCALAR FLUX, SPHERE PROBLEM, MEDIUM TETRAHEDRAL MESH.....	IV-34
FIGURE IV-30: CONTOUR PLOT OF SURFACE AVERAGE SCALAR FLUX, SPHERE PROBLEM, FINE TETRAHEDRAL MESH.....	IV-35
FIGURE IV-31: CONTOUR PLOT OF SURFACE FLUX, MQ ₅ AND LQ ₁₆ , AXIAL VIEW OF FINE SPHERE.....	IV-36
FIGURE IV-32: VARIABILITY OF SCALAR FLUX AT THE SURFACE OF SPHERE PROBLEM, MEDIUM TETRAHEDRAL MESH.....	IV-37
FIGURE IV-33: VARIABILITY IN NET CURRENT THROUGH THE SURFACE, SPHERE PROBLEM, MEDIUM TETRAHEDRAL MESH.....	IV-37
FIGURE IV-34: SURFACE AVERAGE SCALAR FLUX, SPHERE PROBLEM, COARSE TETRAHEDRAL MESH.....	IV-39
FIGURE IV-35: RELATIVE ERROR IN SURFACE AVERAGE SCALAR FLUX, SPHERE PROBLEM, COARSE TETRAHEDRAL MESH.....	IV-39
FIGURE IV-36: RELATIVE ERROR IN SURFACE AVERAGE SCALAR FLUX, SPHERE PROBLEM, MEDIUM TETRAHEDRAL MESH.....	IV-40
FIGURE IV-37: RELATIVE ERROR IN SURFACE AVERAGE SCALAR FLUX, SPHERE PROBLEM, FINE TETRAHEDRAL MESH.....	IV-40
FIGURE IV-38: RELATIVE ERROR IN VOLUME AVERAGE SCALAR FLUX, SPHERE PROBLEM, COARSE TETRAHEDRAL MESH.....	IV-45
FIGURE IV-39: COMPARISON OF CONTOUR PLOTS: SCALAR FLUX, Z = .125 PLANE, SPHERE PROBLEM, PARALLELEPIPED MESH.....	IV-48

FIGURE IV-40 : VOLUME AVERAGE SCALAR FLUX, SPHERE PROBLEM, PARALLELEPIPED MESH	IV-49
FIGURE IV-41: RELATIVE ERROR, VOLUME AVERAGE SCALAR FLUX, SPHERE PROBLEM, PARALLELEPIPED MESH	IV-49
FIGURE IV-42: NET CURRENT, SPHERE PROBLEM, PARALLELEPIPED MESH.	IV-50
FIGURE IV-43: RELATIVE ERROR IN NET CURRENT, SPHERE PROBLEM, PARALLELEPIPED MESH	IV-50
FIGURE IV-44: TIME VS. ERROR IN FLUX, SPHERE PROBLEM, PARALLELEPIPED MESH	IV-51
FIGURE IV-45: TIME VS. ERROR IN CURRENT, SPHERE PROBLEM, PARALLELEPIPED MESH	IV-51

List of Tables

TABLE I-1: VARIABLE DEFINITIONS FOR THE BTE, EQUATION (I-1)	I-4
TABLE III-1: SUMMARY OF QUADRATURE CASE DATA	III-10
TABLE III-2: CONTRIBUTION OF EACH CASE TO EQUATION (III-7)	III-13
TABLE III-3: CASE COMBINATION FOR QUADRATURE OF ORDER N	III-18
TABLE IV-1 : TETRAHEDRAL MESH DATA FOR TEST PROBLEM ONE	IV-7
TABLE IV-2: SURFACE AVERAGE SCALAR FLUX, NET CURRENT, AND RELATIVE ERROR, CUBE PROBLEM, COARSE TETRAHEDRAL MESH	IV-13
TABLE IV-3: SURFACE AVERAGE SCALAR FLUX, NET CURRENT AND RELATIVE ERROR, CUBE PROBLEM, FINE TETRAHEDRAL MESH	IV-13
TABLE IV-4 : VOLUME AVERAGE SCALAR FLUX AND RELETIVE ERROR, CUBE PROBLEM, COARSE TETRAHEDRAL MESH	IV-16
TABLE IV-5: VOLUME AVERAGE SCALAR FLUX, FINE MESH.....	IV-17
TABLE IV-6 :USER TIME IN SECONDS TAKEN TO SOLVE THE CUBE IN CUBE PROBLEM.....	IV-17
TABLE IV-7 : PARALLELEPIPED MESH DATA.....	IV-22
TABLE IV-8: PARALLELEPIPED CUBE DATA SUMMARY	IV-26
TABLE IV-9 : TIME BY QUADRATURE, PARALLELEPIPED MESH, CUBE PROBELEM	IV-27
TABLE IV-10 : TETRAHEDRAL MESH DATA	IV-30
TABLE IV-11: SURFACE AVERAGE SCALAR FLUX AND NET CURRENT, SPHERE PROBLEM, COARSE TETRAHEDRAL MESH	IV-38

TABLE IV-12: SURFACE AVERAGE SCALAR FLUX AND NET CURRENT, SPHERE PROBLEM, MEDIUM TETRAHEDRAL MESH.....	IV-41
TABLE IV-13: SURFACE AVERAGE SCALAR FLUX AND NET CURRENT, SPHERE PROBLEM, FINE TETRAHEDRAL MESH.....	IV-41
TABLE IV-14: VOLUME AVERAGE SCALAR FLUX DATA, COARSE SPHERE	IV-42
TABLE IV-15: VOLUME AVERAGE SCALAR FLUX DATA, MEDIUM SPHERE	IV-43
TABLE IV-16: VOLUME AVERAGE SCALAR FLUX DATA, FINE SPHERE	IV-43
TABLE IV-17 :USER TIME IN SECONDS TAKEN TO SOLVE THE SPHERE PROBLEM	IV-44
TABLE IV-18 : PARALLELEPIPED MESH DATA.....	IV-46
TABLE IV-19: SPHERE DATA SUMMARY, PARALLELEPIPED MESH	IV-46
TABLE IV-20 : TIME BY QUADRATURE, SPHERE PROBLEM, PARALLELEPIPED MESH	IV-47

Abstract

Several new quadrature sets for use in the discrete ordinates method of solving the Boltzmann neutral particle transport equation are derived. These symmetric quadratures extend the traditional symmetric quadratures by allowing ordinates perpendicular to one or two of the coordinate axes.

Comparable accuracy with fewer required ordinates is obtained.

Quadratures up to seventh order are presented. The validity and efficiency of the quadratures is then tested and compared with the LQ_n level symmetric quadratures relative to a Monte Carlo benchmark solution. The criteria for comparison include current through the surface, scalar flux at the surface, volume average scalar flux, and time required for convergence. Appreciable computational cost was saved when used in an unstructured tetrahedral cell code using highly accurate characteristic methods. However, no appreciable savings in computation time was found using the new quadratures compared with traditional S_n methods on a regular Cartesian mesh using the standard diamond difference method. These quadratures are recommended for use in three-dimensional calculations on an unstructured mesh.

I. Introduction

This research developed a set of angular quadratures that are computationally efficient when used with the discrete ordinates method to solve the three-dimensional Boltzmann neutral particle transport equation. The quadrature sets contain directions perpendicular to one or more cardinal directions. These sets are tested for accuracy and computational efficiency. Performance comparisons are made with traditional (level symmetric) quadrature sets. Types of problems and conditions where these quadratures are most applicable are discussed.

Background

The foundation of transport theory is the Boltzmann transport equation (BTE). This equation, formulated over a century ago, was originally developed for the study of the kinetic theory of gases (1: 1). Preliminary study in the field was primarily of the diffusion of light by the atmosphere. Then study began in the early part of the twentieth century on investigating the diffusion of energy through the atmosphere of a star (2: 1). The scale of these problems are such that they can be modeled as semi-infinite media with one-dimensional geometry and therefore the methods of their solution are of limited application (1: 1).

In the 1940s, interest in the military and industrial application of nuclear energy stimulated a tremendous amount of research into neutral particle transport. The incredible urgency involved in the research of nuclear energy induced by the events of World War II necessarily resulted in the development and use of approximate methods for solving the linearized transport equation (2:1).

Motivation

Military and industrial research into the use of nuclear energy using actual nuclear material has decreased substantially in recent years. The comprehensive nuclear test ban treaty (CTBT), if ratified, will eliminate our ability to obtain any further real data on new weapons designs or systems survivability in or near a real threat environment. Some aspects of the radiation environment resulting from a nuclear detonation are simulated at various test sites. These tests can only approximate the actual post detonation environment and are very costly (17). It is currently politically undesirable for private industry to perform research using significant amounts nuclear material or to build new nuclear research facilities. These and other factors have greatly increased the need for accurate computer modeling of nuclear material and effects. The high performance computers needed for this modeling are very expensive, and therefore anything that can increase the efficiency of these machines will translate directly into

substantial savings by increasing their productivity and extending their useful life. Reduction in computation time also increases the practicality of analyzing a large variety of similar scenarios for threat analysis or system optimization.

The Boltzmann Transport Equation

The Boltzmann transport equation (Equation I-1) is a conservation equation for the flux of neutral particles (1: 24). The particles can be neutrons, photons, or any other neutral particle given the nuclear data. The angular flux, ψ , is dependent on position (\vec{r}), direction of motion ($\hat{\Omega}$), on speed or energy (v , E), and time (t). Equation (I-1) represents a balance between the loss rate (right side) and gain rate (left side) of particles that exist at each point of this seven dimensional phase space (3: I-2);

$$\left[\frac{1}{v} \frac{\partial}{\partial t} + \hat{\Omega} \cdot \nabla + \sigma_t(\vec{r}, E, t) \right] \psi(\vec{r}, E, \hat{\Omega}, t) = \int dE' \int d\Omega' \sigma_s(\vec{r}, E \rightarrow E', \hat{\Omega} \cdot \hat{\Omega}', t) \psi(\vec{r}, E', \hat{\Omega}', t) + s(\vec{r}, E, \hat{\Omega}, t) \quad (\text{I-1})$$

where the variables are defined in Table 1.

Table I-1: Variable Definitions for the BTE, Equation (I-1)

Variable	Description
v	magnitude of the velocity
t	time
\mathbf{r}	position
E	energy
σ_t	total macroscopic cross-section for interaction (absorption and scatter)
σ_s	macroscopic scattering cross-section
s	total non-scattering source
ψ	angular flux: a distribution function of particles at point \mathbf{r} , with energy E , moving in direction $\hat{\Omega}$ at time t
$\hat{\Omega}$	unit vector aligned along the streaming direction of particles: it is often shown as three components, or direction cosines, μ , η , ξ defined by $\mu = \hat{\Omega} \cdot \hat{e}_x$, $\eta = \hat{\Omega} \cdot \hat{e}_y$, $\xi = \hat{\Omega} \cdot \hat{e}_z$ as shown in Figure I-1

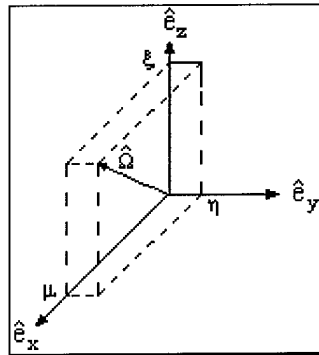


Figure I-1: Direction Cosines

Though discrete ordinates is valid for time dependent problems, this treatment will assume steady state conditions with all time dependence

suppressed; therefore the first term in Equation (I-1) (representing the time rate of change of particles in the phase space) vanishes. The remaining terms represent the steady state balance equation. The second term in the brackets on the left of Equation (I-1) is the streaming operator and represents the loss rate due to particle divergence. The final term in the brackets on the left is the collision operator and represents the loss rate due to particle interaction with the medium. This interaction could be absorption (destroying the particle), or scatter (changing the particle's energy or direction) (3: I-2).

The first term on the right of Equation (I-1) is the gain rate due to particles traveling in other directions that scatter into the given direction, $\hat{\Omega}$. As a consequence of the isotropic material assumption, the distribution of particles scattering into a given direction is not a function of the incident angle, $\hat{\Omega}'$; however it is a function of the angle between the incident direction and final direction, $(\hat{\Omega} \cdot \hat{\Omega}')$. Despite the isotropic material assumption, this dependence on scattering angle means that scattering may be anisotropic (1). The final term represents the gain rate from production of particles by any source mechanism. The source can be internal, such as radioactive decay and fission or external such as solar x-rays or an incident beam. A more detailed discussion of the BTE and definition of its components is presented in section II.

The macroscopic cross sections are functions of position, through spatially varying number density or changes in material, and of energy

through the microscopic cross sections in which fundamental properties of the isotopes are involved. In general the microscopic cross sections could have some additional implicit spatial variation. For example, this could be due to a temperature-dependence through Doppler broadening (1: 6). This research assumes each material is uniform and isotropic and therefore no such implicit spatial dependence exists.

The physical quantities most often of interest to be found via the BTE are the scalar flux ϕ (zeroth angular moment of the vector flux) and the vector current \mathbf{J} (first angular moment). The scalar flux is of interest as it represents the total expected particle path length traveled per unit volume at a given location in the medium. This will determine the reaction rates for such things as fission and neutron activation. The vector current will determine the leakage rate from one region to the next or through boundaries (3: I-3).

Only a limited number of analytic and semi-analytic solutions exist for the BTE. Most of these solutions are for highly idealized problems. Many ingenious methods such as discrete ordinates, Monte Carlo, even-parity, finite-elements, and Green functions have been developed to solve the transport equation and to extend the application of such knowledge. The diffusion equation can be derived from the BTE using several simplifying assumptions regarding the angular dependence. For problems with nearly isotropic scatter, this can yield approximate results (16: 2). Of particular

interest are methods capable of providing solutions to the broad range of geometrical configurations found in nuclear reactor and radiation shielding applications (1: 1). From a military perspective, in addition to the application to power generation, accurate modeling of neutron flux allows for more precise modeling of the yield and effects of nuclear weapons.

The advent of high-speed computing and large storage capacity has led to the refinement and use of two primary numerical methods of attaining a solution to the BTE: the method of discrete ordinates and Monte Carlo (1: 2). Other less used methods will not be examined. The theory and development of the Monte Carlo method will not be discussed in detail; however, Monte Carlo solutions will be used as benchmarks.

Since its evolution from the angular segmentation formulation by Carlson in 1957 discrete ordinates has become a widely used method for solving the integrodifferential form of the transport equation. The discrete ordinates method involves enforcing the transport equation only at discrete angular directions called ordinates. These ordinates are selected such that the flux moments may be evaluated accurately by a weighted sum (1: 118). For example the scalar flux (zeroth flux moment) is

$$\phi(\vec{r}, E, t) = \int d\Omega \psi(\vec{r}, E, \hat{\Omega}, t) \approx \sum_n w_n \psi(\vec{r}, E, \hat{\Omega}_n, t).$$

A more detailed discussion of the flux moments is found in Chapter II. The advantages of the discrete ordinates method are the relatively simple derivation and the subsequent ease of transformation into algorithms of good computational efficiency (1: 116). It also lends itself well to the discretizing of energy into multiple energy groups. A distinct advantage over the Monte Carlo method is that it provides flux and current data everywhere in the problem rather than only at a limited number of locations. A quadrature set is the combination of discrete angles and weights used in a weighted sum to evaluate the flux moments.

There are two independent angular directions for $\hat{\Omega}$. The directions are parameterized by three direction cosines that obey the relationship

$$\mu^2 + \eta^2 + \xi^2 = 1 \quad (\text{I-3})$$

where μ , η , and ξ are shown in Figure I-1.

Once the angular approximation has been made, a spatial discretization scheme must be used. Computational cost and storage requirements are directly proportional to the number of spatial cells and discrete ordinates used. A large number of spatial schemes have been formulated for use in discrete ordinates calculations. They include linear methods such as diamond difference, linear discontinuous, and linear characteristic and non-linear methods such exponential characteristic (9).

The most serious drawback to the discrete ordinates method is the buildup of truncation errors due to the discretized angular and spatial representations (1: 131). The truncation errors can result in random error, which limits the accuracy of the results, or may lead to physically unrealistic results such as negative fluxes or sources. Systematic truncation error may lead to what are known as *ray effects* (21, 8, 3). These are errors caused by the discrete ordinates method of limiting particle motion to discrete directions or *rays*. Flux due to unscattered particles will only be found to occur at points where a line can be drawn from a source to the point in the direction of a discrete ordinate. This causes the scalar flux to be calculated higher than expected at points along discrete ordinate directions and lower between. The method is not well suited to geometry with a strongly peaked flux in a given direction. Generally, a separate method must be used to calculate the first scatter source for such a problem. In order to increase accuracy of the discrete ordinates method and minimize the negative consequences, it is either necessary to increase the number of directions in the angular quadrature, thus increasing the computation time and storage requirements of the computer system, or to develop an alternative quadrature that produces less error with fewer directions. This research concentrates on increasing the accuracy of the discrete ordinates approximation while minimizing the number of angles.

The primary drawback of allowing motion perpendicular to one or more cardinal directions in a quadrature set is that mathematical instability may result when using current computer codes. The resulting zero components of flux often generate run-time errors. The advantages of using directions parallel to cell boundaries are (due to one or two of the direction cosines being zero) the discrete ordinates equations simplify significantly and fewer directions are required for the same order of anisotropy, thus allowing for increased computational efficiency.

Except for the simple case of isotropic scatter, the cross section for scattering will be a function of the scattering angle as well as energy. Separation of the angular and energy dependence is assumed. Traditionally, cross sections are then expanded in orthogonal Legendre polynomials (1: 13). The order of this expansion is another limit to the accuracy obtainable by the discrete ordinates method.

The high performance computers needed to perform these calculations are very expensive, and therefore anything that can increase the efficiency of these machines will translate directly into substantial savings by increasing their useful life. Reduction of computation time also increases the practicality of analyzing a large variety of similar scenarios for threat analysis or system optimization.

Statement of the Problem

The objective of this research is to develop and evaluate new quadrature sets that produce accurate discrete ordinates solutions to the BTE using a minimum number of ordinates. The viability of including ordinates perpendicular to one or two cardinal directions is examined. This includes deriving and implementing the appropriate quadrature angles and weights, and comparing the results with those obtained with standard level-symmetric LQ_n quadratures and with Monte Carlo benchmark solutions.

Scope

This research includes the derivation and implementation of discrete ordinates quadrature sets that include directions perpendicular to one or two cardinal directions. Demonstration of the method including comparison to traditional level-symmetric quadratures with regard to computational cost (execution time) and accuracy of results based on a benchmark calculation is performed. The test problems use three-dimensional Cartesian coordinates with no time or energy dependence. The test problems were run using TETRAN (13), an unstructured mesh tetrahedral cell code developed at the Air Force Institute of Technology and the THREEDANT code of the RSICC Computer Code Collection, DANTSYS 3.0 (14) from Los Alamos National Laboratory (LANL) using a rectangular parallelepiped mesh. LANL's MCNP (Monte Carlo Neutron Photon) transport code package (15) provided

benchmark solutions. Due to current limitations in the TETRAN code still in development, the test problems are defined as one energy group, isotropic scatter transport problems. Multiple levels of spatial mesh refinement are used. The method is tested to identify any variation in performance and determine an optimal usage. The scope of the comparison using the output of the THREEDANT module is limited due to the requirement to modify the developed quadratures in order for the module to run. See chapter IV for a discussion of the modifications. No code changes or new modules were written to augment THREEDANT to obtain a more accurate comparison of the quadrature sets.

General Approach and Sequence of Presentation

In chapter II the integrodifferential form of the Boltzmann transport equations is discretized over angle. A brief discussion of spatial and energy discretization is included. The consequences of discretization are enumerated. The method of generating the new quadrature sets is developed in chapter III. Several quadrature sets of various order are presented. The method is implemented using two test problems and the results are presented in chapter IV. The geometry of each test problem has been selected to, in the first case, exacerbate, then in the second, mitigate the problem of ray effects. Traditional level symmetric quadratures are used on the same test problems. Benchmark calculations were performed on each

test problem using a Monte Carlo simulation. The methods are compared for accuracy and computational efficiency and potential advantages or disadvantages of the method identified. Consideration is given to smoothness, pointwise and global accuracy, ray-effects, and other systematic errors.

Once the method has been tested and analyzed, recommendations for use and for further research are given in the final chapter. Appendices contain complete derivations of the equations used to generate the quadratures as well as any mathematical routines used to solve them. Also, pertinent portions of input and output files of the test problems are included

II. Theory

This chapter will present a development of the discrete ordinates method, the criteria for selecting a quadrature, discuss spatial discretization, and some the consequences of applying these approximations.

The steady state assumptions reduces the Boltzmann transport equation (Equation I-1) to:

$$\hat{\Omega} \cdot \vec{\nabla} \psi(\vec{r}, E, \hat{\Omega}) + \sigma(\vec{r}, E) \psi(\vec{r}, E, \hat{\Omega}) = \int dE' \int d\Omega' \sigma_s(\vec{r}, E \rightarrow E', \hat{\Omega} \cdot \hat{\Omega}') \psi(\vec{r}, E', \hat{\Omega}') + s(\vec{r}, E, \hat{\Omega}) \quad (\text{II-1})$$

In order to yield a convenient normalization over all angles, the incremental solid angle is defined as

$$d\Omega = \frac{d\omega}{2\pi} \frac{d\theta \sin \theta}{2} = \frac{d\omega}{2\pi} \frac{d\mu}{2} \quad (\text{II-2})$$

so that

$$\int d\Omega = \int_0^{2\pi} \frac{d\omega}{2\pi} \int_{-1}^1 \frac{d\mu}{2} = 1. \quad (\text{II-3})$$

Definitions of the above angles are shown in Figure II-1 (1: 11). Equation (II-1) contains terms that are functions of position, scattering angle, and energy. The energy dependence in the discrete ordinates approximation is most often accounted for by dividing the energy range of interest into a number of intervals. It is assumed that for each interval, cross-sections are given as average values over the interval (18: 109). The transport equation is then

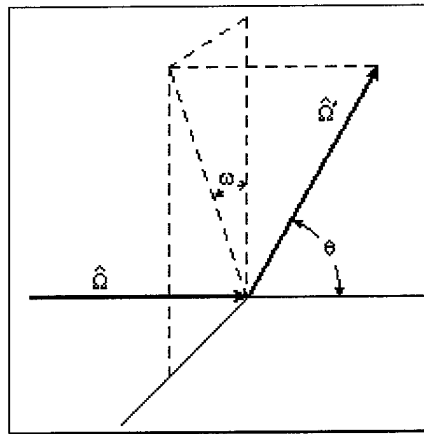


Figure II-1: Particle Entering from Direction $\hat{\Omega}$, Scattering into direction $\hat{\Omega}'$

solved in each energy interval as a mono-energetic equation with particle contributions scattered from outside the energy interval added as a source term and particles scattering from the interval of interest into other energy intervals treated as losses. The resulting equations are known as the *multigroup equations* (1: 61). For clarity, the remainder of the derivations given will be for a mono-energetic system. The Boltzmann equation then becomes the mono-energetic transport equation:

$$\hat{\Omega} \cdot \bar{\nabla} \psi(\bar{r}, \hat{\Omega}) + \sigma(\bar{r}) \psi(\bar{r}, \hat{\Omega}) = \int d\hat{\Omega}' \sigma_s(\bar{r}, \hat{\Omega} \cdot \hat{\Omega}') \psi(\bar{r}, \hat{\Omega}') + s(\bar{r}, \hat{\Omega}). \quad (\text{II-4})$$

In the discrete ordinates method each term of the integrodifferential transport equation is assumed to be a separable function of space and angle and the dependencies are dealt with separately (3: I-3). Both the spatial and angular variables are required to be discretized before the problem may be solved numerically. The angular discretization, being the focus of this research, will be considered first and discussed in some detail while the spatial discretization will be dealt with later.

Angular Discretization

The majority of the derivation that follows is an extension into three-dimensions of the procedure presented by Lewis and Miller (1). The differential scattering cross sections are expanded in orthogonal Legendre polynomials $P_l(\hat{\Omega} \cdot \hat{\Omega}')$ where $\mu_0 = \hat{\Omega} \cdot \hat{\Omega}'$ is the cosine of the scattering angle. The differential scattering cross section may be expressed as

$$\sigma_s(\bar{r}, \hat{\Omega} \cdot \hat{\Omega}') \approx \sum_{l=0}^L (2l+1) \sigma_{sl}(\bar{r}) P_l(\hat{\Omega} \cdot \hat{\Omega}'). \quad (\text{II-5})$$

The scattering moments σ_{sl} are found from

$$\sigma_{sl}(\vec{r}) = \int_{-1}^1 \frac{d\mu_0}{2} \sigma_s(\vec{r}, \mu_0) P_1(\mu_0), \quad (\text{II-6})$$

having taken advantage of the orthogonality property of the Legendre polynomials. The expansion in Equation (II-5) has been truncated at $L+1$ terms, assuming an adequate level of approximation, taking into consideration the degree of anisotropy and the availability of cross section data. For the case of isotropic scatter only the first term of Equation (II-5) is used ($L = 0$) resulting in

$$\sigma_s(\vec{r}, \hat{\Omega} \cdot \hat{\Omega}') \cong \sigma_s(\vec{r}). \quad (\text{II-7})$$

This derivation will not assume isotropic scatter. Combining Equations (II-4) and (II-5) yields

$$\hat{\Omega} \cdot \vec{\nabla} \psi(\vec{r}, \hat{\Omega}) + \sigma(\vec{r}) \psi(\vec{r}, \hat{\Omega}) = \sum_{l=0}^L (2l+1) \sigma_{sl}(\vec{r}) \int d\Omega' P_l(\hat{\Omega} \cdot \hat{\Omega}') \psi(\vec{r}, \hat{\Omega}') + s(\vec{r}, \hat{\Omega}) \quad (\text{II-8})$$

which can be simplified using the Legendre addition theorem (1: 367)

$$P_l(\hat{\Omega} \cdot \hat{\Omega}') = \frac{1}{2l+1} \sum_{m=-l}^l Y_{lm}^*(\hat{\Omega}) Y_{lm}(\hat{\Omega}') \quad (\text{II-9})$$

where the $Y_{lm}(\hat{\Omega})$ are the spherical harmonics and the asterisks signifies the complex conjugate. Using this, the sum on the right hand side of Equation (II-8) becomes

$$\sum_{l=0}^L \sigma_{sl}(\vec{r}) \sum_{m=-1}^1 Y_{lm}^*(\hat{\Omega}) \int d\Omega' Y_{lm}(\hat{\Omega}') \psi(\vec{r}, \hat{\Omega}'). \quad (\text{II-10})$$

The angular integral in expression (II-10) is now just the coefficients resulting from the expansion of the angular flux in spherical harmonics

$$\psi(\vec{r}, \hat{\Omega}) \approx \sum_{l=0}^L \sum_{m=-1}^1 \phi_{lm}(\vec{r}) Y_{lm}^*(\hat{\Omega}). \quad (\text{II-11})$$

with

$$\phi_{lm}(\vec{r}) = \int d\Omega' Y_{lm}(\hat{\Omega}') \psi(\vec{r}, \hat{\Omega}'). \quad (\text{II-12})$$

Substituting this into expression (II-10) gives

$$\sum_{l=0}^L \sum_{m=-1}^1 Y_{lm}^*(\hat{\Omega}) \sigma_{sl}(\vec{r}) \phi_{lm}(\vec{r}). \quad (\text{II-13})$$

Replacing the sum in Equation (II-8) with expression (II-13) yields a form of the transport equation that is convenient for discretization in angle

$$\hat{\Omega} \cdot \bar{\nabla} \psi(\bar{r}, \hat{\Omega}) + \sigma(\bar{r}) \psi(\bar{r}, \hat{\Omega}) = \sum_{l=0}^L \sum_{m=-l}^l Y_{lm}^*(\hat{\Omega}) \sigma_{sl}(\bar{r}) \phi_{lm}(\bar{r}) + s(\bar{r}, \hat{\Omega}). \quad (\text{II-14})$$

In the discrete ordinates approximation, Equation (II-14) is enforced only for a set of discrete directions yielding

$$\hat{\Omega}_n \cdot \bar{\nabla} \psi_n(\bar{r}) + \sigma(\bar{r}) \psi_n(\bar{r}) = \sum_{l=0}^L \sum_{m=-l}^l Y_{lm}^*(\hat{\Omega}_n) \sigma_{sl}(\bar{r}) \phi_{lm}(\bar{r}) + s(\bar{r}, \hat{\Omega}_n), \quad (\text{II-15})$$

where $\psi_n(\bar{r}) \equiv \psi(\bar{r}, \hat{\Omega}_n)$. The scalar flux is approximated by

$$\phi(\bar{r}) = \sum_{n=1}^N w_n \psi_n(\bar{r}), \quad (\text{II-16})$$

and the flux moments of Equation (II-12) are approximated by

$$\phi_{lm}(\bar{r}) = \sum_{n=1}^N w_n Y_{lm}(\hat{\Omega}_n) \psi_n(\bar{r}). \quad (\text{II-17})$$

By defining the right hand side of Equation (II-15) as the emission density or scattering source $q_n(\vec{r})$ and substituting Equation (II-17) for the flux moments, Equation (II-15) becomes

$$\hat{\Omega}_n \cdot \vec{\nabla} \psi_n(\vec{r}) + \sigma(\vec{r}) \psi_n(\vec{r}) = q_n(\vec{r}) \quad (\text{II-18})$$

where

$$q_n(\vec{r}) = s(\vec{r}, \hat{\Omega}_n) + \sum_{l=0}^L \sum_{m=-l}^l Y_{lm}^*(\hat{\Omega}_n) \sigma_{sl}(\vec{r}) \sum_{n'=1}^N w_{n'} Y_{lm}(\hat{\Omega}_{n'}) \psi_{n'}(\vec{r}) \quad (\text{II-19})$$

The most common way of solving Equation (II-18) is the *iteration on the scattering source* form of Von Neuman's series solution (1: 80). The method's usefulness is derived from the fact that if the right side of Equation (II-18) is known, solving for $\psi(\vec{r})$ is usually straightforward. The iteration is defined by modifying Equation (II-18) to

$$[\hat{\Omega}_n \cdot \vec{\nabla} + \sigma(\vec{r})] \psi_n^{i+1}(\vec{r}) = q_n^i(\vec{r}) \quad (\text{II-20})$$

where i is the iteration index. Equation (II-19) likewise becomes

$$q_n^i(\vec{r}) = s(\vec{r}, \hat{\Omega}_n) + \sum_{l=0}^L \sum_{m=-l}^l Y_{lm}^*(\hat{\Omega}_n) \sigma_{sl}(\vec{r}) \sum_{n'=1}^N w_{n'} Y_{lm}(\hat{\Omega}_{n'}) \psi_{n'}^i(\vec{r}). \quad (\text{II-21})$$

The system of Equations (II-20) and (II-21) must be solved to convergence at each \vec{r} of interest.

Before proceeding to the methodology of choosing a quadrature set, a brief discussion of the spatial discretization which allows for the approximation of the those terms which are now function of the spatial variable only will be helpful.

Spatial Discretization

Discretization of the spatial variable in three dimensions can take many forms. The most common method is to divide each of the three Cartesian spatial directions, x , y , and z , into i , j , and k intervals respectively resulting in a three dimensional grid containing $i \times j \times k$ rectangular parallelepiped cells. Another method gaining popularity is to generate an unstructured mesh of tetrahedra. All cross sections are taken to be piecewise constant and therefore not allowed to vary inside a given cell. Various methods exist then to calculate the angular flux ψ_n for each value of n in each cell given appropriate boundary conditions. THREEDANT uses diamond difference (DD) with negative flux fix up in a structured Cartesian mesh, and TETRAN has the capability of using linear characteristic (LC), exponential characteristic (EC) or step characteristic (SC) on an unstructured

tetrahedral mesh. Each of these methods and many more are discussed and derived in detail elsewhere (1,2,3,8,9,16).

Consequences of Discretization

Several problems arise when using discrete ordinates. Any time computations are performed on a computer, truncation errors will occur. The effects of truncation error will accumulate with each computation. Truncation errors therefore limit the accuracy achievable by computational methods. With each refinement of the spatial or angular mesh, the mathematical model more closely resembles the continuous analytical solution, however the number of computations also increases. Though truncation error associated with each calculation should decrease with mesh refinement, there is a limit to the accuracy gained by continued mesh refinement as the number of calculations gets increasingly large. This effect is most visible in three-dimensional problems where the number of cells increases as the cube of the linear refinement. Another, more systematic problem arises due to the angular discretization called ray effects. The phenomenon is most evident in problems with localized sources and small scattering cross sections (1:195).

When the scattering cross section is small, a substantial percentage of particles traveling from a localized source to an area of interest will be uncollided. This will result in a peaked distribution about the discrete ordinates. Clearly these results are physically unrealistic. Ray effects

manifest as oscillations (1: 197), peaks about a region where an ordinate can be traced from a source region and valleys in between. As the order of the angular approximation increases so does the number of oscillations, which also tend to decrease in the amount of deviation from a smooth curve. If the oscillations are uniform about the correct curve, then the integral of the scalar flux over the boundary will still yield good results (1: 200). When the scattering source makes a large contribution to the scalar flux, ray effects tend to be mitigated. The scattering source tends to be distributed over a large area and is often nearly isotropic. This gives a more uniform angular distribution of neutrons.

Numerical diffusion is a consequence of the spatial discretization and truncation errors due to spatial differencing. For example, if a beam of neutrons were to enter the lower left corner of a pure absorbing cube of material traveling along the cube diagonal, one would expect the attenuated beam to exit only at the upper right corner. In the spatial walk of the discrete ordinates calculation, each cell is considered to have a distribution of flux through out the cell and flux can only enter and exit the faces of the cells. For a mesh consisting of regular parallelepiped cells, this means the beam entering the cell in the bottom left corner will exit that cell through the top and sides. The fraction entering the adjacent cells is determined by the incident angle of the beam. This will continue through the spatial walk resulting in a smearing out of the beam. This effect, to a small extent, may

mitigate ray-effects. A more complete discussion of numerical diffusion can be found in reference 3 where is referred to as *quasi-ray effect*.

III. Method

The primary desire when selecting a quadrature set is to maximize accuracy while minimizing the number of ordinates. The primary source of computational cost of obtaining a discrete ordinates solution to the BTE is in the spatial integration. A complete walk through the spatial mesh is required for each ordinate. Thus minimizing the number of ordinates reduces the computational cost by minimizing the number spatial walks required. Other concerns are the mitigation of numerical artifacts both systematic and nonsystematic such as truncation errors, ray effects, and numerical diffusion. With these concerns in mind, this work will present a method of generating simultaneous sets of polynomial equations, which produce quadrature sets based on exact integration of spherical harmonics. Quadrature sets up to order seven are presented.

Zero Components

The key difference in the quadratures presented here from those seen elsewhere is the addition of ordinates with zero components for one or two of the direction cosines. There have been several reasons for not using zero components in the past, primarily stemming from arguments in one or two-dimensional geometry. In these problems, vertical vector flux does not propagate through the problem. The infinite path length resulting from the reciprocal cosine term in the spatially discretized mesh must also be dealt

with. Discontinuity in the vector flux at a vacuum boundary can lead to ambiguity in the meaning of $\psi(\mu = 0)$ at the boundary when using a regular Cartesian mesh. Also, it can be shown that $\psi(\mu = 0)$ is not truly an independent variable when discretized in 2-D and therefore contributes little to the accuracy of the solution (19: 132).

When three-dimensional quadratures are developed, they are often an extension of one and two-dimensional cases. The use of even order in traditional quadrature sets, when applied to 3-D problems has invariably been due to the even order used in the lower dimensional base. The use of diamond difference (DD) is also pervasive in old computer codes. DD codes will not accept zero components without special handling routines being developed. There is often a desire when developing quadrature sets to generate results that will run on the legacy codes without modification. This is unfortunate, as modern parallel computers are capable of handling far greater complexities than the computers for which these codes were developed. The development of computer codes capable of performing discrete ordinates calculations on an unstructured mesh eliminates many of the problems associated with special directions. More accurate characteristic methods of dealing with the spatial integration do not have the same problems dealing with zero components as the DD method.

Quadrature Derivation

The derivation of these polynomial equations for the generation of quadrature sets is based on methodology developed by Dr. Kirk Mathews (25) as an extension of work by B.G. Carlson and others (5). The basic quadrature sets presented here are defined over the entire unit sphere, but can be represented in the principal octant or its edges. The principal octant is where the components of $\hat{\Omega}$ are all positive. We require the quadrature set to meet the *total symmetry* condition. Total symmetry, sometimes referred to as cubic symmetry, requires the quadrature set to remain invariant under all axis exchanges, ninety-degree rotations about a cardinal axis, and reflections across the $x - y$, $x - z$, or $y - z$ planes. An axis exchange operation is the same as a reflection across any $x = y$, $x = -y$, $x = z$, $x = -z$, $y = z$, or $y = -z$ plane. The discrete ordinates can be represented as points on the surface of the unit sphere. These points represent where the tips of the unit vectors corresponding to each ordinate lie on the unit sphere. A *base set* refers to those ordinates in the original *hextant* of the principal octant. The original hextant is a spherical triangle covering a one sixth area of the principal octant. Figure III-1 shows the unit sphere with the principle octant shaded and an expanded view of the principle octant with the original hextant shaded. A complete quadrature set can be built by choosing points in any hextant and reflecting the points by performing successive axes exchange

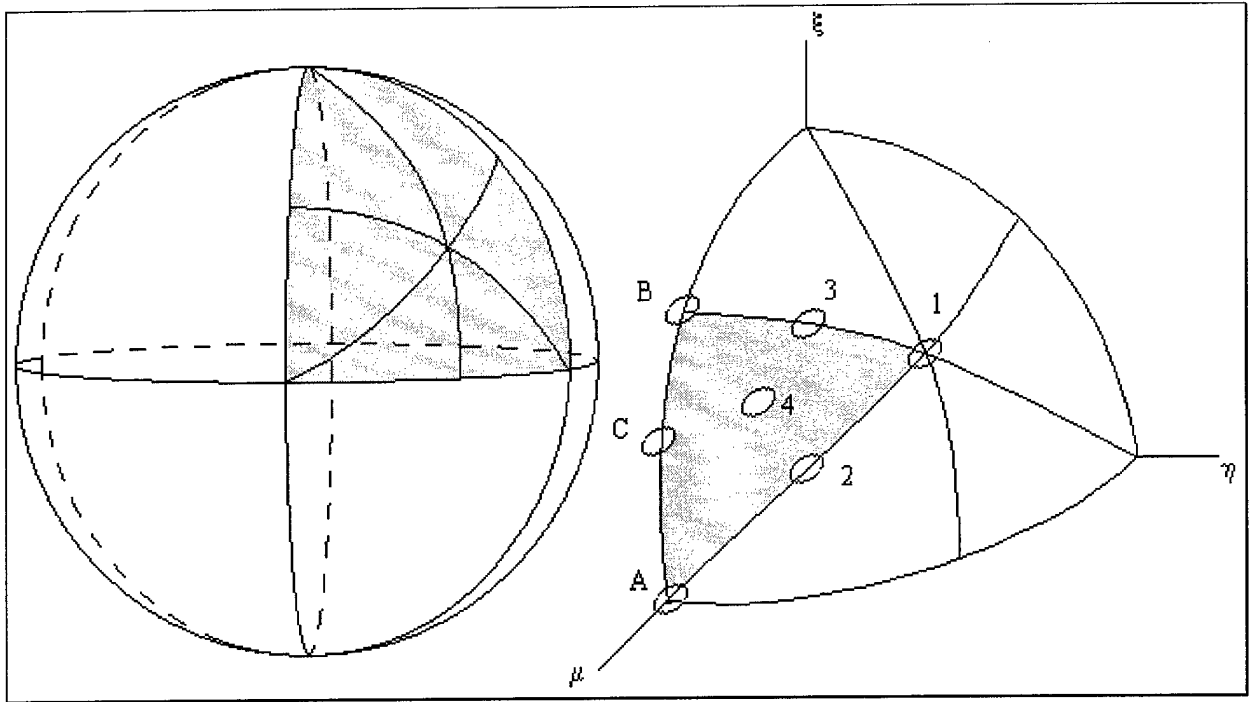


Figure III-1: Unit Sphere and Principal Octant Showing Quadrature Base Set Cases and Designators

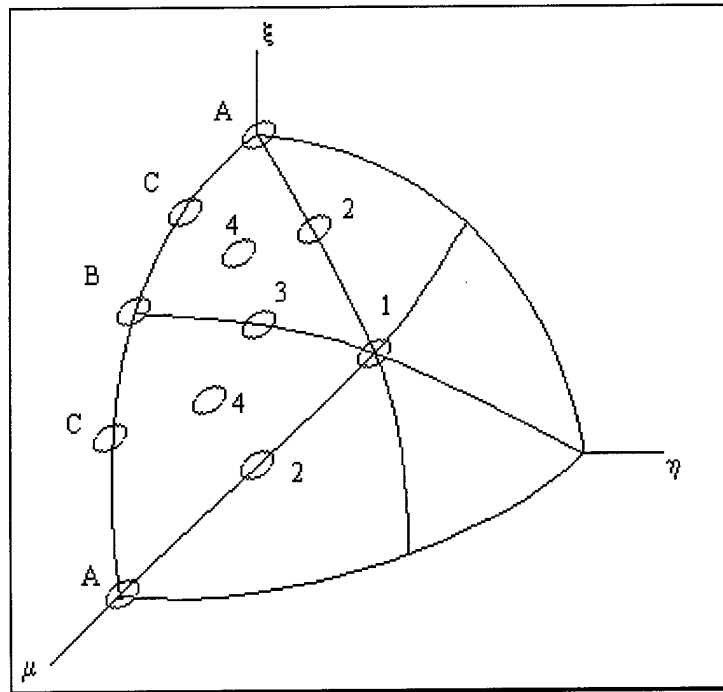


Figure III-2: $\mu \leftrightarrow \xi$ Exchange Operation

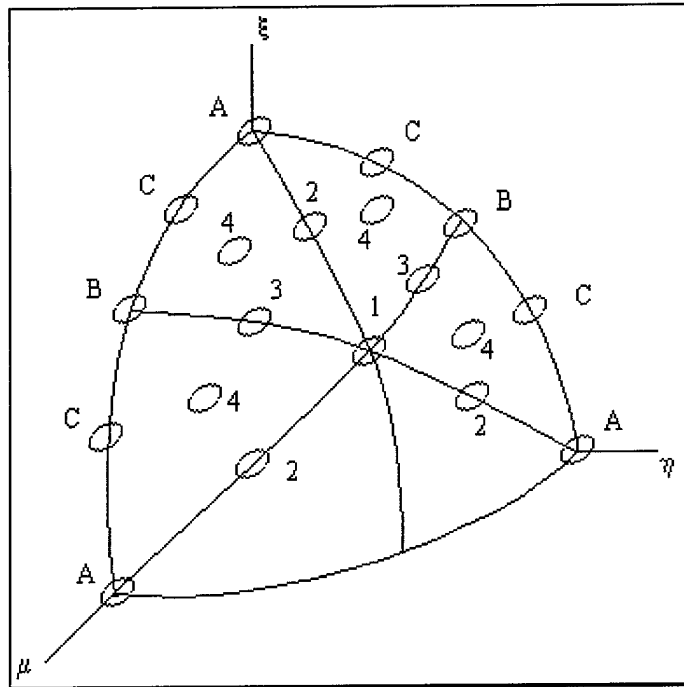


Figure III-3: $\mu \leftrightarrow \eta$ Exchange Operation

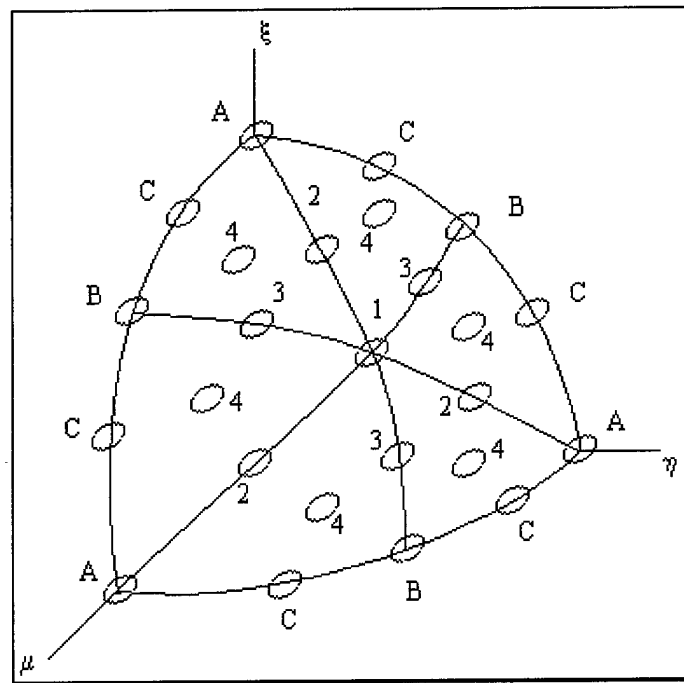


Figure III-4: Complete Principal Octant after $\xi \leftrightarrow \eta$ Exchange Operation

operations as shown in Figures III-2 through 4 (25). The remaining ordinates are generated by sequential reflections across the x-y, x-z and y-z planes.

The directions $\hat{\Omega}_n$ constitute a discrete set of values of $\hat{\Omega}$ over its entire domain (6: 2). If ψ has a convergent expansion in spherical harmonics, then from Equations (II-15) and (II-17) we see that a necessary condition for choosing the ordinates and weights is that the spherical harmonic orthogonality condition up to the desired order be satisfied, that is

$$\int d\Omega Y_{lm}(\hat{\Omega}) Y_{l'm'}^*(\hat{\Omega}) = \sum_{n=1}^N w_n Y_{lm}(\hat{\Omega}_n) Y_{l'm'}^*(\hat{\Omega}_n) = \delta_{ll'} \delta_{mm'} \quad (\text{III-1})$$

for all $0 \leq l, l' \leq L$, $-l \leq m \leq l$, and $-l' \leq m' \leq l'$ with the desired order of precision L . The $l = l' = m = m' = 0$ case provides the normalization condition for the weights,

$$\sum_n^N w_n = 1. \quad (\text{III-2})$$

We also require that $w_n > 0$ to reduce to possibility of obtaining physically unrealistic results.

Because of the symmetry requirements and the exchangeability of coordinates, Equation (III-1) will be satisfied if the moments equations,

$$\int \mu^i d\Omega = \sum_{n=1}^N w_n \mu_n^i, \quad i = 0, 1, \dots, 2L \quad (\text{III-3})$$

are satisfied exactly. In Equation (III-3) i is an exponent not a superscript.

This condition is enough to ensure that $\int \mu^i \eta^j \xi^k d\Omega$ will integrate exactly for all $0 \leq i, j, k \leq 2L$ with $i + j + k \leq 2L$ (25). Also due to symmetry, if $i, j,$ or k is odd, the integral is exactly zero. This is because the integration in Equation (III-1) can be represented as the integration of a product Legendre polynomials, which are intern polynomials of $\mu = \cos(\theta)$, and $e^{i(m-m')\phi}$.

Symmetry guarantees the exponential will integrate exactly because for every ϕ_n there exists with equal weight and equal μ_n a $\phi_{n'}$ that equals $\phi_n + \pi$. The terms in the summation therefore cancel except when $m = m'$, which results in the exponential reducing to unity. The odd powered terms are exactly zero because cosine integrates to zero over the range of -1 to 1 .

Finally, the case where $i = 0$ and the case where $i = 2$ are not independent. For the $i = 0$ case, Equation (III-3) becomes

$$\int d\Omega = 1 = \sum_{n=1}^N w_n, \quad (\text{III-4})$$

and for the $i = 2$ case

$$\int \mu^2 d\Omega = \frac{1}{3} = \sum_{n=1}^N w_n \mu_n^2 . \quad (\text{III-5})$$

Because of the symmetry requirements, the μ_n^2 values with equal weights will always exist in sets of three that sum to one (this can readily be seen by examining the most general case (case 4) in appendix B with $k = 1$). Equation (III-5) therefore becomes

$$\frac{1}{3} = \sum_{n=1}^N \frac{1}{3} w_n . \quad (\text{III-6})$$

Equation (III-6) and Equation (III-3) are not linearly independent. We can therefore replace the system of Equations (III-3) with

$$\int \mu^{2k} d\Omega = \frac{1}{2k+1} = \sum_{n=1}^N w_n \mu_n^{2k} , \quad k = 1, 2, \dots, L. \quad (\text{III-7})$$

The system of Equations (III-7) may have a solution or solutions providing the number of equations, L , is equal to the total number of free parameters (degrees of freedom): the total number of independent values for w_n and μ_n .

It is important to make clear that the criteria used for the selection of a quadrature set is that it will evaluate, without quadrature error, integrals of the sort

$$\int Y_{lm}^*(\hat{\Omega})f(\hat{\Omega})d\Omega$$

for any $N \geq l$; which means

$$\int Y_{lm}^*(\hat{\Omega})Y_{l'm'}(\hat{\Omega})d\Omega$$

must integrate with out error. This is why Equation (III-3) requires μ^i to integrate exactly for $i = 0$ to $2L$. Symmetry assures getting all the odd powers exactly while the degrees of freedom in the weights and angles are used to get the even powers. Thus five degrees of freedom integrate the coefficients of a fifth order expansion. P_5 anisotropic scatter needs this order of expansion. Chapter II discusses the expansion of the scattering cross section. With highly anisotropic scattering, a high order expansion may be needed to get accurate results. This requires the discrete ordinates order to be at least as high. Computational efficiency with highly anisotropic scattering therefore becomes of even greater concern. Therefore, obtaining the desired order of expansion with fewer ordinates is very desirable.

The objective is then to use the most reasonable value of L and minimize N , maintain total symmetry, and produce accurate transport results. The desired (or available) precision of the arithmetic, computation cost, and the order of the Legendre expansion of the scattering cross section will determine the most reasonable value of L .

Figure III-4 shows the principle octant and the various possible cases for points to be located and satisfy all symmetry requirements. The four cases not on the edge of the octant correspond with the cases 1 through 4 presented by Carlson (5) and have 1, 3, 3, and 6 points in the octant (hence 8, 24, 24, 48 points on the unit sphere) with 1, 2, 2, and 3 degrees of freedom respectively. The three additional cases, A, B, and C, are shared by two or more octants. Case A points are on a primary axis. Case B points are in a zero plane with the remaining two components equal. Case C points are in a zero plane but the remaining two components are not equal. There are a total of 6, 12, and 24 points over the unit sphere with 1, 1, and 2 degrees of freedom for cases A, B, and C respectively. Table III-2 provides a summary of pertinent information regarding each case.

Table III-1: Summary of Quadrature Case Data

Case	Total Points on Unit Sphere	Degrees of Freedom	Parameters to be Determined	Ordinates per Degree of Freedom
1	8	1	w	8
2	24	2	w, μ	12
3	24	2	w, μ	12
4	48	3	w, μ , η	16
A	6	1	w	6
B	12	1	w	12
C	24	2	w, μ	12

Cases A and 1 have the fewest ordinates per degree of freedom and are therefore preferred. Case 4 is the most expensive and also the most difficult to calculate and is to be avoided. The remaining cases are equivalent in this regard.

To distinguish these quadrature sets from those previously developed the notation MQ_n is adopted for a quadrature of order n . To uniquely solve for a quadrature set of order n , the total degrees of freedom in the equation set used must also equal n . This is accomplished by selecting a combination of cases from Table III-1 such that the sum of the degrees of freedom equals n . Equation (III-7) is then used to determine the free parameters. Care must be taken to uniquely identify the quadrature being referenced because there may be multiple quadrature sets of the same order. For example, to find an MQ_5 quadrature case 1 + case 2 + case A + case B will provide the needed degrees of freedom. A different MQ_5 quadrature results from selecting case 4 + case C. Further discussion of notation is presented later.

When selecting the cases, those cases with no free angles may only be selected once; otherwise a case may be used multiple times. Each free parameter must be uniquely identified. For example, for case 3 + case 3 + case A, the free parameters would be $\{(w_3, \mu_3, \eta_3), (w_{3'}, \mu_{3'}, \eta_{3'}), (w_A)\}$ resulting in an MQ_7 quadrature.

Because for each case only one point on the sphere is independent, the others resulting from exchange and reflection operations, we are able to write

a set of equations for each case that depends only on the free parameters of that point. This series of equations is then inserted into the system of

Equations (III-7). For case 1, $\mu_1 = \eta_1 = \xi_1 = \frac{1}{\sqrt{3}}$ in the primary octant with

w_1 to be determined and a total of eight points over the sphere. Therefore,

the contribution of case 1 to Equation (III-7) is

$$w_1 \left[\left(\frac{1}{\sqrt{3}} \right)^{2k} + \left(\frac{1}{\sqrt{3}} \right)^{2k} + \left(\frac{1}{\sqrt{3}} \right)^{2k} + \left(\frac{1}{\sqrt{3}} \right)^{2k} + \left(-\frac{1}{\sqrt{3}} \right)^{2k} + \left(-\frac{1}{\sqrt{3}} \right)^{2k} + \left(-\frac{1}{\sqrt{3}} \right)^{2k} + \left(-\frac{1}{\sqrt{3}} \right)^{2k} \right] = 8w_1 \left(\frac{1}{3} \right)^k$$

$k = 1, 2, \dots, L.$ (III-8)

The contributions of the other cases are found analogously. A complete derivation of each case is given in Appendix A and is summarized in Table III-2. Note that cases 2 and 3 have the same form of contribution equation.

If the angle solved for is less than $\frac{1}{\sqrt{3}}$ then this is a case 2 ordinate and the

angle is μ , if the angle is greater than $\frac{1}{\sqrt{3}}$ then a case 3 ordinate results and

the angle is η . The column labeled "Cosines" gives the equations or values

needed to find the initial (μ, η, ξ) triplet. The rest of the quadrature is then

generated by the operations described previously. As an example, for the

Table III-2: Contribution of Each Case to Equation (III-7)

Case	Contribution	Cosines (μ, η, ξ)
1	$8w_1 \left(\frac{1}{3}\right)^k$	$\left(\frac{1}{\sqrt{3}}, \frac{1}{\sqrt{3}}, \frac{1}{\sqrt{3}}\right)$
2	$8w_2 \left[\mu_2^{2k} + 2 \left(\frac{1 - \mu_2^2}{2} \right)^k \right]$	$\left(\mu_2, \sqrt{\frac{1 - \mu_2^2}{2}}, \sqrt{\frac{1 - \mu_2^2}{2}} \right)$
3	$8w_3 \left[\eta_3^{2k} + 2 \left(\frac{1 - \eta_3^2}{2} \right)^k \right]$	$\left(\sqrt{\frac{1 - \eta_3^2}{2}}, \eta_3, \sqrt{\frac{1 - \eta_3^2}{2}} \right)$
4	$16w_4 \left[\mu_4^{2k} + (1 - \mu_4^2 - \eta_4^2)^k + \eta_4^{2k} \right]$	$\left(\mu_4, \eta_4, \sqrt{1 - \mu_4^2 - \eta_4^2} \right)$
A	$2w_A$	$(1, 0, 0)$
B	$8w_B \left(\frac{1}{2}\right)^k$	$\left(\frac{1}{\sqrt{2}}, 0, \frac{1}{\sqrt{2}}\right)$
C	$8w_C \left[\mu_C^{2k} + (1 - \mu_C^2)^k \right]$	$\left(\mu_C, 0, \sqrt{1 - \mu_C^2} \right)$

MQ₅ quadrature using case 1 + case 2 + case A + case B, the following equations result

$$2w_A + 8w_B \left(\frac{1}{2}\right)^k + 8w_1 \left(\frac{1}{3}\right)^k + 8w_2 \left[\mu_2^{2k} + 2 \left(\frac{1 - \mu_2^2}{2}\right)^k \right],$$

$k = 1, 2, 3, 4, 5.$ (III-9)

These equations were entered into a Mathematica™ (20) notebook and solved using built-in functions. A listing of the notebook is found in Appendix B.

The solution for Equations (III-9) is shown in Table III-3. Including all unique permutations of the cosines will complete the principal octant. For example, there are two additional case A ordinates with the same weight as the one shown and having cosines (0, 1, 0) and (0, 0, 1) respectively. There are no additional case 1 ordinates as there are no more unique permutations of the cosines. Figure III-3 shows the distribution of these points on the principal octant. Both the exact solution and the decimal fractions of the weights are given. The weights are all positive, as required, which reduces the likelihood of physically unrealistic results such as negative flux. They are also similar in magnitude, providing for better conditioning of the problem.

From Table III-1 we see that there are fifty total directions and five degrees of freedom for this quadrature. For comparison, an LQ₁₀ quadrature also has five degrees of freedom but has 120 total directions over the unit sphere requiring 2.4 times the computational cost (assuming both calculations converge in the same number of iterations). The LQ₆ level symmetric quadrature has 48 directions but only three degrees of freedom. Table III-3

also gives the base sets for an MQ_3 and an MQ_7 quadrature set. Table III-4 shows the number of discrete ordinates required to obtain a desired number of degrees of freedom for various MQ_n and LQ_n quadrature sets.

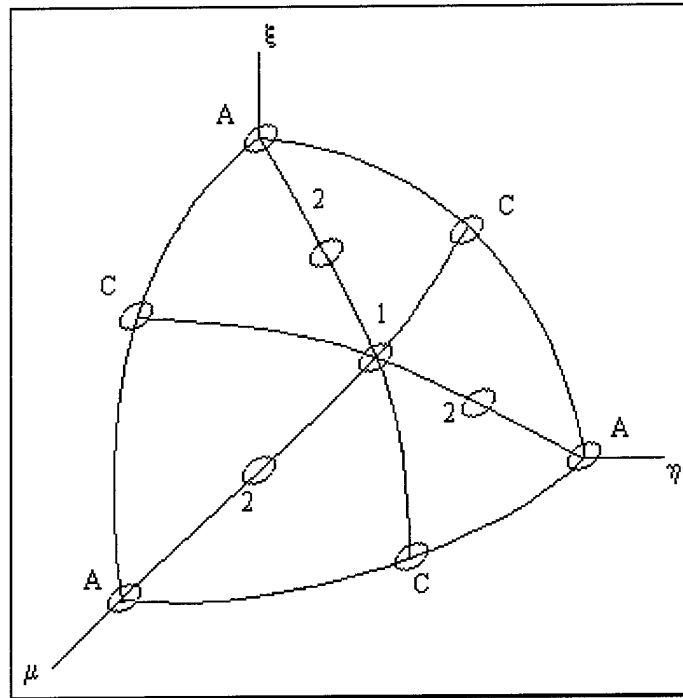


Figure III-5: Example MQ_5 Quadrature Layout

Table III-3: Some Possible MQ_n Quadrature Base Sets

Order	Class	weight	μ	η	ξ
n = 3	A	1/21 .047619047619	1	0	0
	B	9/280 .0321428571429	$1/\sqrt{2}$	0	$1/\sqrt{2}$
	1	4/105 .0380952380952	$1/\sqrt{3}$	$1/\sqrt{3}$	$1/\sqrt{3}$
n = 5	A	4 / 315 .0126984126984	1	0	0
	B	64 / 2835 .0225749559083	$1/\sqrt{2}$	0	$1/\sqrt{2}$
	1	27 / 1280 .0210937500000	$1/\sqrt{3}$	$1/\sqrt{3}$	$1/\sqrt{3}$
	2	14641 / 725760 .020173335379	$3/\sqrt{11}$	$1/\sqrt{11}$	$1/\sqrt{11}$
n = 7	A	.00904818883016	1	0	0
	B	.02103246043743	$1/\sqrt{2}$	0	$1/\sqrt{2}$
	C	.00645149153857	.954580866940172	0	0.29795195665031
	1	.01827941392342	$1/\sqrt{3}$	$1/\sqrt{3}$	$1/\sqrt{3}$
	2	.01634375972737	.875317087598172	.34192104070871	.34192104070871

Table III-4: Comparison of Computational Cost of MQ_n versus LQ_n

Degrees of Freedom	MQ _n Cases Used	LQ _n Required	MQ _n : Total Number of Ordinates on Unit Sphere	LQ _n : Total Number of Ordinates on Unit Sphere
1	A	S ₂	6	8
3	A, B, 1	S ₆	26	48
5	A, B, 1, 2	S ₁₀	50	120
7	A, B, C, 1, 2	S ₁₂ / S ₁₄ *	74	168 / 224
9	A, B, 1, 2, 4	S ₁₆	110	288

*S₁₂ only has six degrees of freedom and S₁₄ has eight. No level symmetric S_n quadrature has 7 degrees of freedom.

For the MQ₇ quadrature in Table III-3, the exact values are not given,

because Mathematica was not able to solve this set of equations exactly.

Instead a numerical solutions was obtained using a numerical solving built-

in, NSolve. As the order of the quadrature increases the complexity of the polynomial system of equations increases substantially. Only for the lowest order quadrature sets was I able to obtain exact solutions.

These quadrature sets were tested with a computer algorithm to verify they met the orthogonality condition in Equation (III-1) to double precision. Many more combinations of cases are available than are presented here. Quadrature sets can be tailored using Table III-2 and Equation 3 to best fit the geometry of the problem. Appendix C shows several additional quadrature sets.

Generating the sets of equation to solve is a straightforward matter, solving them is often a challenge. Some of the equation sets do not have real solution that I have been able to find. The requirement of positive weights also eliminates some possibilities. Appendix B contains some of the work I did in attempting to get valid quadrature sets. Table III-6 summarizes a significant number of possible quadrature set combinations and the results of my efforts. Only those combinations using at least one of the new cases are shown. The "2(3)" notation in the Cases column is intended to show that the resulting equations when selecting a case 2 or a case 3 are mathematically equivalent as discussed above. An entry in the results column of one valid found means a valid quadrature set was found for the resulting system of equations, no valid means all the solutions had either negative weights, imaginary values or cosines greater than one. No solution means that the

system of equations did not provide any solutions, good or bad. Empty spaces are quadrature combinations I have not tried and those marked with “tried”, means they were attempted, but I was unable to solve the equations. The letters in the order column are a method to distinguish different quadratures of like order, for example M_{5b} . Valid quadrature sets are presented in Appendix C

Table III-3: Case Combination for Quadrature of Order n

Order	Cases	Results	
3	a	AB1	One valid found
	b	C1	One valid found
	c	AC	No solution
	d	BC	No solution
5	a	AB12(3)	One valid found
	b	AC2(3)	One valid found
	c	BC2(3)	One valid found
	d	C4	One valid found
	e	ABC1	No solution
	f	C12(3)	No valid
	g	AB4	Tried
	h	A23	
	i	B23	
	j	A13	
	k	B13	
7	a	ABC12(3)	One valid found
	b	AC23	One valid found
	c	ABC4	Tried
	d	AC14	
	e	AB14	Tried
	f	AB42(3)	
	g	AB123	No valid
9	a	ABC123	Tried
	b	ABC2(3) 4	Tried
	c	Etc.	

Though trial and error can yield valid quadrature sets it may be possible to gain some direction when selecting the cases to use. Since the method is based on the exact integration of spherical harmonics, selecting cases based on features of the spherical harmonics of the order being matched may yield systems of equations that are more readily solved. Figure III-6 (12) shows the first few spherical harmonics.

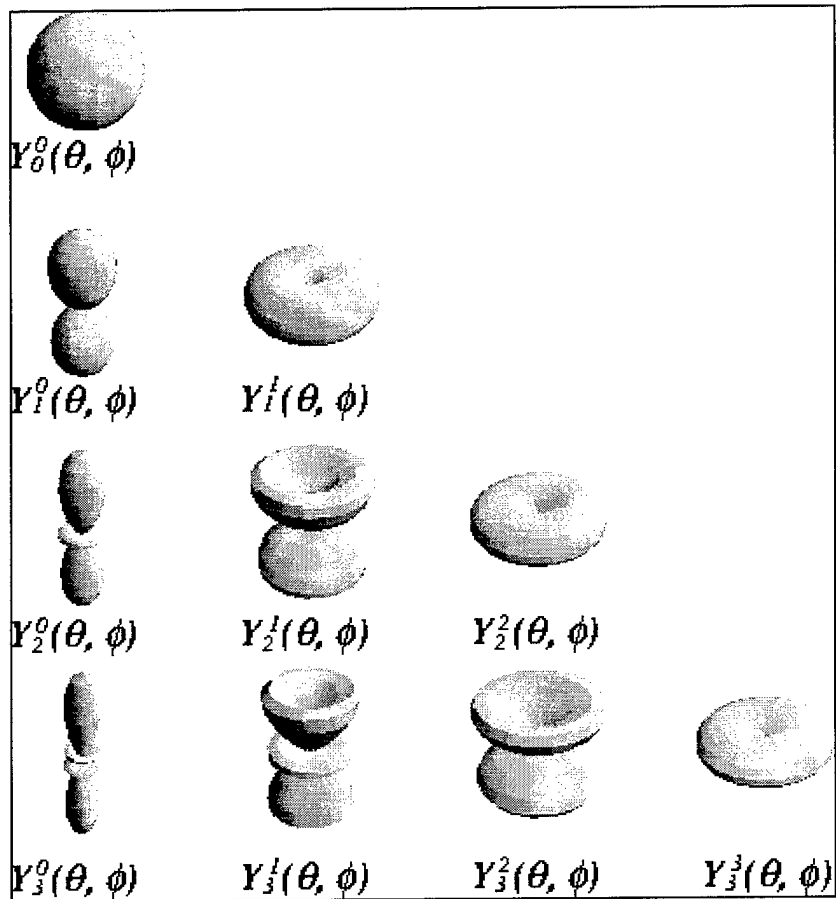


Figure III-6 :Spherical Harmonics, $Y_l^m(\theta, \phi)$

The three quadratures show in Table III-3 where tested and compared with level symmetric quadratures. These quadratures were chosen because they are the sets with the fewest ordinates for the given order. Also they

have ordinates which are reasonable dispersed over the unit sphere and the weights are all about the same order of magnitude. The MQ_{5a} quadrature was shown in Figure III-5, the MQ_{3a} and MQ_{7a} quadrature sets are shown in Figures III-7 and III-8.

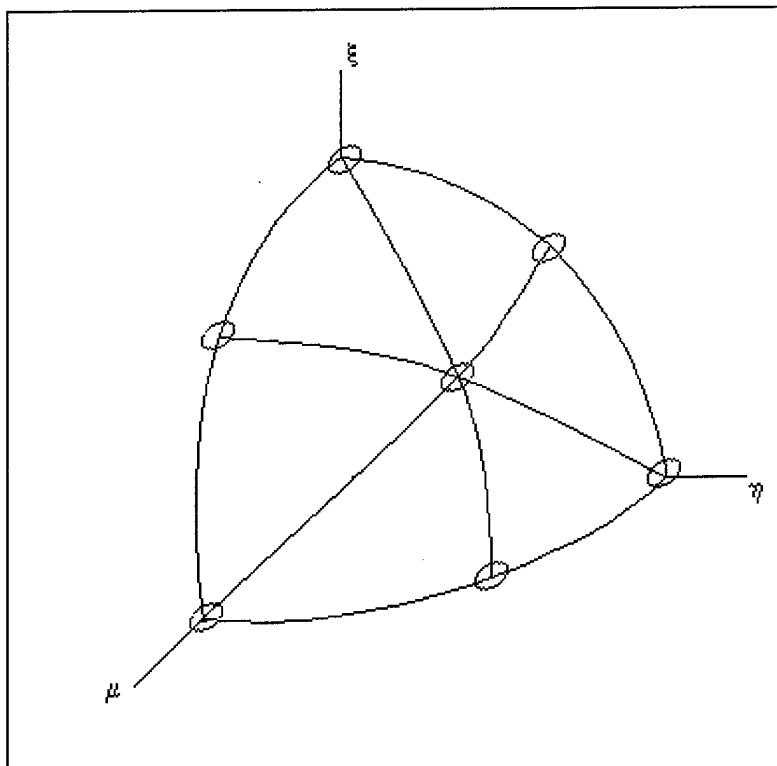


Figure III-7: MQ_{3a} Quadrature Layout

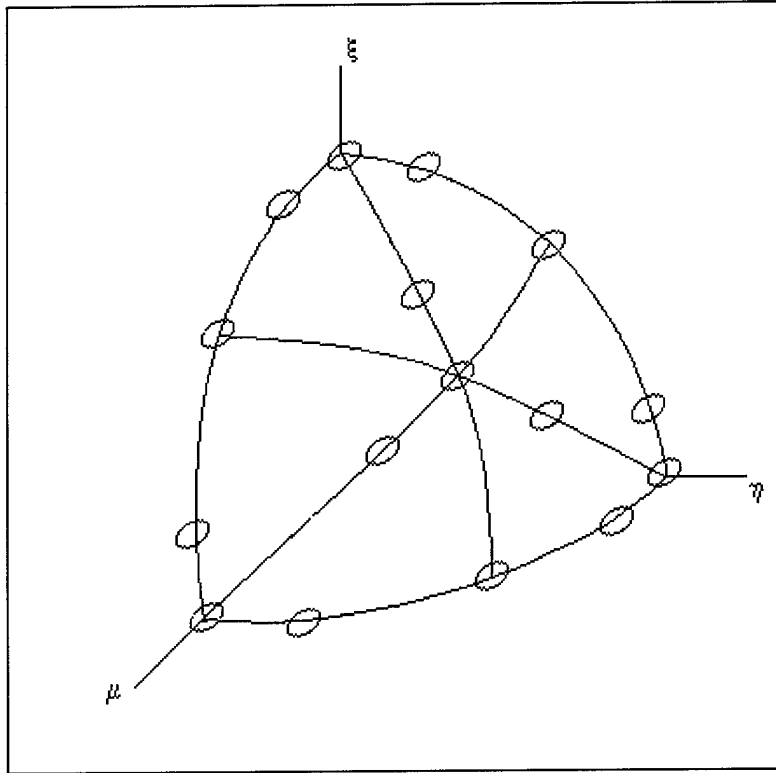


Figure III-8: MQ7a Quadrature Layout

IV. Results

Some of the new quadrature sets were tested on two problems and compared with the level symmetric LQ_n quadratures. The first problem is a cube source inside a cube shield region and was designed to exacerbate ray effects. The second problem is a spherical source region in a spherical shield. This problem was selected to reduce ray-effects. Due to the symmetry of this problem, the solution should also be symmetric; therefore any deviation from smooth behavior must be due to the method of calculation. Each test problem was run on the TETRAN code using the linear characteristic (LC) method for handling the spatial computations. The MQ_3 , MQ_5 , and MQ_7 quadrature sets from Table III-3 are compared with the standard LQ_4 , LQ_{10} , and LQ_{16} level symmetric quadrature sets. For brevity, no letter subscript will be used with the MQ_n quadratures. Each problem was also run on the THREEDANT module of the DANTSYS code package using Diamond Difference with negative flux fix-up (DZ). Some quadratures with zero ordinates would cause the code to produce nan (not a number) values for some of the output. The case A ordinates did not cause problems, but the case B and C would. The input file for THREEDANT requires μ , η , and the weights to be entered. The program calculates the value of ξ . For the case B and C ordinates, when ξ should be zero, instead a nan would be reported. Error handling routines prevent the code from failing but the output is not useful. By reducing the precision of the quadrature angles input into THREEDANT, the code does

run and provide output. Presumably because the value of ξ , though very near zero, is sufficiently large so as not to cause problems.

In order to overcome the limitations of THREEDANT with regard to the expectation that the ordinates not lie on the edges of an octant and to the total number of directions in a quadrature set, it was necessary to make further modifications. THREEDANT defines a quadrature only in the principle octant, the remaining angles generated by reflection operations. This also requires the weights that should lie on a boundary to be divided by the number of octants among which it is shared. For example, in order for the normalization of the weights to be correct the weight of a case B or C ordinate must be divided by two. Also, the number of ordinates in a quadrature must match the number of ordinates expected. The variable *isn* in the input file must be set to the value of *n* for the LQ_n quadrature intended for use (there are provisions for other quadrature types not of relevance here). The LQ_n level symmetric quadratures are selected by default if no quadrature information is given. If a quadrature set is entered, the number of ordinates supplied for the principle octant must match the number in a LQ_n quadrature for the value of *n* supplied. This number is given by $N = n(n + 2) / 8$. For the MQ_3 quadrature there are seven angles in the principle octant. The closest LQ_n quadrature with at least that many ordinates is LQ_8 with ten ordinates. Therefore, to run the MQ_3 quadrature, the variable *isn* must be set to eight and the first seven ordinates in the

quadrature array are filled with the MQ_3 values. The remaining three slots in the quadrature array are filled with dummy angles with the weights set to zero. This fix will maintain the quadrature set's ability to integrate properly. The disadvantage of this fix is a loss of computational efficiency because the code still has to perform computations using the dummy values that do not contribute to the solution. Valid comparisons of computational efficiency between the MQ_n and LQ_n sets using THREEDANT are therefore limited.

The TETRAN calculations were performed on the IBM SP located at the major shared resource center (MSRC) of Wright Patterson AFB. These problems were run on a single node, consisting of an RS/6000 P2SC model 595 processor with a clock speed of 135MHz and 1Gb of memory (23). The THREEDANT code was run on an IBM RS-6000/590 workstation using the AIX 3.2.5 operating system with 256 Mb of memory and operating at 67MHz. The convergence tolerance for each problem was 10^{-6} .

A benchmark solution was obtained for each problem using a Monte Carlo simulation generated with MCNP (15). MCNP is a general three-dimensional simulation code widely used and accepted. MCNP results are the average of the computed quantity over all histories. Each history is a simulation of one particle's motion through the media. MCNP also provides the estimated statistical relative error, R , at the one standard deviation level defined as the sample standard deviation divided by the sample mean.

Problem Definition

The cube problem uses the geometry shown in Figure IV-1. The mesh shown is for clarity and not used in calculation. This problem is a three-dimensional extension of the two-dimensional problem presented by Lathrop (21) and discussed in references 1 and 3. The source region is a 2x2x2 cm

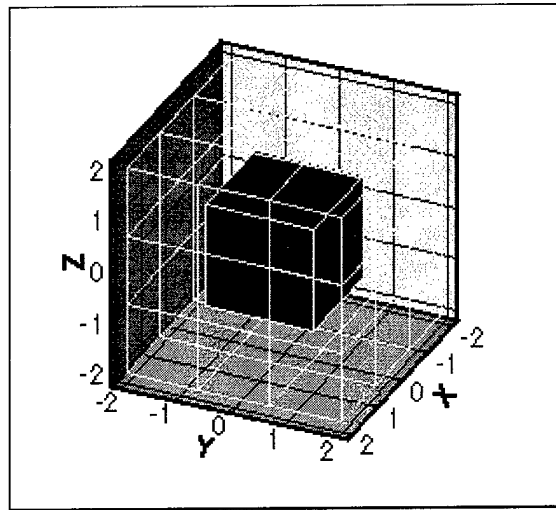


Figure IV-1: Geometry for the Cube in Cube Problem

cube centered in a 4x4x4 cm cube with the source normalized to one over the source volume. The second problem, shown in Figure IV-2, is a spherical source region in a spherical shield region. Problem two used a source region with a radius of 1.5 cm normalized to one over the volume and a shield region with a radius of 3 cm. Figure IV-2 shows the finest tetrahedral mesh used with TETRAN. The source and shield regions have the same nuclear data

for all test problems. Vacuum boundaries are used outside all shield regions.

The total cross section, σ_t , is $\frac{3}{4} \text{ cm}^{-1}$ with a scattering to total cross section

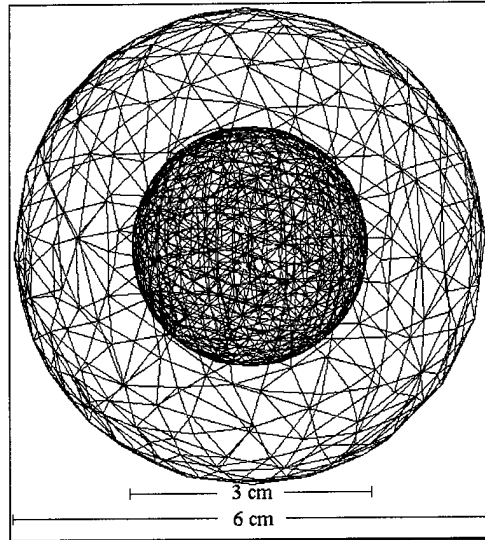


Figure IV-2: Geometry for the Sphere in Sphere Problem

ratio of $\frac{\sigma_s}{\sigma_t} = \frac{2}{3}$. This results in a mean free path of $\frac{4}{3} \text{ cm}$. The MCNP

benchmark solution gives the volume average scalar flux in each region, the average scalar flux at the outer surface and the net current through each surface.

Test Problem One – Cube Source in Cube Shield

The first test problem is a simple 4x4x4 cm cube with vacuum boundaries and a uniformly embedded isotropically-emitting source of strength $1.0 \text{ cm}^{-3} \text{ sec}^{-1}$. The source is constrained to the 2x2x2 cm center

region of the cube. The nuclear data is given above. The MCNP solution for this problem was run with one million histories. The statistical relative error, R as defined above, is .003 for surface data and .0007 for volume data.

Tetrahedral Mesh

Each tetrahedral mesh was generated using the Pro/Mesh module of Pro/Engineer (22). This problem was run with two levels of mesh refinement. The meshes are shown in Figure IV-3. Table IV-1 gives the tetrahedral mesh information for test problem one. For clarity, only the surface cells are show for the fine mesh.

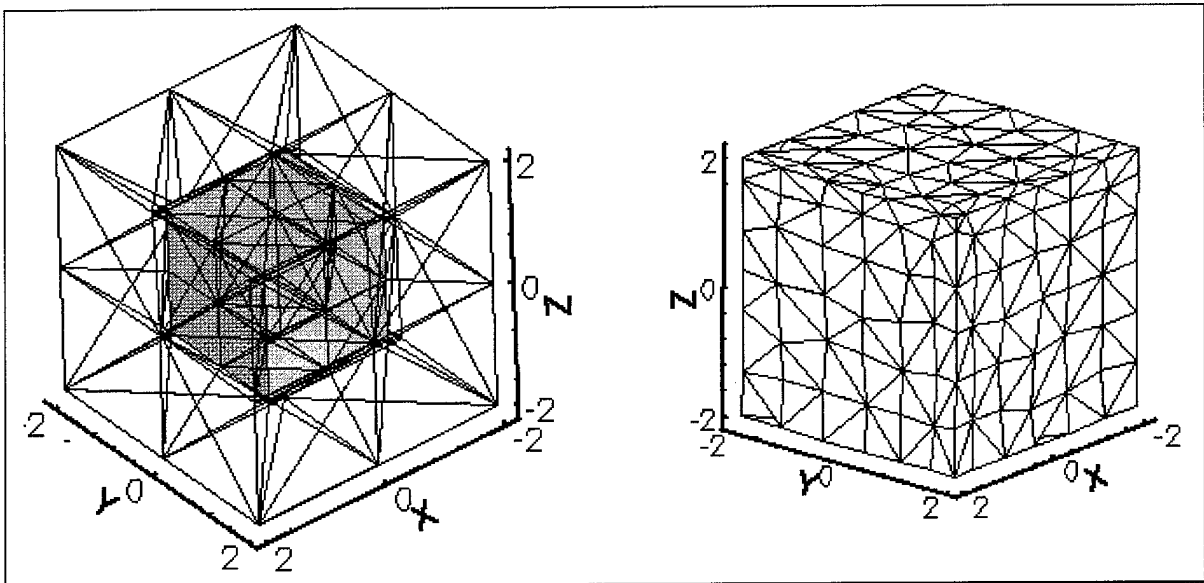


Figure IV-3: Tetrahedral Meshes Used in Test Problem One

Table IV-1 : Tetrahedral Mesh Data for Test problem One

Mesh	Total Tetrahedra	Cells in Source Region	Net Volume of Source Region	Average Optical Thickness
Coarse	191	47	8.0	1.203
Fine	1513	162	8.0	0.5997

For a right regular problem geometry the tetrahedral mesh does very well in matching the region volumes, even with a relatively coarse mesh. Here the average optical thickness is defined as the mean path length through a cell measured in mean-free paths. The accuracy of each quadrature relative to the benchmark will be examined first.

Figure IV-4 shows contour plots of the surface average scalar flux for the coarse mesh for the MQ₇ and LQ₁₆ quadrature sets. Figure IV-5 shows the same data for the fine mesh. The plots of the other quadrature sets are very similar and are not shown. The TETRAN code gave the scalar flux at the center of each cell and at the surface of each cell on the boundary. To generate these plots it was necessary to have values at the nodes. Each node value was approximated as the average of the cell center values for each tetrahedron shared by that node. This averaging may effect the variability of the actual surface data. Also from these figures, the flux distribution's dependence on cell geometry and orientation is very evident. These contour plots show little dependence on quadrature. Contour plots of the net current out the cell faces at the surface are very similar to those for the scalar flux

and are not presented. These plots indicate that the new quadratures do not cause any significant loss in uniformity and that it is the spatial mesh which is the primary source of surface variation in scalar flux and current. The variability of the data does decrease slightly with quadrature order. For low order quadrature sets the LQ_n sets have less variability than the MQ_n sets but this difference is minor. Using the tetrahedral mesh, it is very difficult to get a qualitative comparison of quadrature sets using individual data points. The integral values provide a clearer method of comparison.

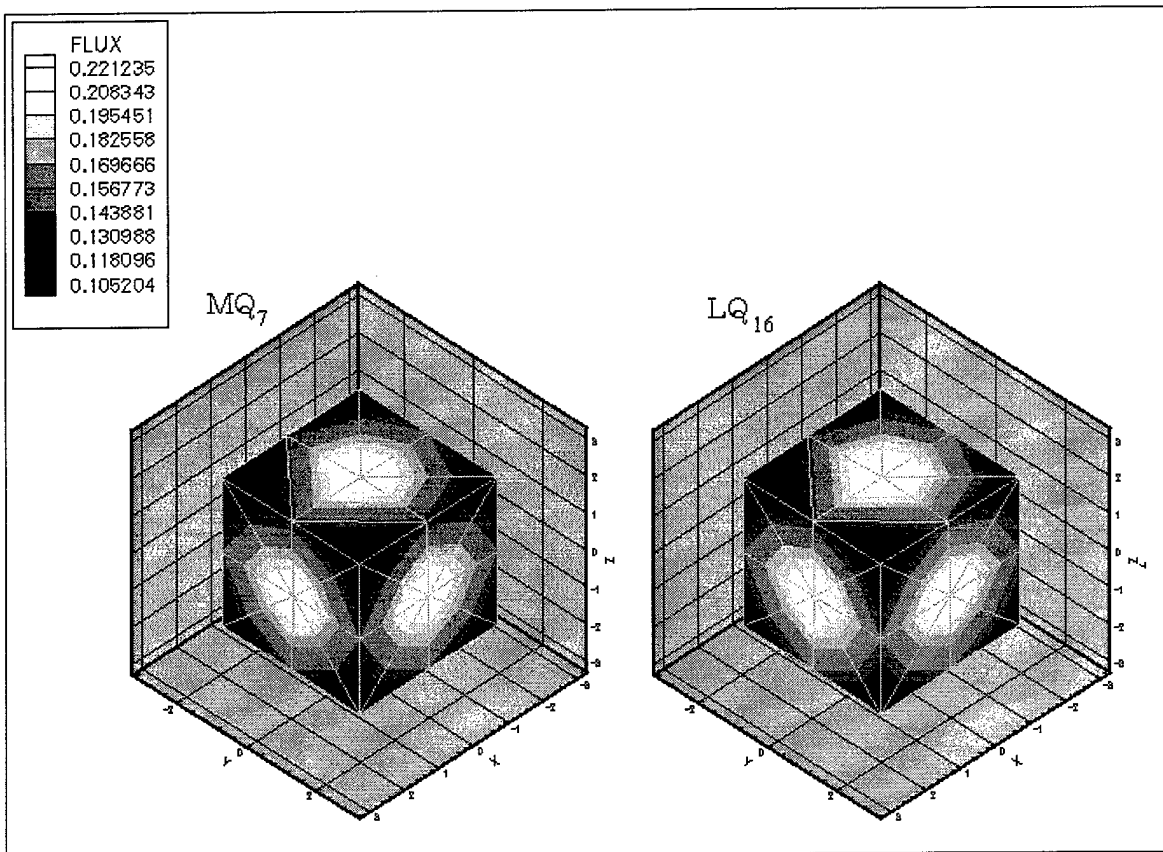


Figure IV-4: Contour Plot of the Surface Average Scalar Flux, Cube Problem, Coarse Tetrahedral Mesh

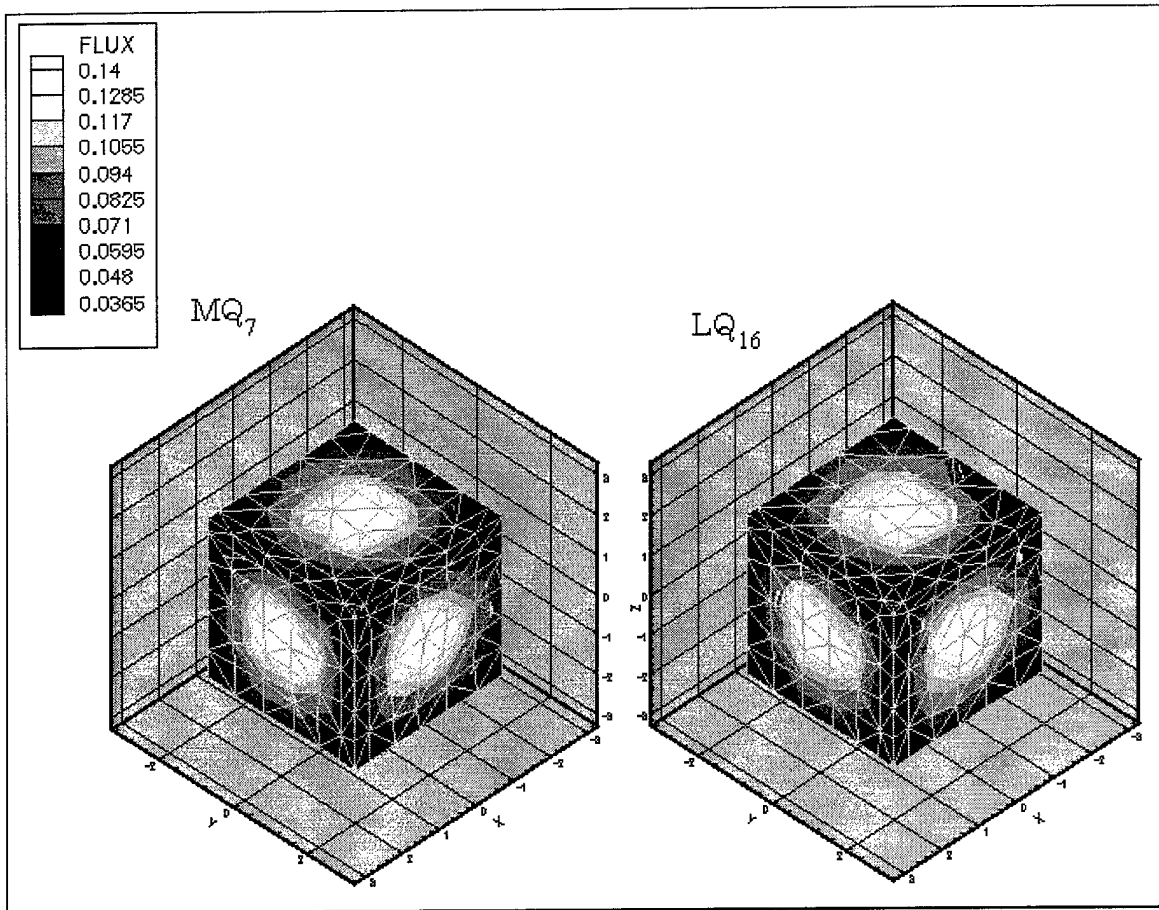


Figure IV-5: Contour Plot of Surface Average Scalar, Cube Problem, Fine Tetrahedral Mesh

The surface average scalar flux for each quadrature and mesh are shown in comparison with the MCNP benchmark calculation in Figures IV-6 and 7. The surface average is calculated as the sum of the product of the flux at the vacuum interface of a surface cell and the area of that cell's face divided by the total surface area,

$$\phi_{\text{surface average}} = \frac{\sum_{\text{cells on surface}} \phi_{\text{cell}} A_{\text{cell}}}{\sum_{\text{cells on surface}} A_{\text{cell}}}$$

The net current out of the cube is similarly shown in Figures IV-8 and 9. The benchmark is shown with error bars indicating the statistical error R. With the exception of the surface flux calculation for the fine tetrahedral mesh, these plot show there is little significant difference in the accuracy achieved by the quadratures tested.

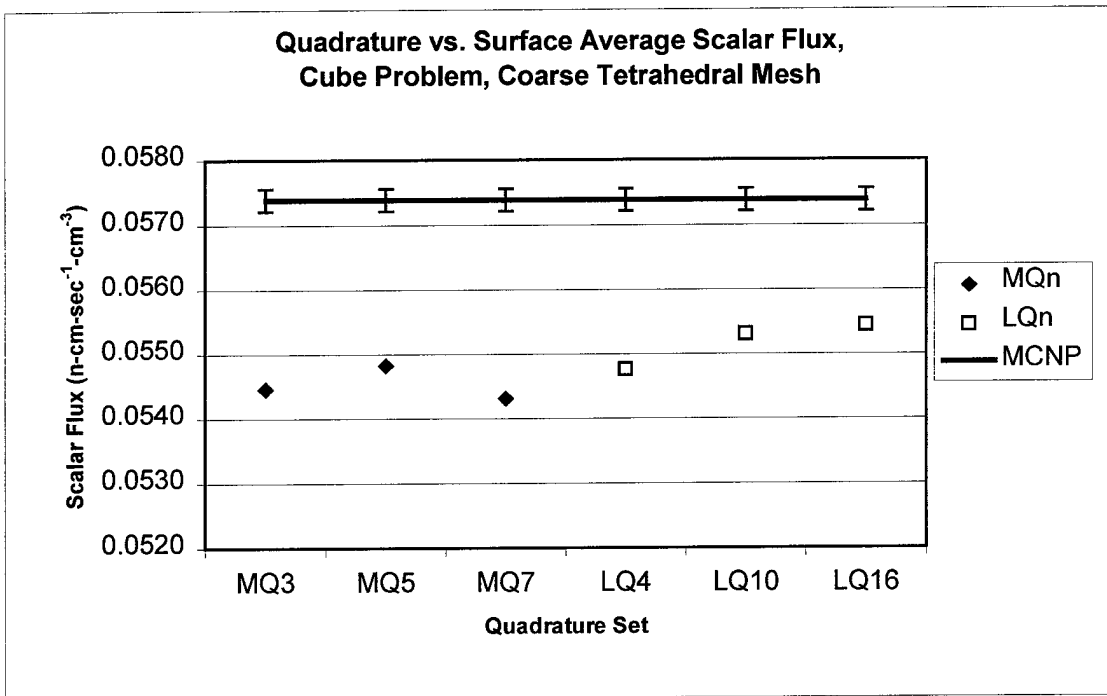


Figure IV-6: Surface Average Scalar Flux, Cube Problem, Coarse Tetrahedral Mesh

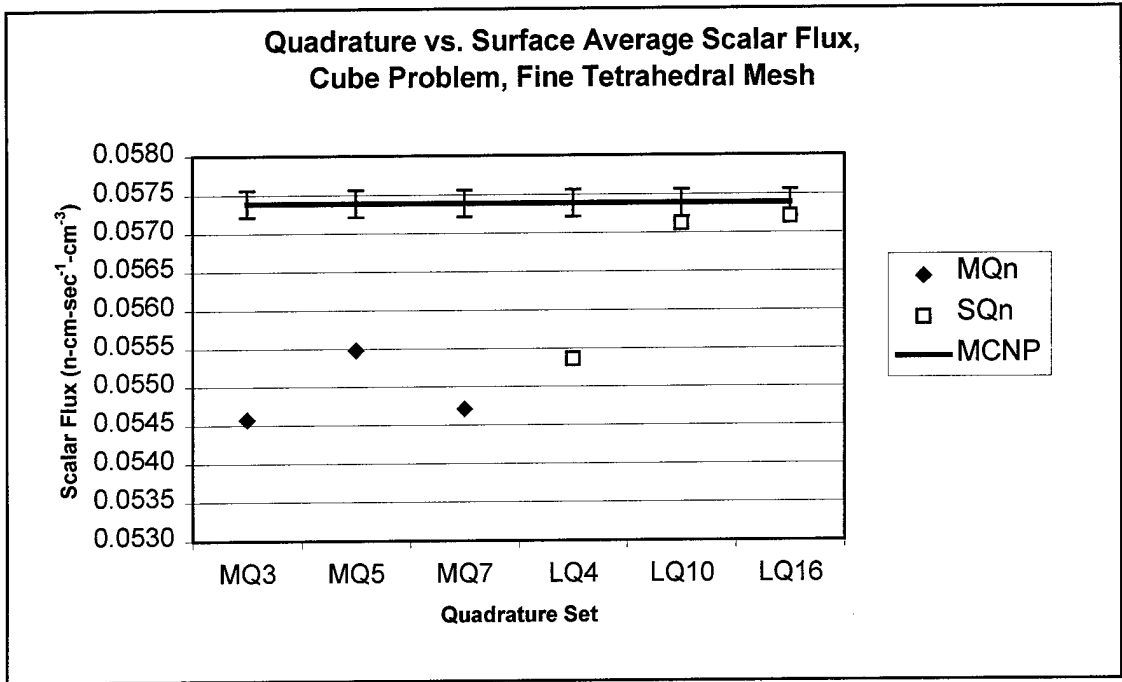


Figure IV-7: Surface Average Scalar Flux, Cube Problem, Fine Tetrahedral Mesh

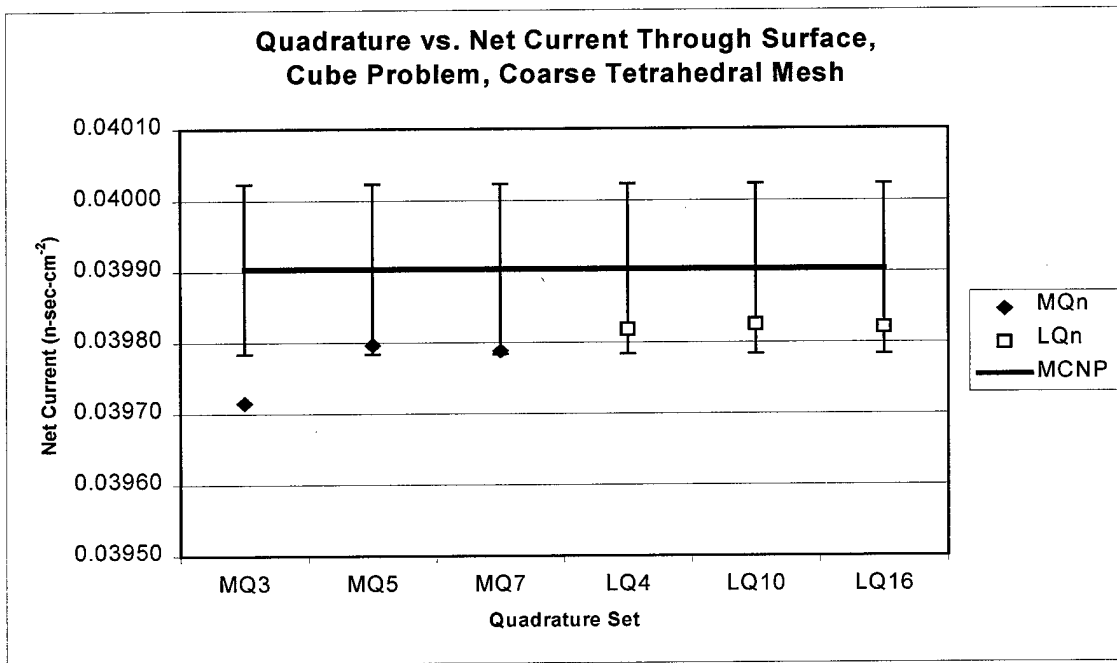


Figure IV-8: Net Current Through the Surface, Cube Problem, Coarse Tetrahedral Mesh

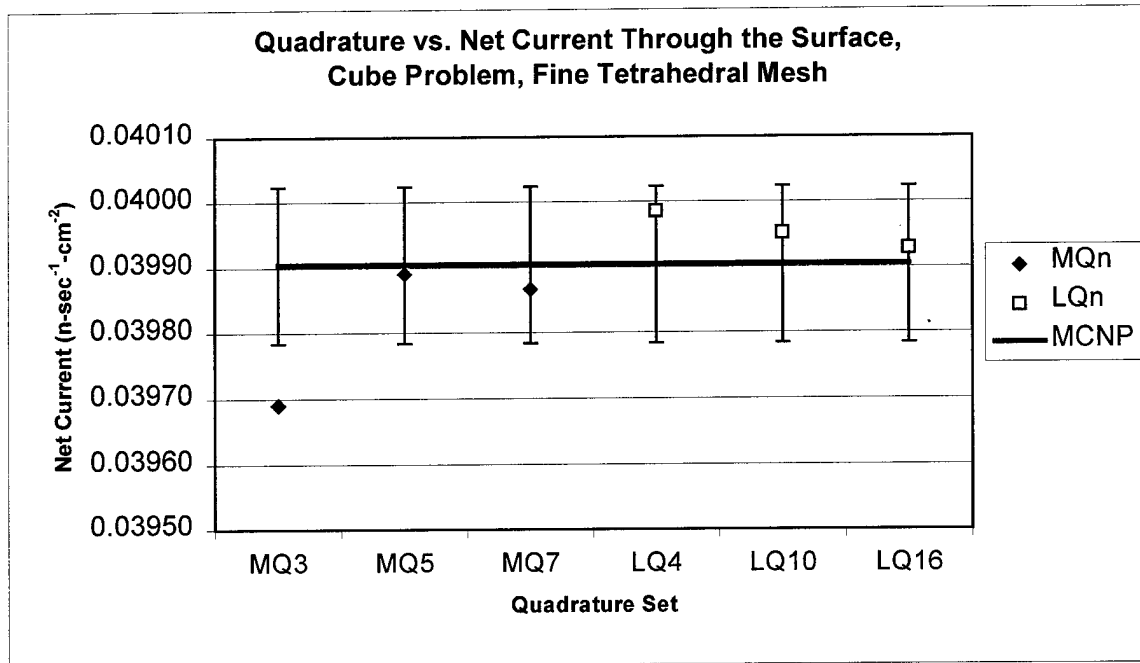


Figure IV-9: Net Current Through the Surface, Cube Problem, Fine Tetrahedral Mesh

The absolute value of the relative error, ε , is defined as

$$\varepsilon = \frac{|\phi_{\text{benchmark}} - \phi_{\text{calculated}}|}{\phi_{\text{benchmark}}} \quad (\text{IV-1})$$

The absolute value of the relative error for the current is found analogously to the flux. The flux, current, and relative error are summarized in Tables VI-2 and 3 for test problem one. The value for ε given for the MCNP entry is actually the statistical error R and is shown for reference.

Table IV-2: Surface Average Scalar Flux, Net Current, and Relative Error, Cube Problem, Coarse Tetrahedral Mesh

Quadrature	Scalar Flux	ϵ	Net Current	ϵ
MQ ₃	0.054461034	0.05100	0.039715347	0.004732
MQ ₅	0.054827230	0.04462	0.039796675	0.002693
MQ ₇	0.054314746	0.05355	0.039788637	0.002895
LQ ₄	0.054765258	0.04570	0.039818522	0.002146
LQ ₁₀	0.055312273	0.03617	0.039825301	0.001976
LQ ₁₆	0.055447146	0.03382	0.039821360	0.002075
MCNP	0.05739	0.003	0.03990	0.003

Table IV-3: Surface Average Scalar Flux, Net Current and Relative Error, Cube Problem, Fine Tetrahedral Mesh

Quadrature	Scalar Flux	ϵ	Net Current	ϵ
MQ ₃	0.054574800	0.04902	0.03969063	0.005351
MQ ₅	0.055480478	0.03324	0.03989043	0.0003442
MQ ₇	0.054711298	0.04664	0.03986661	0.0009411
LQ ₄	0.055361991	0.03530	0.03998596	0.002050
LQ ₁₀	0.057121652	0.004641	0.03995183	0.001194
LQ ₁₆	0.057210746	0.003090	0.03992792	0.000595
MCNP	0.05739	0.003	0.03990	0.003

For the surface values the LQ_n quadratures have slightly better accuracy. The difference in relative error between quadrature sets tested is small for the coarse cube. In the fine cube the LQ_n quadrature sets do better for scalar flux but the MQ₅ and MQ₇ provide comparable results for net current.

Figures IV-10 - 13 show the volume average scalar flux in each region and quadrature with the MCNP solution. The volume average is calculated

as the sum of the product of cell flux and cell volume divided by the total region volume,

$$\phi_{\text{average}} = \frac{\sum_{\text{cells in region}} \phi_{\text{cell}} V_{\text{cell}}}{\sum_{\text{cells in region}} V_{\text{cell}}}$$

The source and shield regions are shown. Tables IV-4 and 5 summarize this data as well as present the relative error.

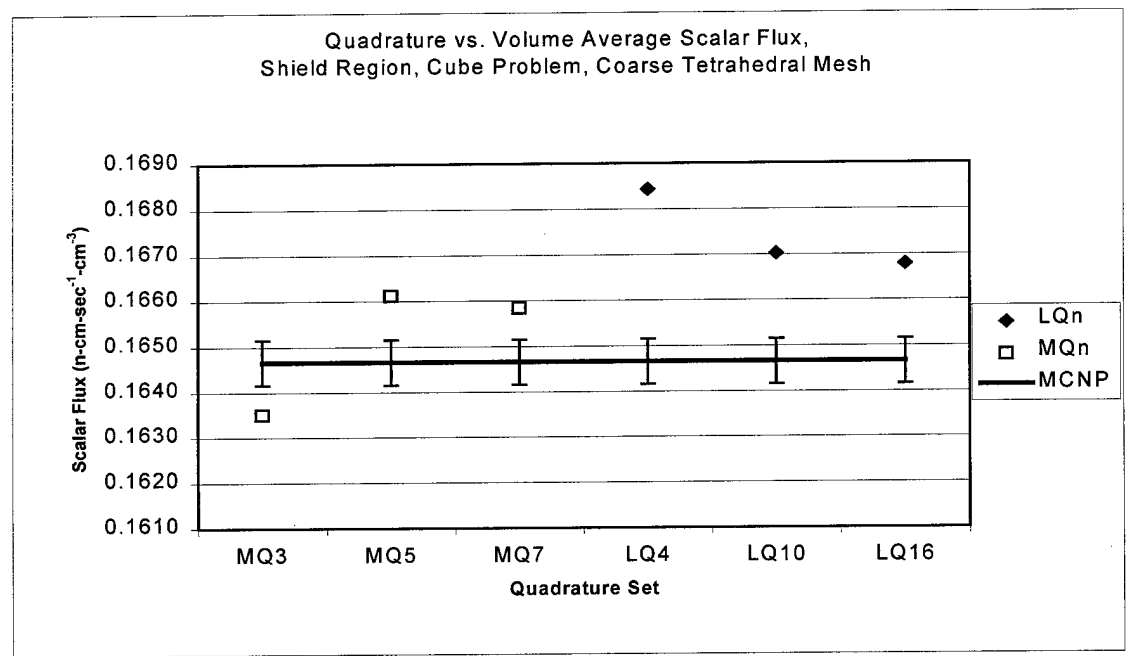


Figure IV-10: Volume Average Scalar Flux, Shield Region, Cube Problem Coarse Tetrahedral Mesh

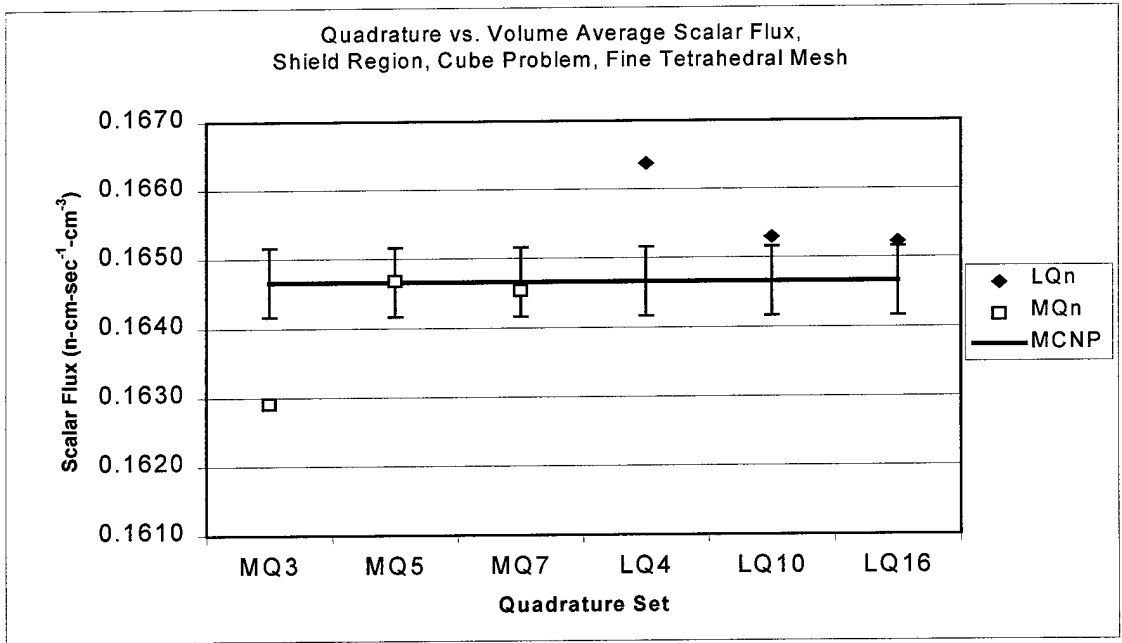


Figure IV-11 Volume Average Scalar Flux, Shield Region, Cube Problem, Fine Tetrahedral Mesh

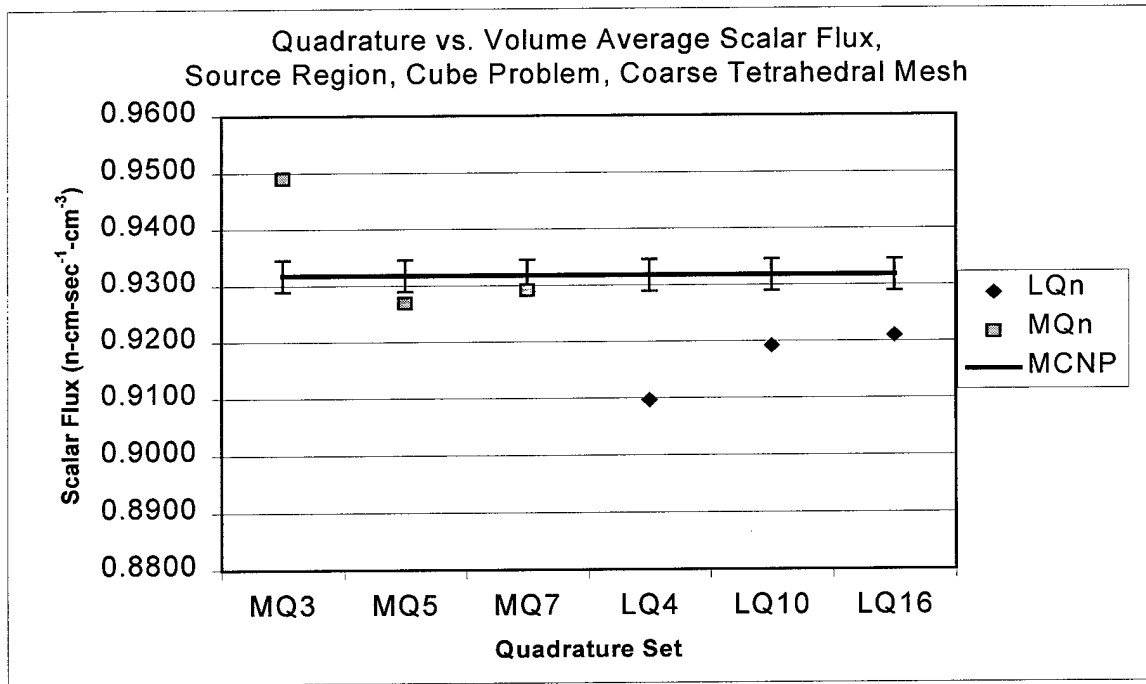


Figure IV-12: Volume Average Scalar Flux, Source Region, Cube Problem, Coarse Tetrahedral Mesh

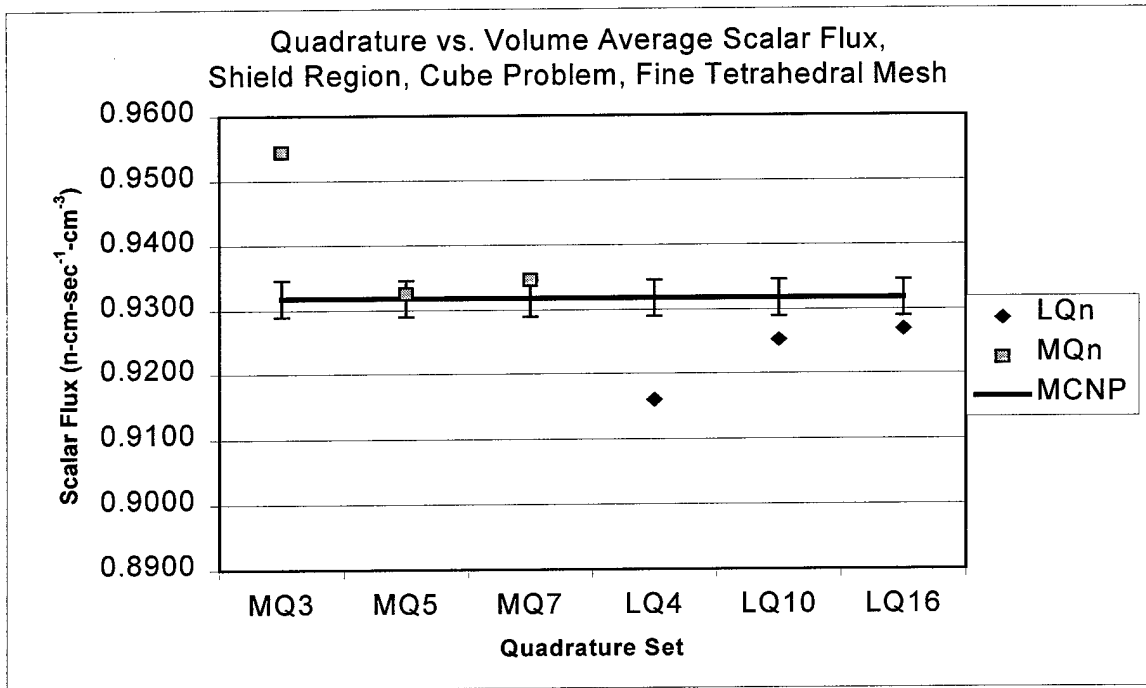


Figure IV-13: Volume Average Scalar Flux, Source Region, Fine Cube

Table IV-4 : Volume Average Scalar Flux and Relative Error, Cube Problem, Coarse Tetrahedral Mesh

Quadrature	Region	Volume Average Scalar Flux	MCNP Benchmark +/- .07%	Relative Error
MQ ₃	Source	0.9490771	0.93175	0.018596
	Shield	0.1635121	0.16466	0.0069711
MQ ₅	Source	0.9269118	0.93175	0.0051926
	Shield	0.1661212	0.16466	0.0088739
MQ ₇	Source	0.9291961	0.93175	0.0027409
	Shield	0.1658497	0.16466	0.0072253
LQ ₄	Source	0.9096752	0.93175	0.023692
	Shield	0.1684340	0.16466	0.022920
LQ ₁₀	Source	0.9191761	0.93175	0.013495
	Shield	0.1670303	0.16466	0.014395
LQ ₁₆	Source	0.9209707	0.93175	0.011569
	Shield	0.1668003	0.16466	0.012998

Table IV-5: Volume Average Scalar Flux, Fine Mesh

Quadrature	Region	Volume Average Scalar Flux	MCNP Benchmark +/- .07%	Relative Error
MQ ₃	Source	0.9544397	0.93175	0.024352
	Shield	0.1629156	0.16466	0.010594
MQ ₅	Source	0.9324943	0.93175	0.00079882
	Shield	0.1646805	0.16466	0.00012450
MQ ₇	Source	0.9346356	0.93175	0.0030970
	Shield	0.1645381	0.16466	0.00074031
LQ ₄	Source	0.9160339	0.93175	0.016867
	Shield	0.1663769	0.16466	0.010427
LQ ₁₀	Source	0.9252458	0.93175	0.0069806
	Shield	0.1652950	0.16466	0.0038564
LQ ₁₆	Source	0.9269132	0.93175	0.0051911
	Shield	0.1652210	0.16466	0.0034068

The MQ_n quadrature set performed better than the LQ_n quadrature set for the volume average data in all but the MQ₃ case on the fine mesh.

Computational efficiency was measured as the user time on the IBM SP taken to solve the problem. Table IV-6 shows the user time for each quadrature and each mesh. Recall the convergence tolerance for all problems was 10⁻⁶.

Table IV-6 :User Time in Seconds Taken to Solve the Cube in Cube Problem

Quadrature	Coarse Mesh (sec)	Iterations to Convergence	Fine Mesh (sec)	Iterations to Convergence
MQ ₃	9.51	20	96.75	20
MQ ₅	18.43	19	187.55	20
MQ ₇	26.73	19	274.3	20
LQ ₄	9.58	19	92.77	20
LQ ₁₀	48.15	19	459.17	20
LQ ₁₆	116.75	19	1100.61	20

For these quadratures to be of value, they must provide increased computational efficiency while maintaining comparable error, or they must provide increased accuracy in comparable time. Figures IV-14 through 17 show plots of user time versus the absolute value of relative error for the surface average scalar flux and net current through the surface. Data points nearer to the origin represent better performance. For these surface averaged values the LQ_n quadrature sets perform better on this problem except for the current through the surface on the fine mesh, where the MQ_5 and MQ_7 quadratures perform well. Figures IV-18 and 19 show the volume average scalar flux versus relative error. The MQ_n quadrature sets have consistently better performance, providing less error for the computation cost in all cases except for the MQ_3 on the fine mesh. These plots clearly show the savings in computational costs while maintaining accurate transport results.

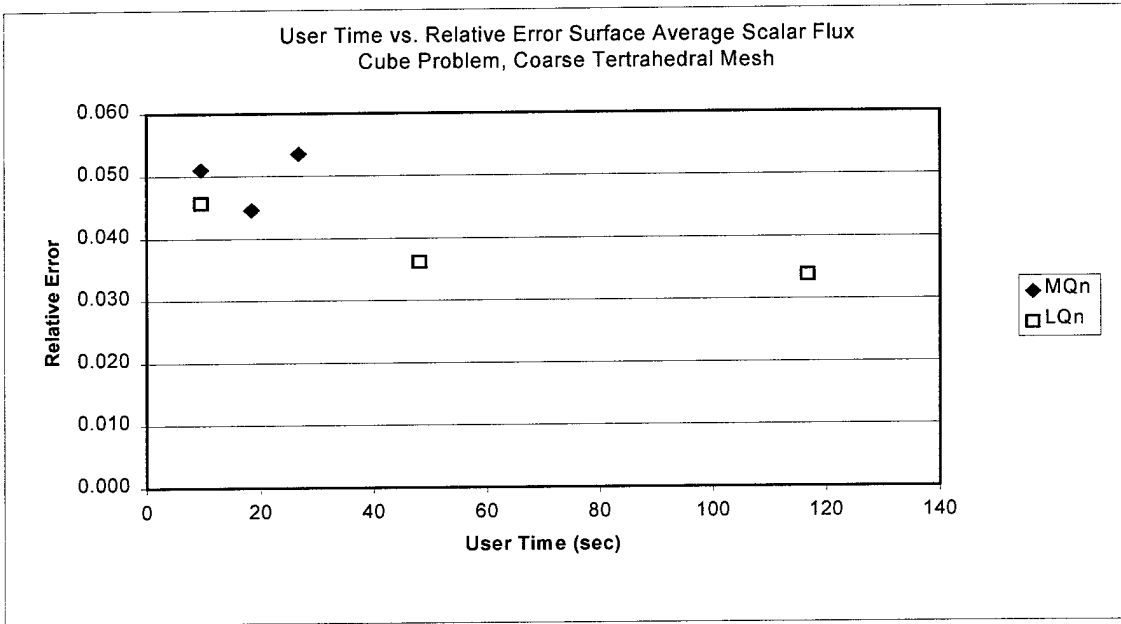


Figure IV-14: Computational Efficiency, Surface Flux, Cube Problem, Coarse Tetrahedral Mesh

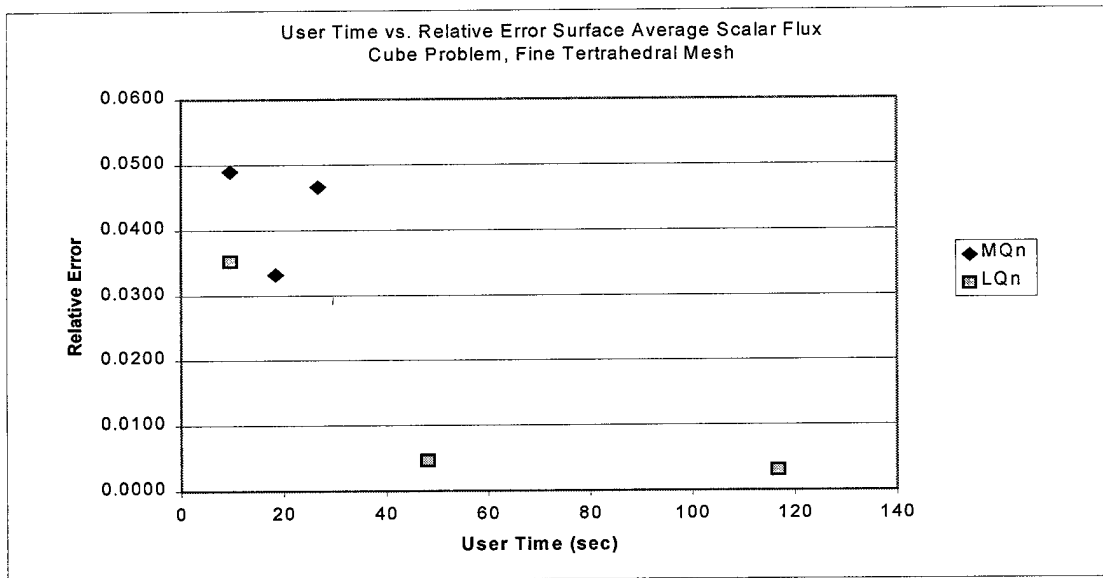


Figure IV-15: Computational Efficiency, Surface Flux, Cube Problem, Fine Tetrahedral Mesh

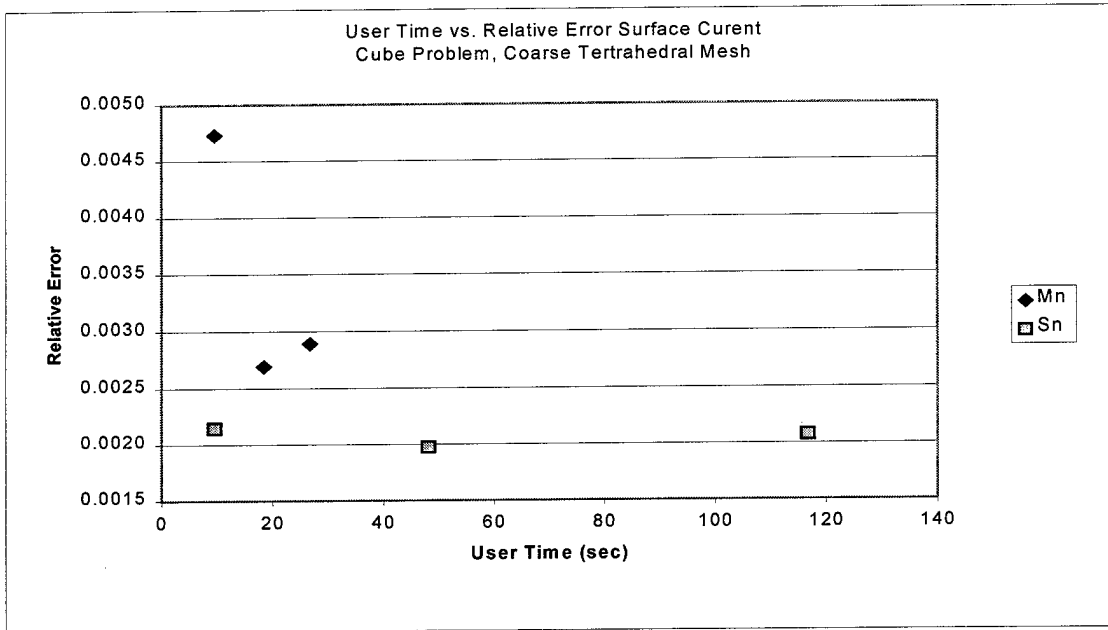


Figure IV-16: Computational Efficiency, Surface Current, Cube Problem Coarse Tetrahedral Mesh

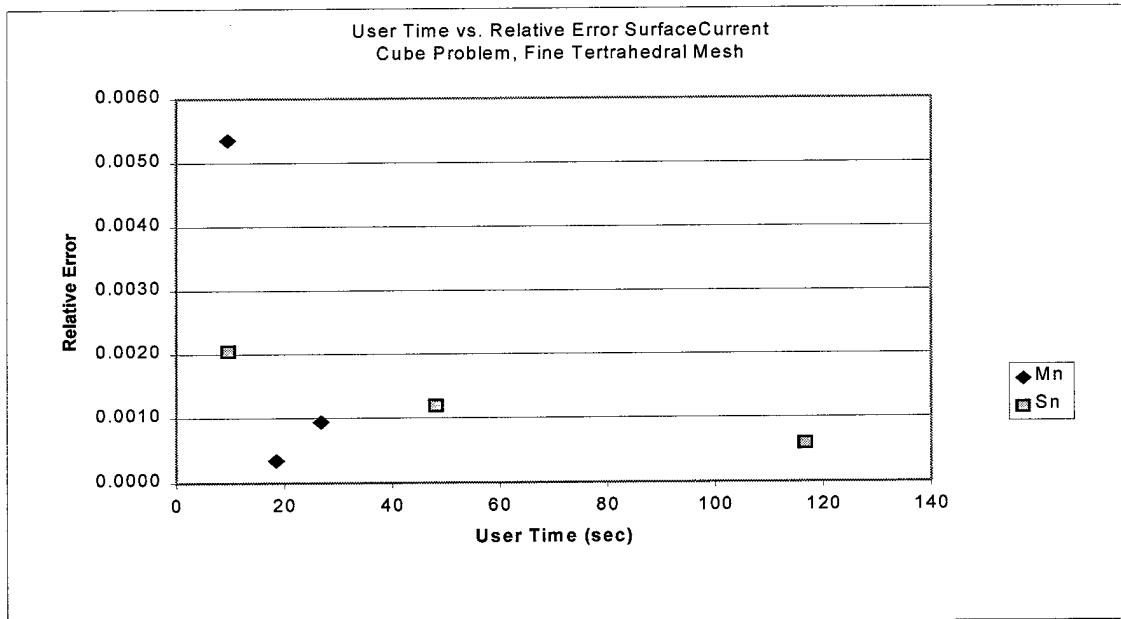


Figure IV-17: Computational Efficiency, Surface Current, Cube Problem Fine Tetrahedral Mesh

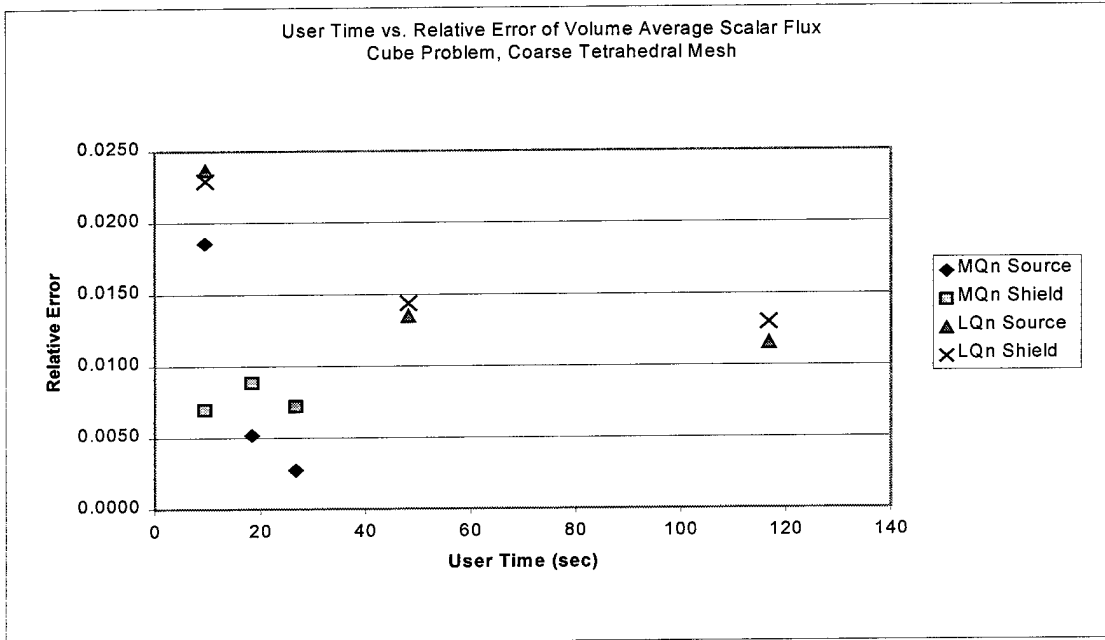


Figure IV-18: Computational Efficiency, Volume Average Scalar Flux, Cube Problem Coarse Tetrahedral Mesh

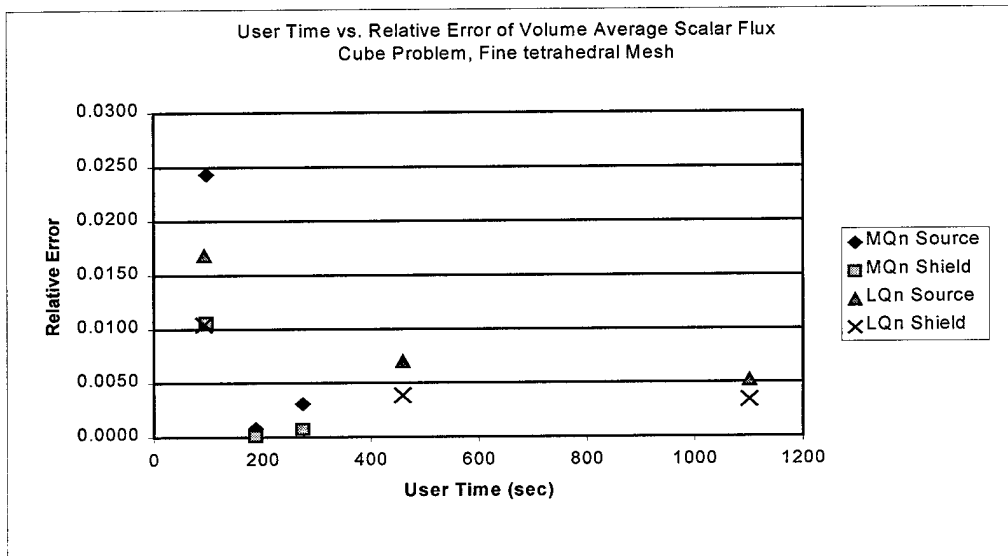


Figure IV-19: Computational Efficiency, Volume Average Scalar Flux, Cube Problem Fine Tetrahedral Mesh

Parallelepiped Mesh

This problem was run with one mesh. The mesh is 16x16x16 cells in the principal octant. Reflective boundaries were used on three sides. This results in a 2x2x2 cm cube which is one corner of the test problem containing one eighth of the volume. The solution to the remaining seven eighths of the problem is assumed to be the same by symmetry. The source is normalized to .125 over this source volume which is one eighth of a complete source cube. Data for the parallelepiped mesh is shown in Table VI-7. The volumes of the regions are easily conserved with this meshing method. The number in parenthesis in the volume column is for an equivalent volume if reflective boundaries had not been used.

Table IV-7 : Parallelepiped Mesh Data

Total Cells	Cells in Source Region	Net Volume of Source Region	Optical Thickness
4096	512	1.0 (8.0)	.09375

Figure IV-20 shows a contour plot of the cell center scalar flux for the base layer of cells ($Z = .125$ cm plane) using each quadrature set. The flux shows a significant dependency on quadrature for this mesh. The MQ₃ case shows a very pronounced ray effect. The higher order quadrature sets show better behavior.

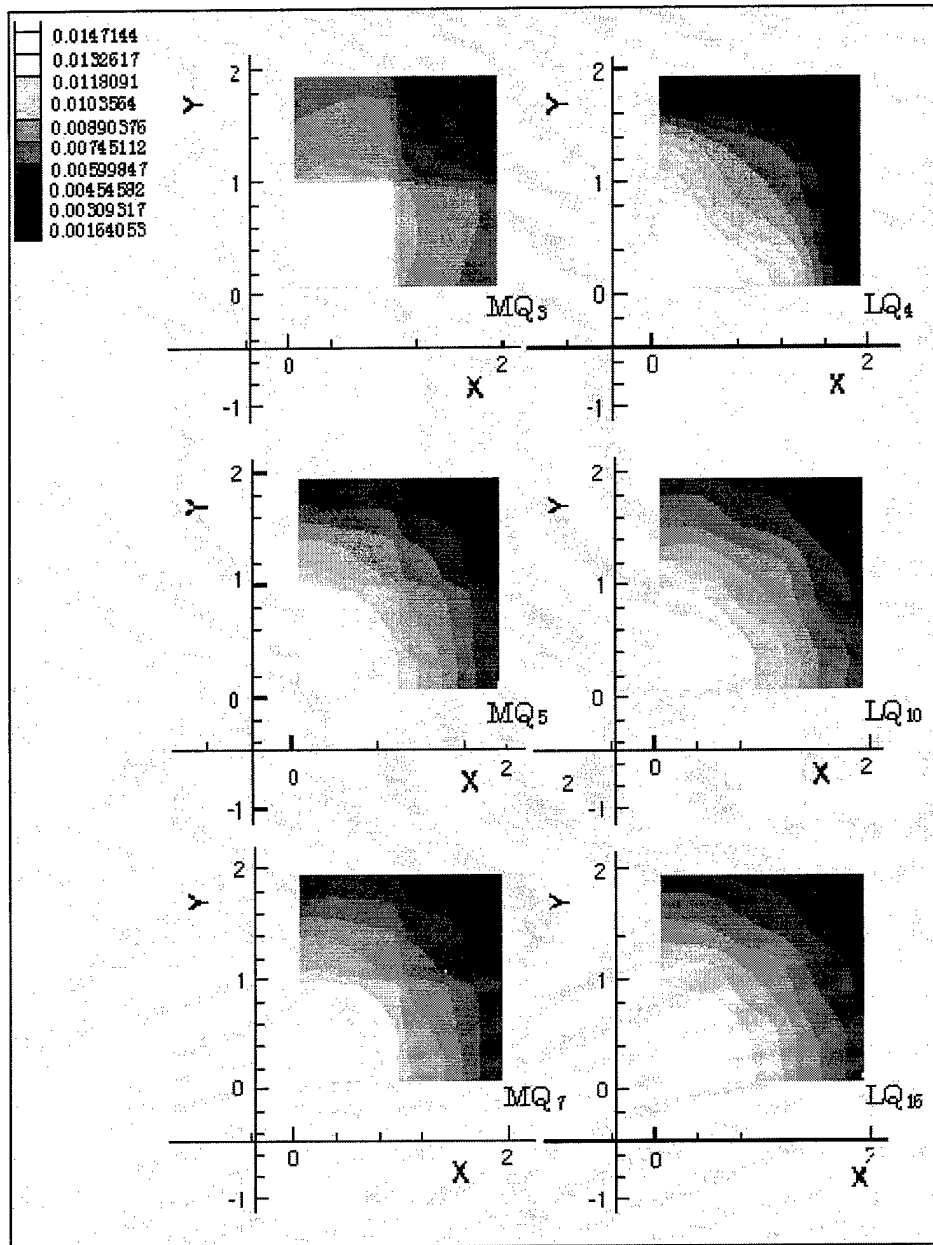


Figure 20: Contour Plot of Scalar Flux in the $Z = .125\text{cm}$ Plane, Cube Problem, Parallelepiped Mesh

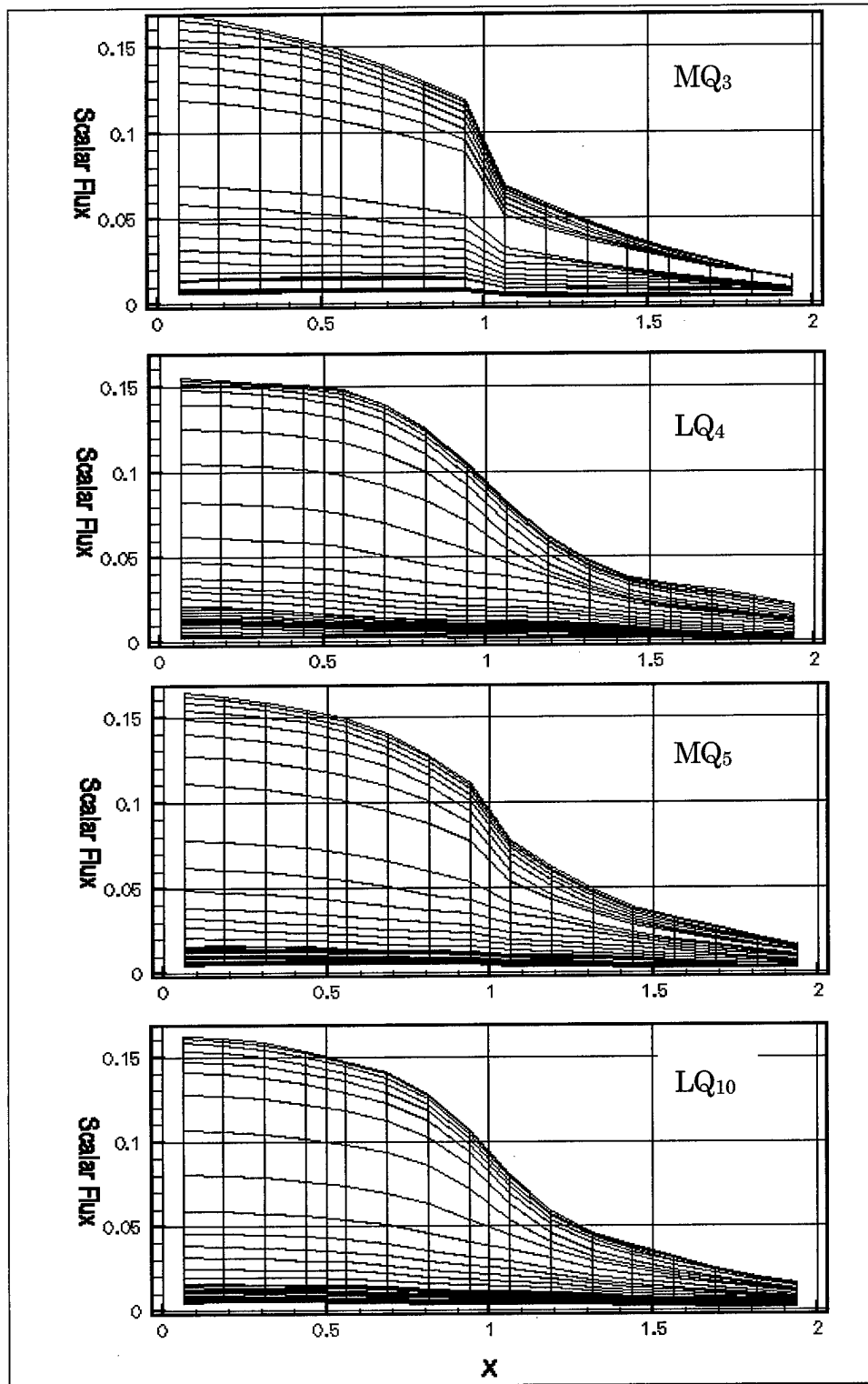


Figure IV-21: Scalar Flux at Cube Surface

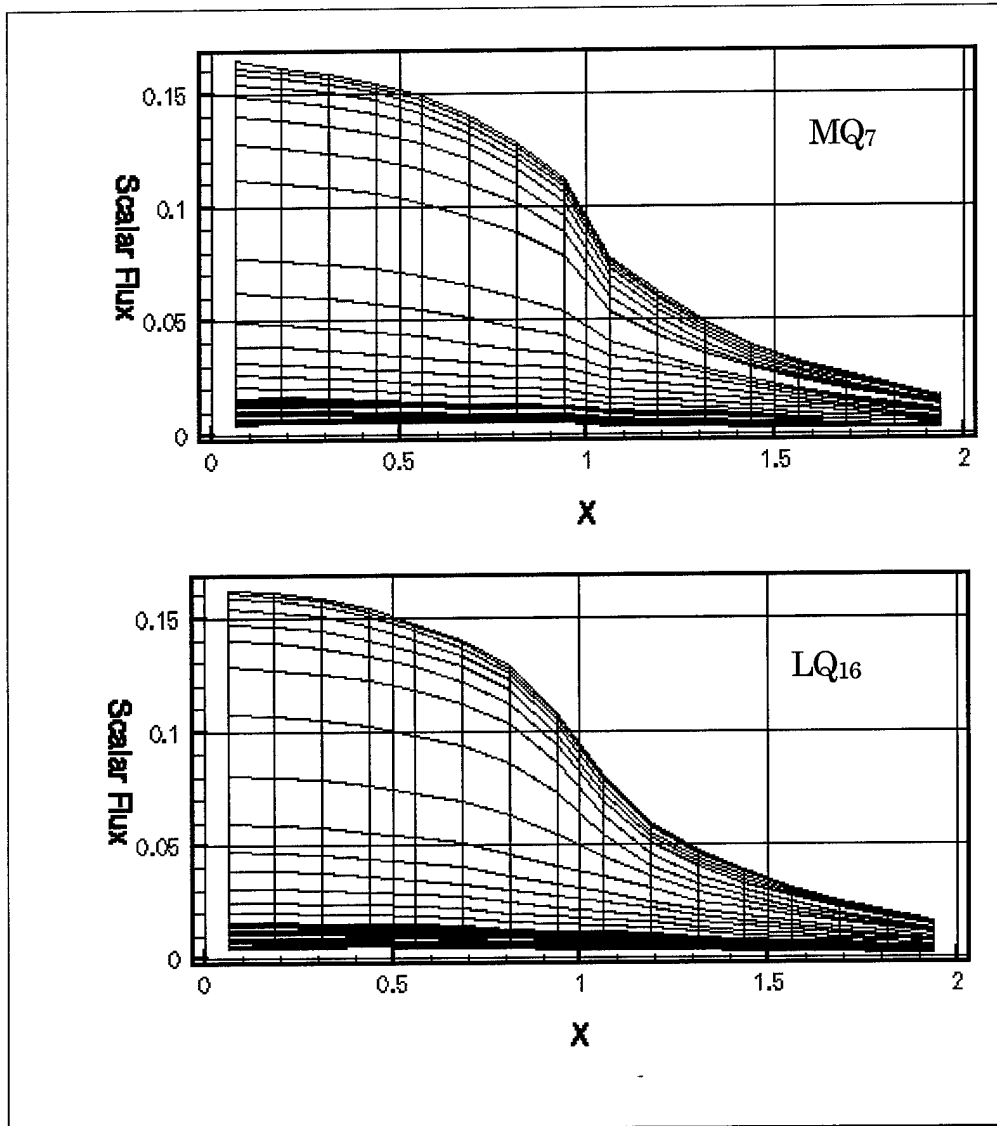


Figure IV-21 (Continued): Scalar Flux at Cube Surface

Figure IV-21 shows a comparison of the flux at the top layer of cells ($Z = 1.875$ plane). Each successively lower line represent a step of one cell width in the positive y direction starting at $y = .125$. The lower order MQ_n quadratures display a substantial drop in flux when crossing from the source to shield region. This is still evident in the MQ_7 quadrature but is not as pronounced. This is evidently a ray effect due to the ordinates perpendicular to the axes. Figure IV-22 shows the volume average scalar flux for each quadrature compared with the MCNP benchmark. All quadrature sets performed well, with error less than one percent except for LQ_4 . MQ_5 and LQ_{16} performed very well, both with error less than 0.1 percent. The net current through the surface for each quadrature and the MCNP solution are plotted in Figure IV-23. This data is summarized in Table IV-8 with the relative error for each quadrature.

Table IV-8: Parallelepiped Cube Data Summary

Quadrature	Flux	ϵ	Net Current	ϵ
MQ3	0.2622893	0.0066899	0.059428	0.489260
MQ5	0.2607804	0.0008985	0.059805	0.498714
MQ7	0.2609637	0.0016024	0.059759	0.497565
LQ4	0.2558341	0.0180855	0.061041	0.529702
LQ10	0.2601124	0.0016650	0.059972	0.502898
LQ16	0.2604749	0.0002739	0.059881	0.500627

Figures IV-24 and 25 shows the relative error vs. computation time. The lines were added for clarity connecting the MQ_n and LQ_n quadratures with separate lines by increasing order. When using the THREEDANT code

with these quadratures the convergence time is not as direct a function of the number of angles in the quadrature set as it is when using TETRAN. This is primarily due to the added dummy angles required. For Example, both the MQ₃ and MQ₅ quadrature used $isn = 8$, requiring the input of 10 ordinates. For the MQ₃ case, three of the ordinates were dummy values with zero weights but for the MQ₅ all ten ordinates are used. The MQ₇ quadrature used $isn = 12$, requiring 21 ordinates, five of which were dummy values. In addition, since THREEDANT uses quadrature sets input by octant, redundant calculations are made for the case A, B, and C ordinates that lie on octant boundaries. Despite this, the MQ_n quadratures still seem to have better computational efficiency when examining integral values. Table IV-9 shows the computation times for each quadrature sets.

Table IV-9 : Time by Quadrature, Parallelepiped Mesh, Cube Probelem

Quadrature	Time (sec)	Iterations to Convergence
MQ3	3.6	10
MQ5	3.03	8
MQ7	11.49	8
LQ4	1.91	9
LQ10	5.56	8
LQ16	24.39	8

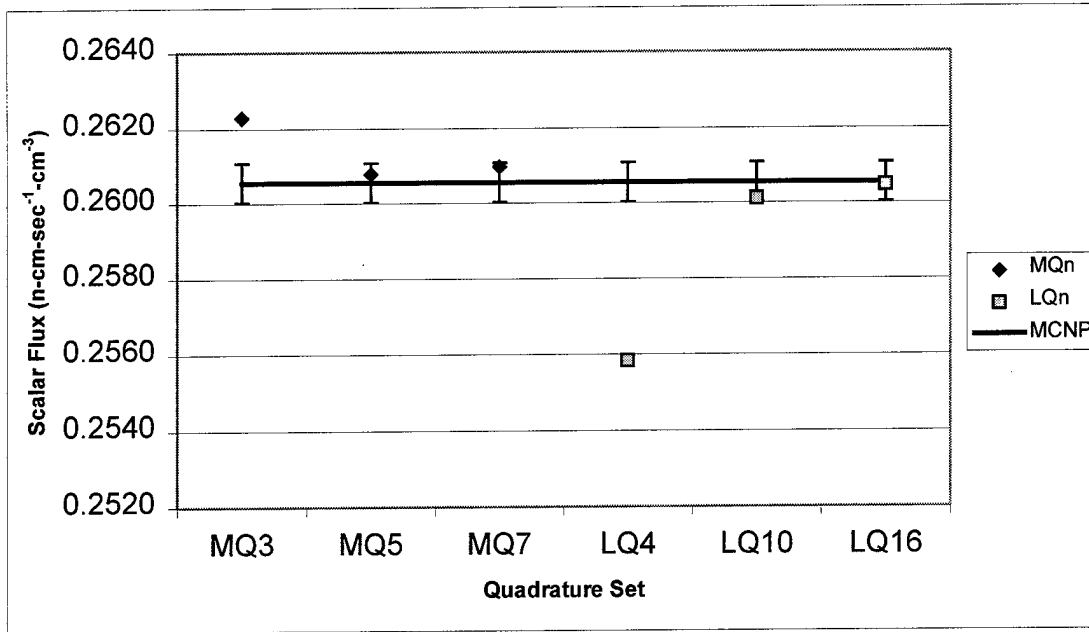


Figure IV-22 :Volume Average Scalar Flux, Cube Problem, Parallelepiped Mesh

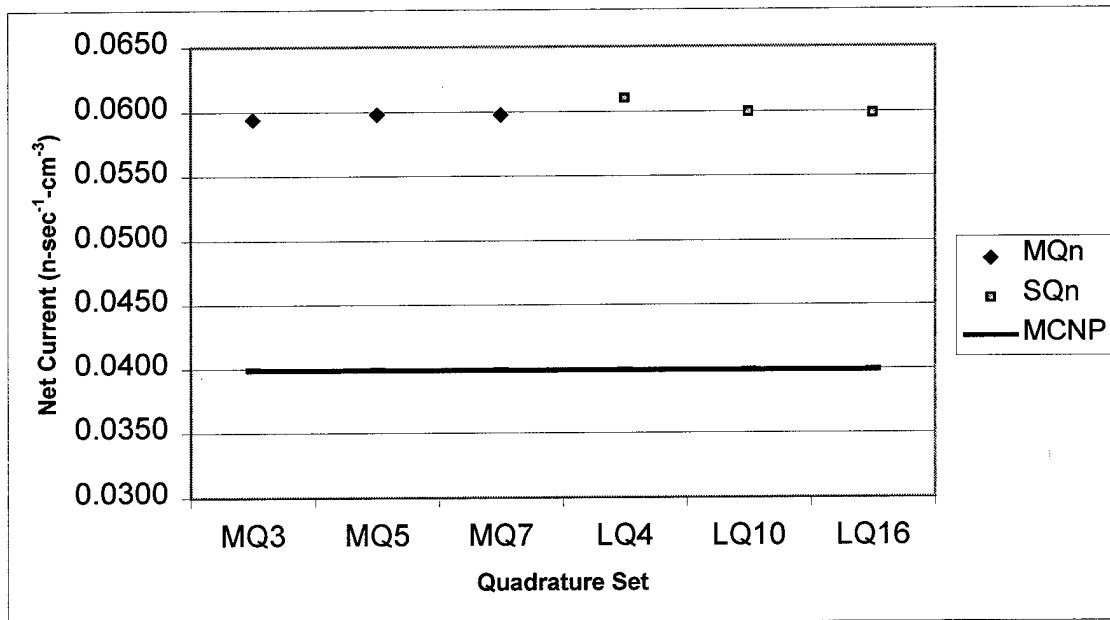


Figure IV-23: Net Current through the Surface, Cube Problem, Parallelepiped Mesh

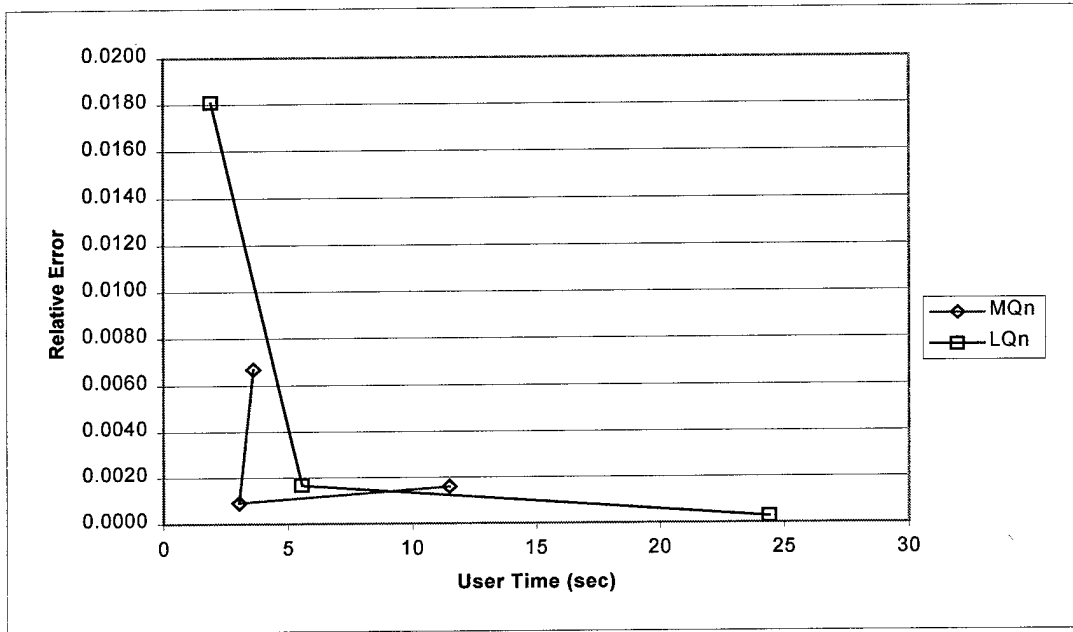


Figure IV-24: User Time vs. Relative Error in Volume Average Scalar Flux, Cube Problem, Parallelepiped Mesh

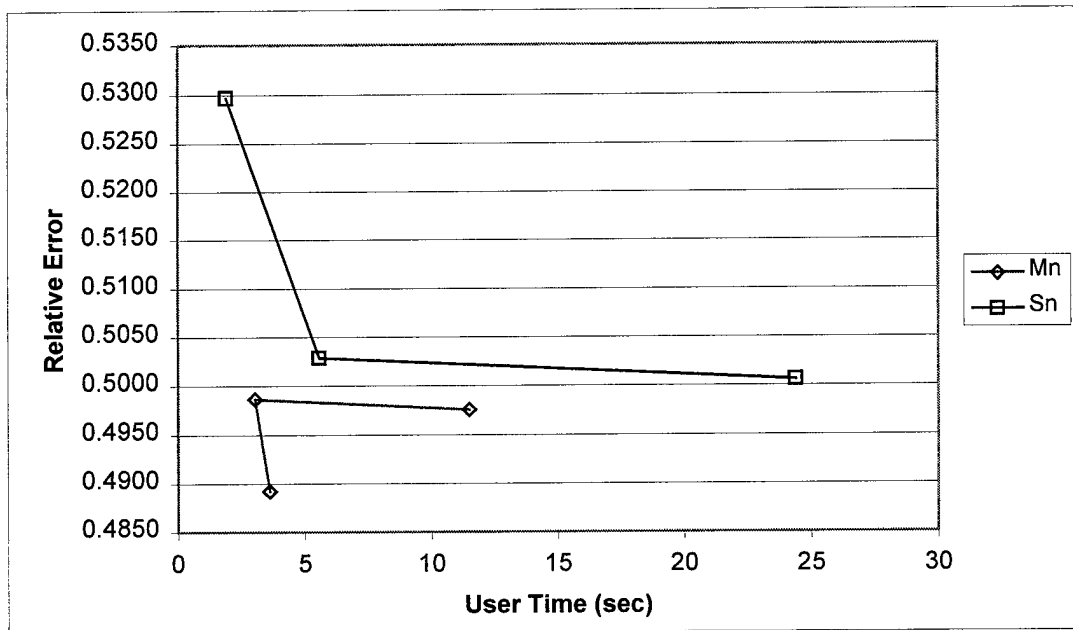


Figure IV-25: User Time vs. Relative Error in Net Current through the Surface, Cube Problem, Parallelepiped Mesh

Test Problem Two – Spherical Source in Spherical Shield

The second test problem is a 3 cm radius sphere with vacuum boundaries and a uniformly embedded isotropically emitting source of strength $1.0 \text{ cm}^{-3} \text{ sec}^{-1}$. The source is constrained to a 1.5 cm radius sphere in the center. The nuclear data is the same as the previous problem. The same computer systems and convergence tolerance that were used in problem one were used for problem two.

Tetrahedral Mesh

This problem was run with three levels of mesh refinement. The structure for each mesh is shown in Figure IV-26. Table IV-10 gives the tetrahedral mesh information for test problem two. The volumes shown are the sums of the tetrahedron volumes in each region. This is compared with 14.14 and 98.96 cm^{-3} for an actual spherical volume. For curved geometry the

Table IV-10 : Tetrahedral Mesh Data

Mesh	Total Tetrahedra	Cells in Source Region	Mesh Volume in Source Region (cm ³)	Mesh Volume in Shield Region (cm ³)	Average Optical Thickness
Coarse	211	14	5.885	82.24	1.1317
Medium	896	152	11.69	93.48	0.84944
Fine	6632	2033	13.74	96.46	0.40539

tetrahedral mesh does not conserve volume very well until a very fine mesh is used. This is a fault in the design of mesh generators. They are usually used

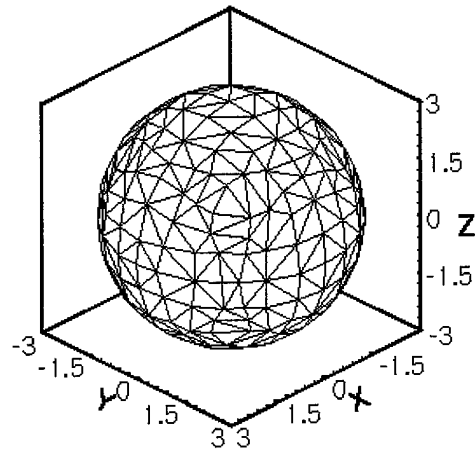
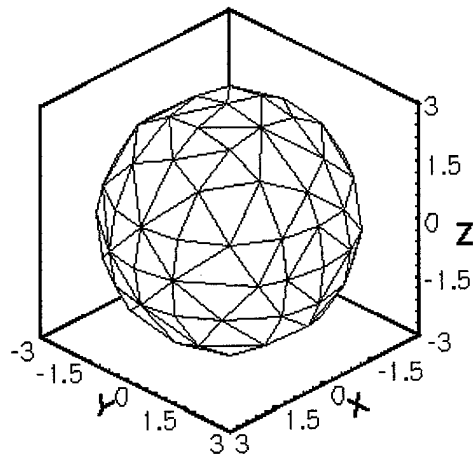
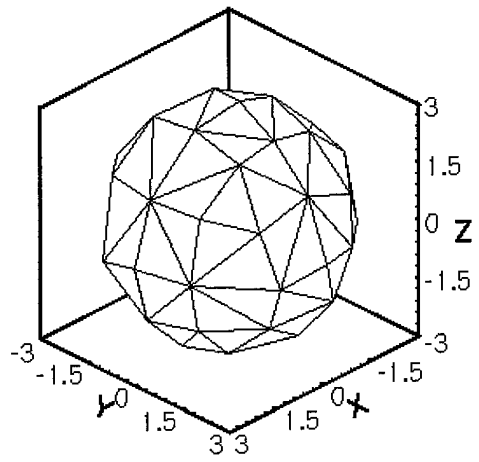


Figure IV-26: Tetrahedral Mesh Structures Used in Problem 2

for finite elements mechanics calculations where volume is not an issue. Figure IV-27 shows the source region for the coarsest mesh. This figure shows how difficult it is to mesh curved regions. The accuracy of each quadrature will again be examined first.

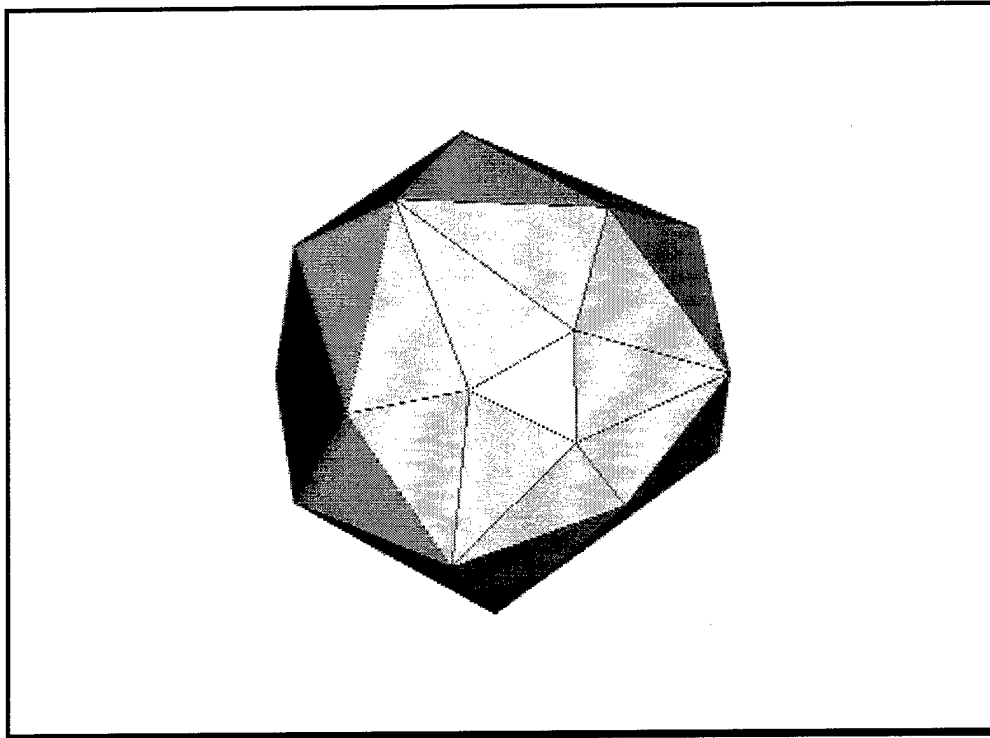


Figure IV-27: Source Region for Sphere Problem, Coarse Mesh

Figure IV-28-30 shows contour plots of the surface average scalar flux at the surface layer of tetrahedra for each mesh and various quadrature sets. Due to the similarity of the plots, not all of the quadratures are presented. The same method of node averaging was used to present this data. These contour plots also show little dependency on quadrature. To better show the quadrature dependence, Figure IV-31 shows contour plots of the fine sphere using MQ₃ and LQ₁₆ quadrature sets, looking from the $-x$, x , and z directions

respectively. The orientation can be seen from the standard arrowhead \odot , signifying the positive direction is out of the page, or tail \otimes , signifying the positive direction is into the page, notation at the origin of each plot. Also from this figure, an unusual asymmetry can be seen. There is a biasing in the positive x direction. This appears to be due to a problem in the TETRAN code that is currently under investigation. The degree of variability in the surface average scalar flux can be seen in Figure IV-32. This figure shows the TETRAN calculated surface flux arbitrarily ordered by magnitude for the medium mesh. Due to the symmetry of the problem the actual flux should be uniform over the surface. The shape of this curve remains the same as the mesh is made more or less refined, however the magnitude of the peak increases to about .11 for the coarse mesh and decreases to about .065 for the fine mesh. These plots are not shown. Figures IV-33 shows the net surface current in the same manner as the scalar flux. This data is ordered by the magnitude of the scalar flux to allow comparison with the previous figure. The current and scalar fluxes have similar trends but do vary independently. Only the MQ₇ and LQ₁₆ data is presented here, the other quadratures have similar behavior.

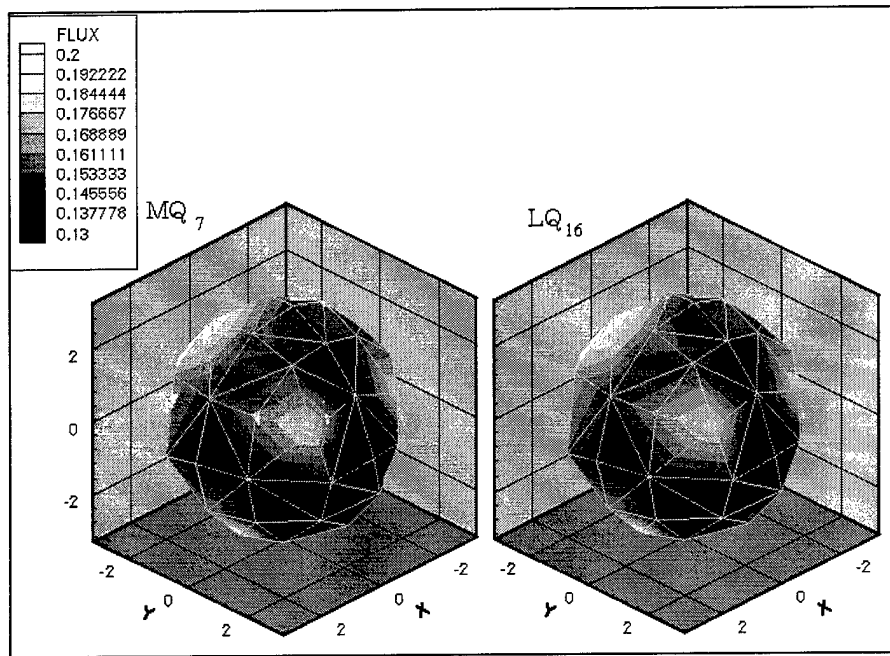


Figure IV-28: Contour Plot of Surface Average Scalar Flux, Sphere Problem,
Coarse Tetrahedral Mesh

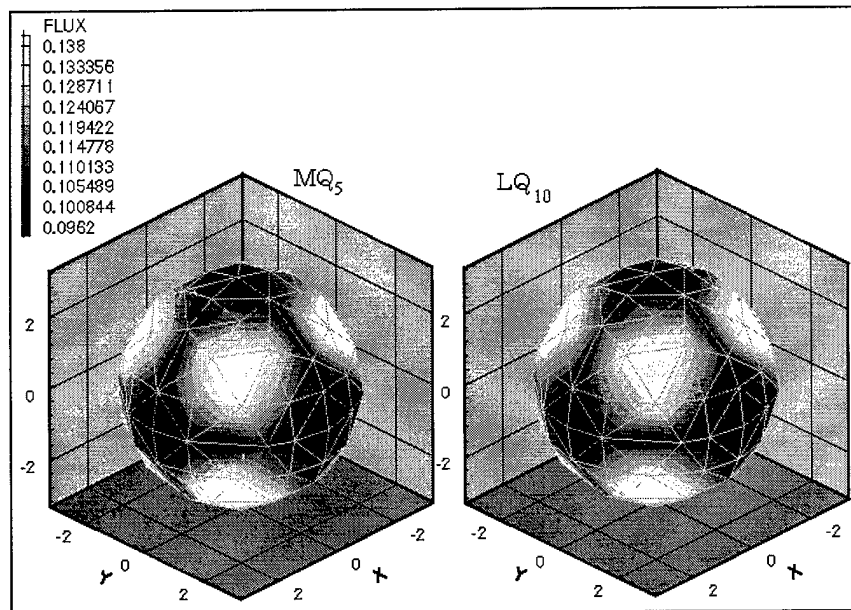


Figure IV-29: Contour Plot of Surface Average Scalar Flux, Sphere Problem,
Medium Tetrahedral Mesh

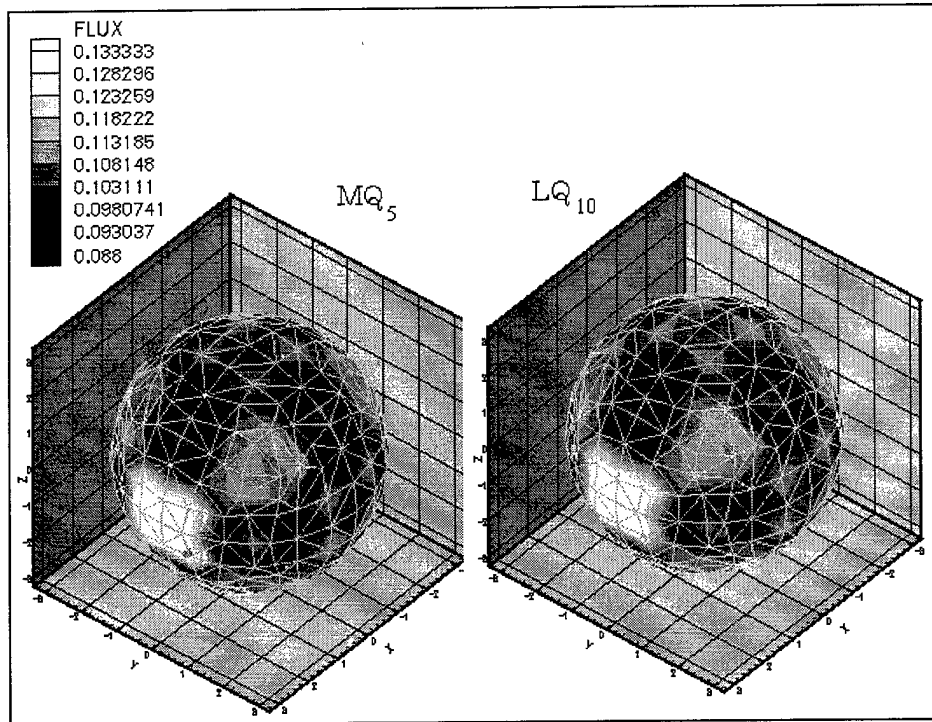


Figure IV-30: Contour Plot of Surface Average Scalar Flux, Sphere Problem,
Fine Tetrahedral Mesh

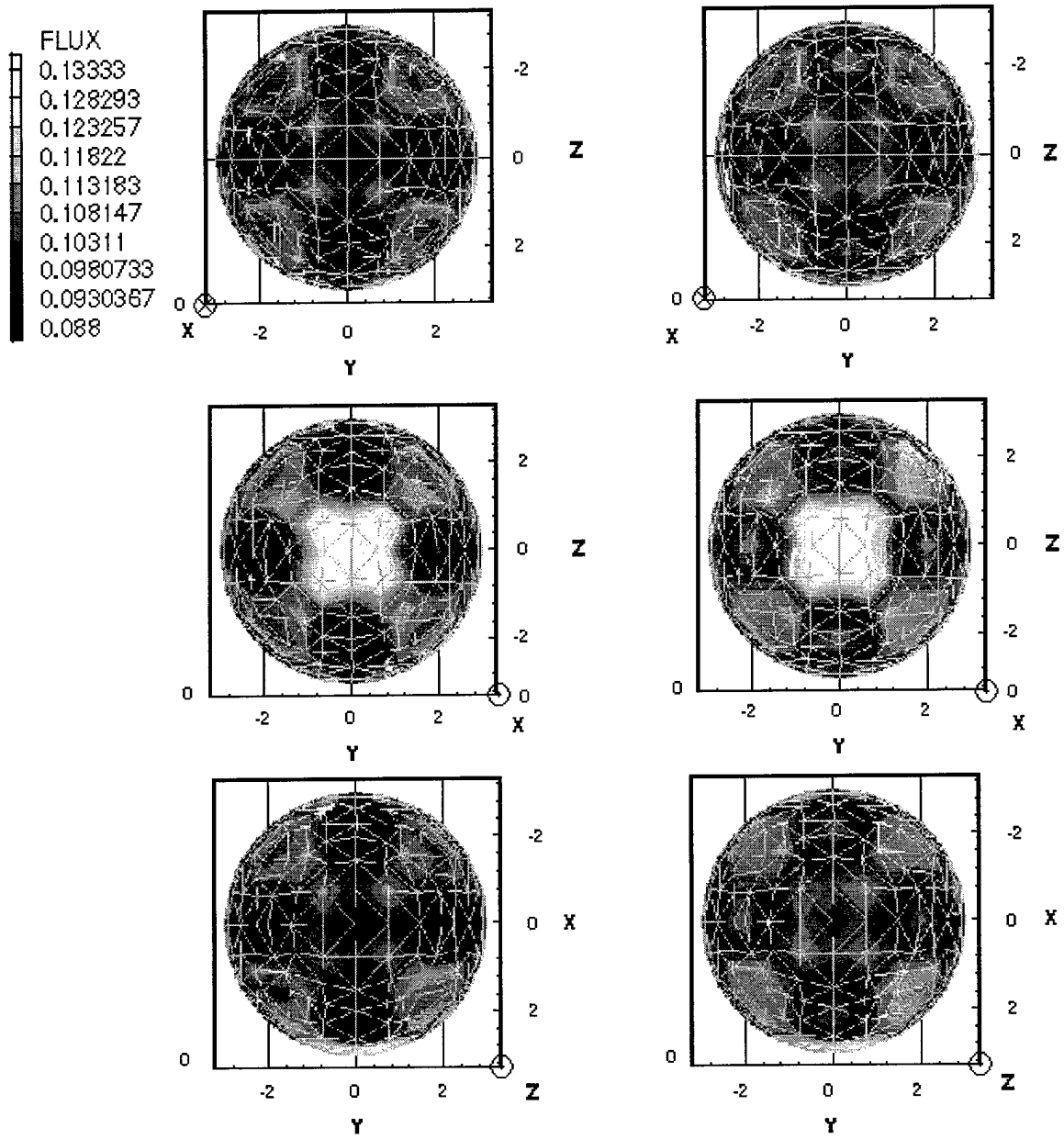


Figure IV-31: Contour Plot of Surface Flux, MQ₅ and LQ₁₆, Axial View of Fine Sphere

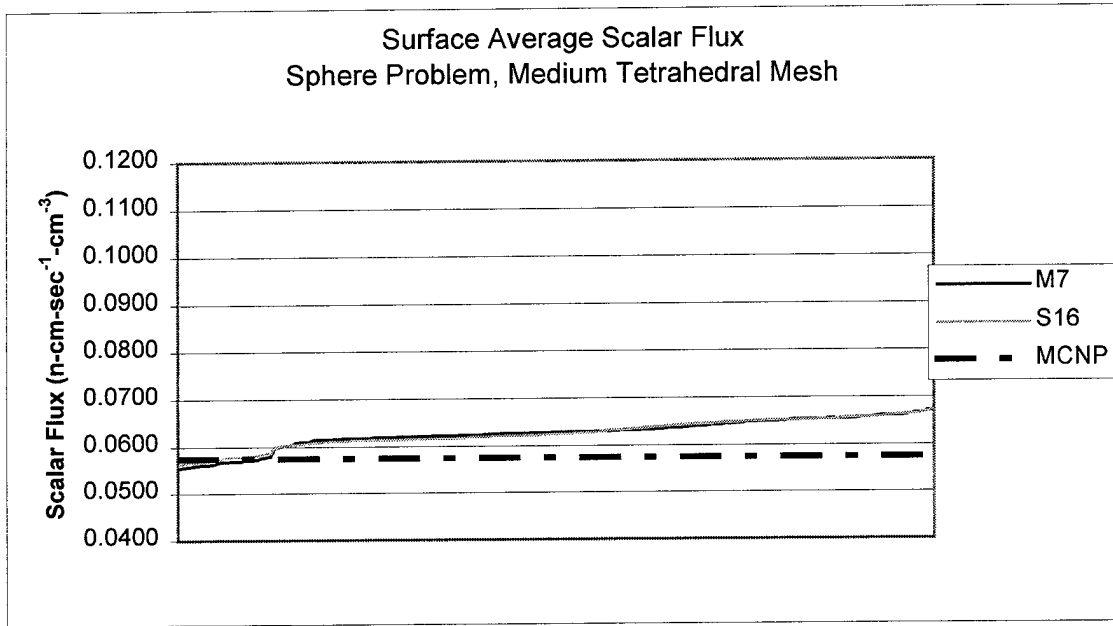


Figure IV-32: Variability of Scalar Flux at the Surface of Sphere Problem, Medium Tetrahedral Mesh

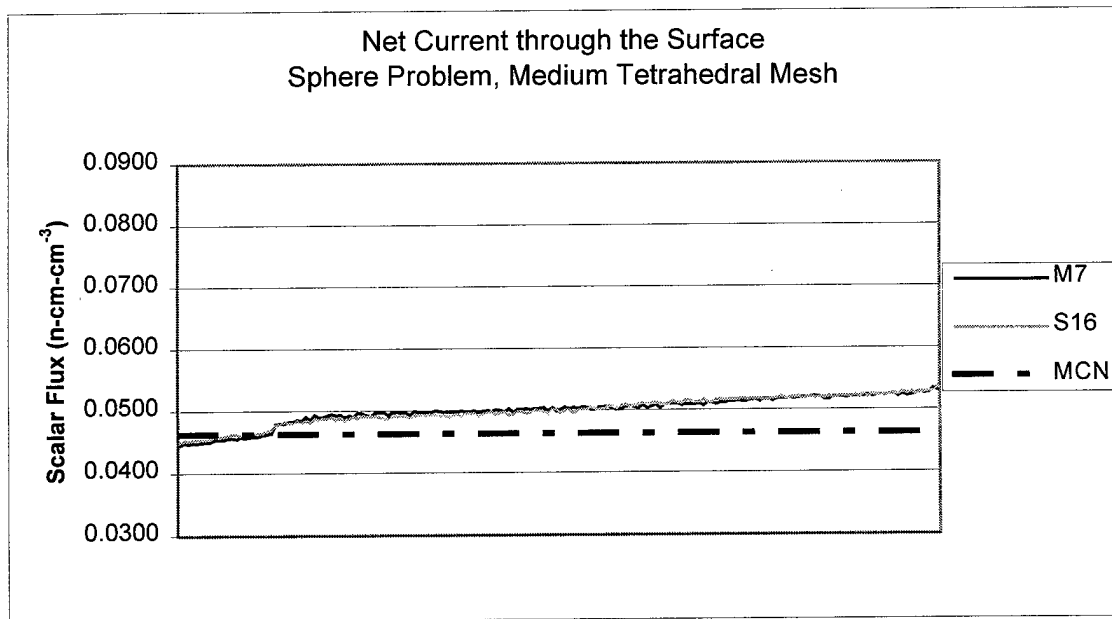


Figure IV-33: Variability in Net Current through the Surface, Sphere Problem, Medium Tetrahedral Mesh

The surface average scalar flux and net current through the surface show little dependence on quadrature. Figure IV-34 shows this for the scalar flux on the coarse sphere. The small differences in accuracy can be seen in a plot of relative error versus quadrature as shown in Figures IV-35-37 for the scalar flux. Plots of the net current are similar and are not presented. Regardless of mesh, the quadratures have comparable performance in approximating the surface values. The relative error for this geometry is much larger than for the cube problem above. This is primarily attributed to the poor job the mesh does in matching the curved surfaces. Though the MQ_n sets do appear to have less error for the surface flux on the coarser two meshes, the difference is small and, as can be seen from Figure IV-34, has little significance. This information is summarized in Tables VI-11-13.

Table IV-11: Surface Average Scalar Flux and Net Current, Sphere Problem, Coarse Tetrahedral Mesh

Quadrature	Scalar Flux	ϵ	Net Current	ϵ
MQ_3	0.072776076	0.2663	0.05724275	0.2363
MQ_5	0.072876460	0.2681	0.05722983	0.2360
MQ_7	0.072896331	0.2684	0.05722878	0.2360
LQ_4	0.072993465	0.2701	0.05720223	0.2354
LQ_{10}	0.073059529	0.2712	0.05723194	0.2360
LQ_{16}	0.073047543	0.2710	0.05723134	0.2360
MCNP	0.05747	0.003	0.04630	0.003

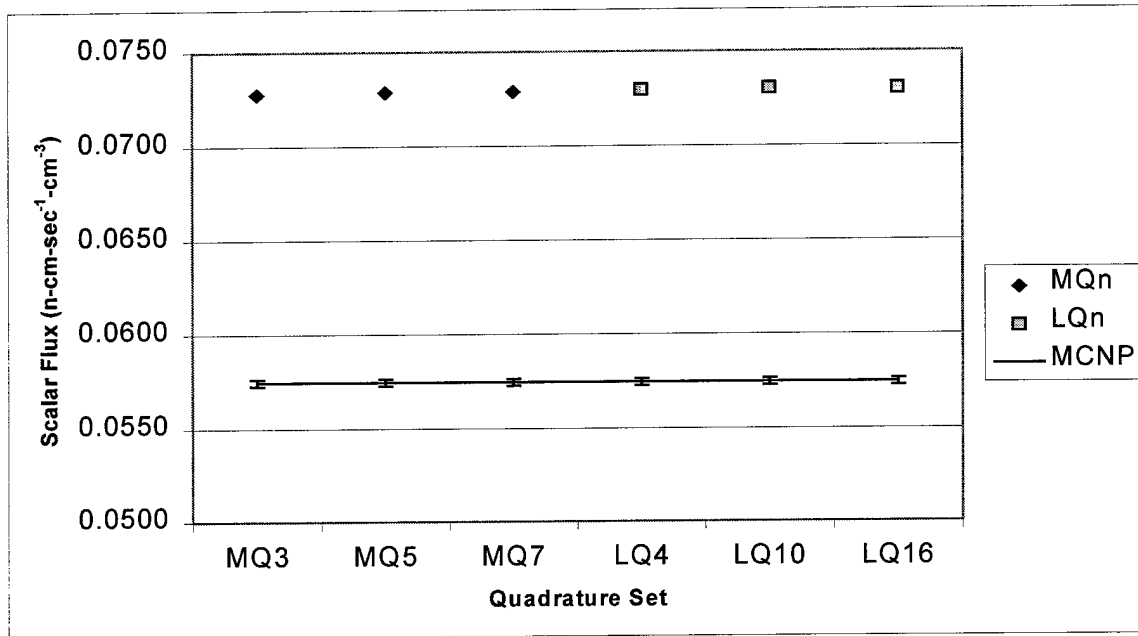


Figure IV-34: Surface Average Scalar Flux, Sphere Problem, Coarse Tetrahedral Mesh

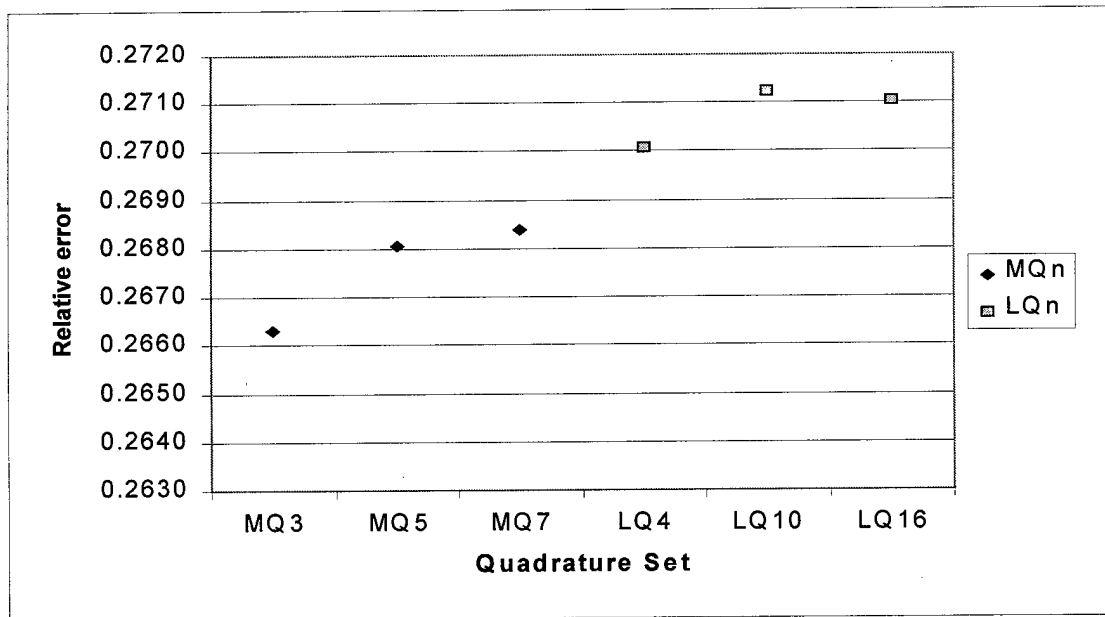


Figure IV-35: Relative Error in Surface Average Scalar Flux, Sphere Problem, Coarse Tetrahedral Mesh

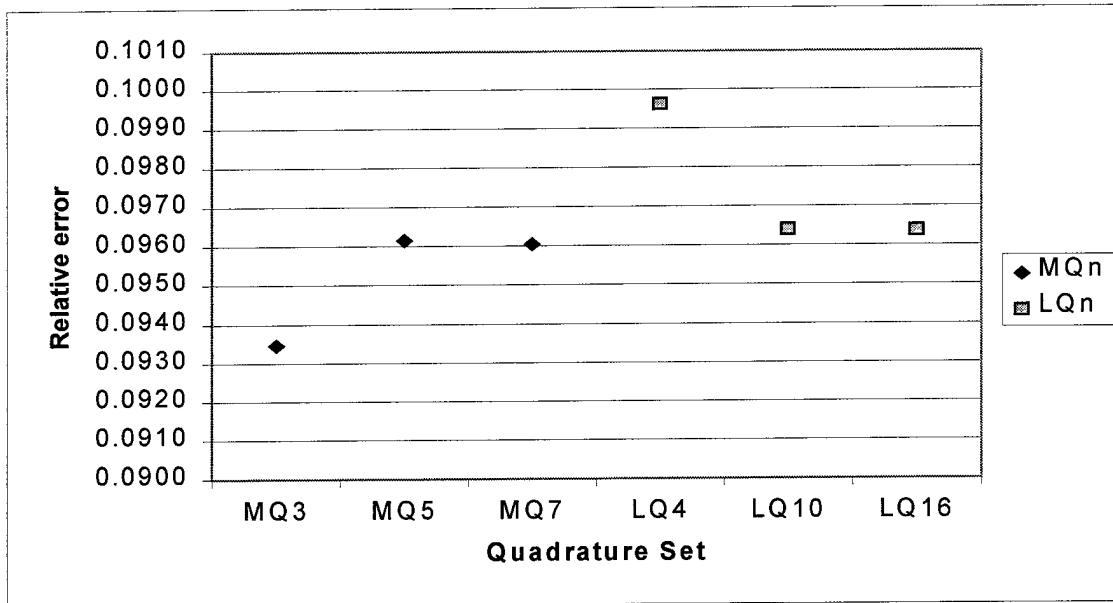


Figure IV-36: Relative Error in Surface Average Scalar Flux, Sphere Problem, Medium Tetrahedral Mesh

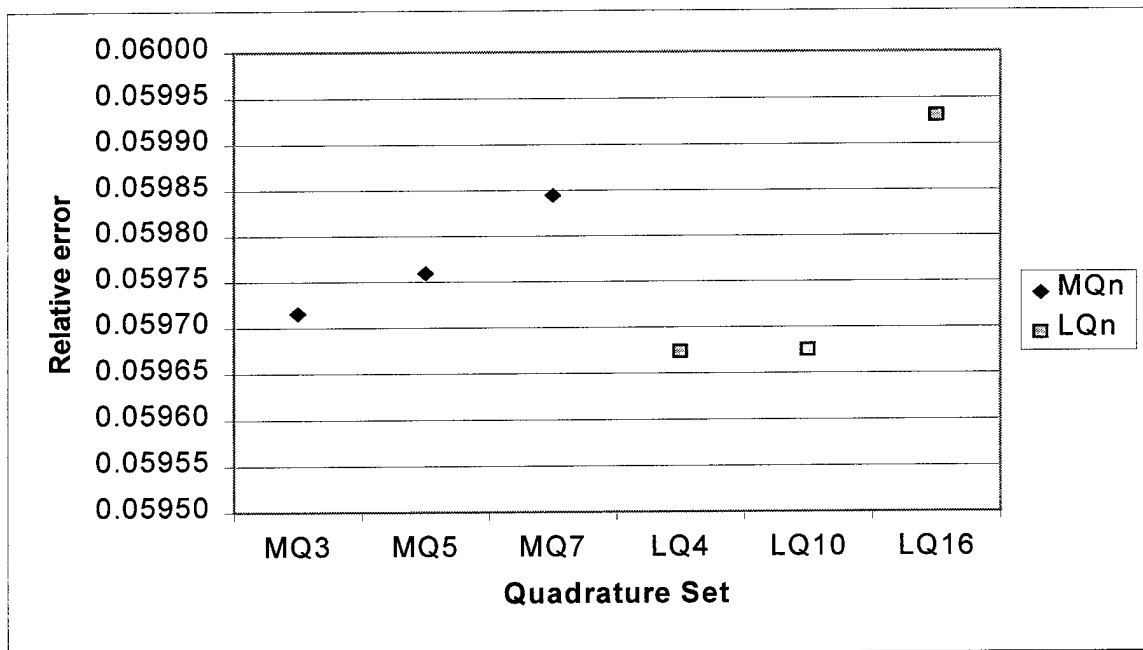


Figure IV-37: Relative Error in Surface Average Scalar Flux, Sphere Problem, Fine Tetrahedral Mesh

Table IV-12: Surface Average Scalar Flux and Net Current, Sphere Problem,
Medium Tetrahedral Mesh

Quadrature	Scalar Flux	ϵ	Net Current	ϵ
MQ ₃	0.062842334	0.0935	0.05024186	0.0851
MQ ₅	0.062996823	0.0961	0.05027019	0.0857
MQ ₇	0.062990863	0.0960	0.05026612	0.0856
LQ ₄	0.063196562	0.0996	0.05028158	0.0859
LQ ₁₀	0.063011997	0.0964	0.05028019	0.0859
LQ ₁₆	0.063010129	0.0964	0.05027461	0.0858
MCNP	0.05747	0.003	0.04630	0.003

Table IV-13: Surface Average Scalar Flux and Net Current, Sphere Problem,
Fine Tetrahedral Mesh

Quadrature	Scalar Flux	ϵ	Net Current	ϵ
MQ ₃	0.060902901	0.0597	0.04857312	0.0490
MQ ₅	0.060905444	0.0598	0.04857166	0.0490
MQ ₇	0.060910336	0.0598	0.04857333	0.0490
LQ ₄	0.060900515	0.0597	0.04857391	0.0490
LQ ₁₀	0.060900610	0.0597	0.04856642	0.0489
LQ ₁₆	0.060915316	0.0599	0.04856830	0.0489
MCNP	0.05747	0.003	0.04630	0.003

Tables IV-14 and 15 summarize the volume average data. All quadratures show nearly equal performance in calculating the volume average scalar flux

Table IV-14: Volume Average Scalar Flux Data, Coarse Sphere

Quadrature	Region	Volume Average Scalar Flux	MCNP Benchmark +/- .2%	ϵ
MQ ₃	Shield	0.259490998	0.17601	0.47430
	Source	2.073454733	1.29600	0.59989
MQ ₅	Shield	0.260540247	0.17601	0.48026
	Source	2.059669935	1.29600	0.58925
MQ ₇	Shield	0.260516136	0.17601	0.48012
	Source	2.060075531	1.29600	0.58956
LQ ₄	Shield	0.261797736	0.17601	0.48740
	Source	2.043972732	1.29600	0.57714
LQ ₁₀	Shield	0.260675794	0.17601	0.48103
	Source	2.057621449	1.29600	0.58767
LQ ₁₆	Shield	0.26067187	0.17601	0.48101
	Source	2.05772263	1.29600	0.58775

for a given mesh. By examining the errors in the source region shown in Tables IV-15 and 16 an interesting phenomenon can be detected when refining the mesh from the medium to the fine sphere. The error in the source region increases from about one percent up to about nine percent. The expected trend is for error to decrease with this level of mesh refinement. The source of this increase in error is suspected to be the same unresolved problems in the TETRAN code that induced the biasing mentioned earlier. This only seems to become detectable when running fine mesh problems. It is suspected that a very small biasing in the positive x direction that only accumulates significantly for very fine meshes is caused by a tetrahedron splitting algorithm used by TETRAN. The magnitude of this problem does

not appear to vary with quadrature and therefore we can still use this output for relative comparisons between quadrature sets.

Table IV-15: Volume Average Scalar Flux Data, Medium Sphere

Quadrature	Region	Volume Average Scalar Flux	MCNP Benchmark +/- .2%	ϵ
MQ ₃	Shield	0.206680395	0.17601	0.17425
	Source	1.313078744	1.29600	0.01318
MQ ₅	Shield	0.20660516	0.17601	0.17383
	Source	1.312631187	1.29600	0.01283
MQ ₇	Shield	0.206585308	0.17601	0.17371
	Source	1.312932737	1.29600	0.01307
LQ ₄	Shield	0.206521942	0.17601	0.17335
	Source	1.312863629	1.29600	0.01301
LQ ₁₀	Shield	0.20670228	0.17601	0.17438
	Source	1.311474207	1.29600	0.01194
LQ ₁₆	Shield	0.206639441	0.17601	0.17402
	Source	1.312184651	1.29600	0.01249

Table IV-16: Volume Average Scalar Flux Data, Fine Sphere

Quadrature	Region	Volume Average Scalar Flux	MCNP Benchmark +/- .2%	Absolute Relative Error
MQ ₃	Shield	0.19327010	0.17601	0.09806
	Source	1.18027900	1.29600	0.08929
MQ ₅	Shield	0.19331830	0.17601	0.09834
	Source	1.17998870	1.29600	0.08951
MQ ₇	Shield	0.19331458	0.17601	0.09832
	Source	1.17996012	1.29600	0.08954
LQ ₄	Shield	0.19331059	0.17601	0.09829
	Source	1.17996978	1.29600	0.08953
LQ ₁₀	Shield	0.19336766	0.17601	0.09862
	Source	1.17981243	1.29600	0.08965
LQ ₁₆	Shield	0.19334904	0.17601	0.09851
	Source	1.17988161	1.29600	0.08960

Computational efficiency was measured in the same fashion as for problem one. Table IV-17 shows the user time for each quadrature and each mesh.

Table IV-17 :User Time in Seconds Taken to Solve the Sphere Problem

Quadrature	Coarse Mesh	Medium Mesh	Fine Mesh
MQ ₃	13.46	62.73	531.79
MQ ₅	25.78	121.17	1015.44
MQ ₇	37.99	177.87	1494.66
LQ ₄	12.48	58.87	491.42
LQ ₁₀	62.47	278.98	2471.91
LQ ₁₆	149.05	701.37	5788.87

Figure IV-38 shows a plot of data from Table IV-14 of user time versus relative error in the volume average scalar flux for the coarse mesh. This curve is nearly flat. Curves for the other levels of mesh refinement and for the net current are similar. The lack of significant features implies the quadratures have already converged to the minimum error obtainable by the discrete ordinates method even for the lowest order quadrature. This is not surprising considering the simple nature of the problem.

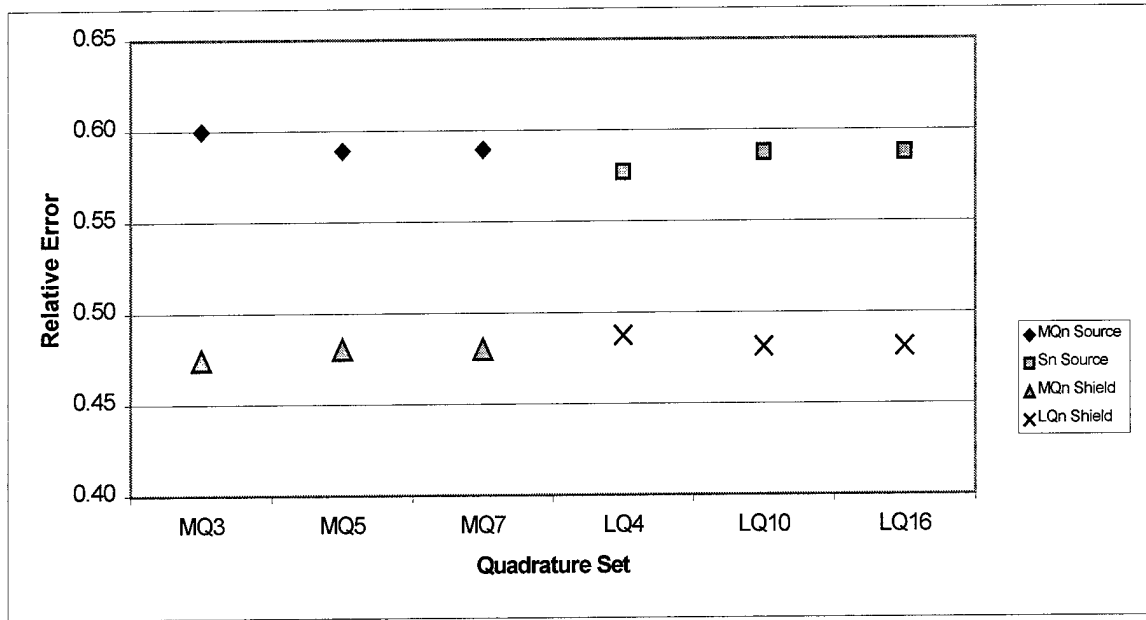


Figure IV-38: Relative Error in Volume Average Scalar Flux, Sphere Problem, Coarse Tetrahedral Mesh

Parallelepiped Mesh

Only one mesh was used for this problem. As in the cube case, reflective boundaries were used on three sides and the problem was run using a one eighth section of the sphere. The remainder of the problem is assumed to be the same by symmetry. Data for the parallelepiped mesh is shown in Table VI-18. The numbers in parentheses in the volume columns are for an entire sphere if reflective boundaries had not been used. The volumes shown here are compared with 98.96 and 14.14 cm³ for an actual spherical volume. This method of mesh generation has a difficult time matching curved surfaces.

Table IV-18 : Parallelepiped Mesh Data

Total Cells in Problem	Cells in Material	Cells in Source Region	Net Volume of Shield (cm ³)	Net Volume of Source Region (cm ³)
3375	1464	211	10.02 (80.2)	1.688 (13.5)

The cells are cubes .1 cm across corresponding to .075 optical thickness. The source volume was allowed to bulge into the shield region a small amount to allow for closer volume modeling. Figure IV-39 shows contour plots of the scalar flux in the x-y plane cutting through the origin. Despite the rough geometry of the mesh, the results are fairly uniform. Figure IV-40 shows the volume average scalar flux and Figure 41 shows the relative error. All quadrature sets did well, with error less than two percent. This data is summarized in Table IV-19

Table IV-19: Sphere Data Summary, Parallelepiped Mesh

Quadrature	Volume Average Scalar Flux	Relative Error	Net Current	Relative Error
MQ ₃	0.3110153	0.0158015	0.047224	0.019887
MQ ₅	0.3111058	0.0155153	0.047246	0.020359
MQ ₇	0.3111027	0.0155251	0.047224	0.019871
LQ ₄	0.3107919	0.0165086	0.047302	0.021565
LQ ₁₀	0.3111415	0.0154021	0.047215	0.019677
LQ ₁₆	0.3112716	0.0149906	0.047218	0.019755

Figure IV-42 shows the net current by quadrature with the MCNP benchmark. Again, the results show little deviation by quadrature. Figures IV-43 and 44 show the relative error vs. computation time. Neither quadrature method seems to have a clear advantage.

Table IV-20 : Time by Quadrature, Sphere Problem, Parallelepiped Mesh

Quadrature	Time (sec)
MQ3	3.24
MQ5	3.3
MQ7	9.58
LQ4	2.92
LQ10	5.81
LQ16	22.97

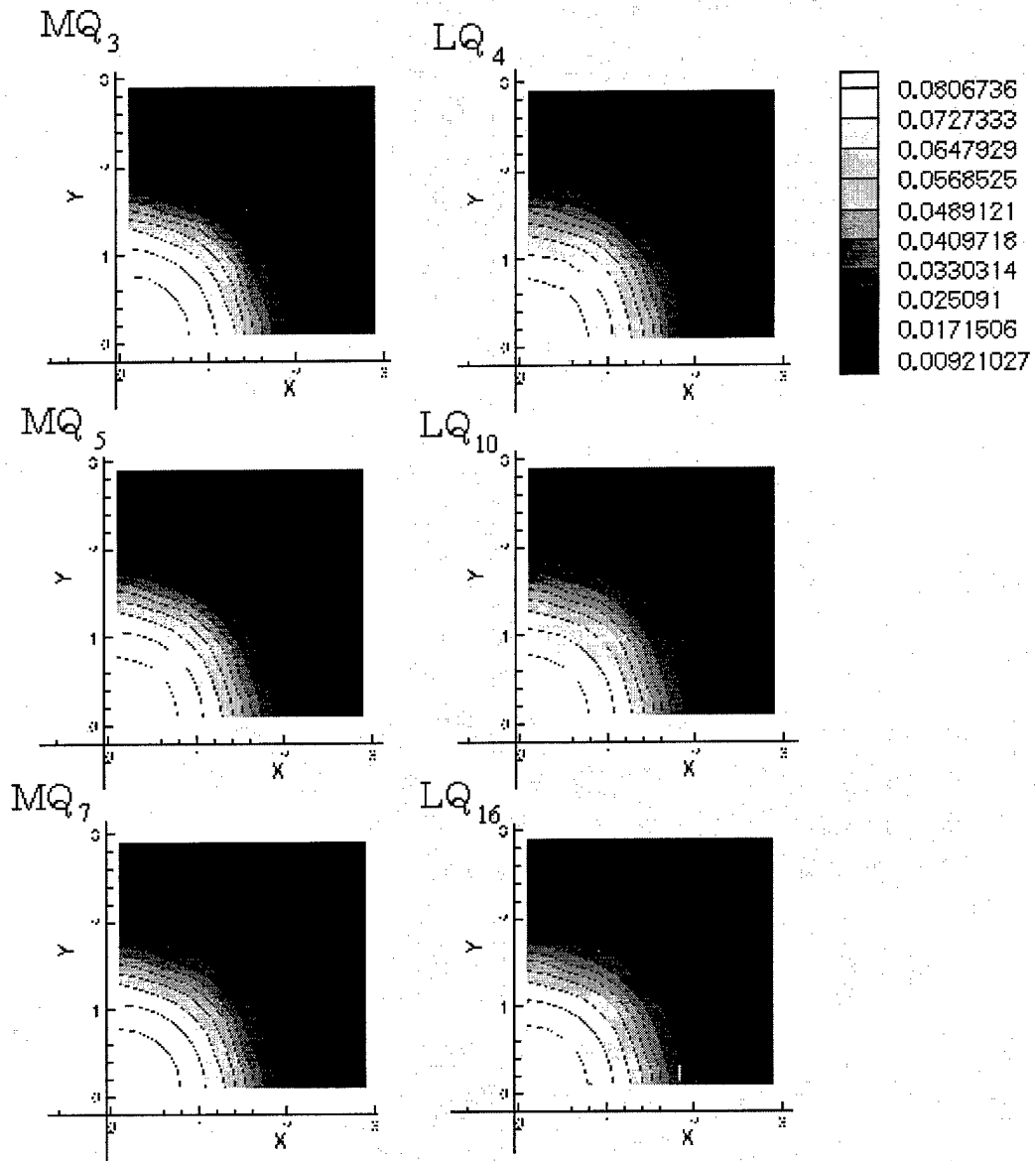


Figure IV-39: Comparison of Contour Plots: Scalar Flux, $Z = .125$ plane, Sphere Problem, Parallelepiped mesh

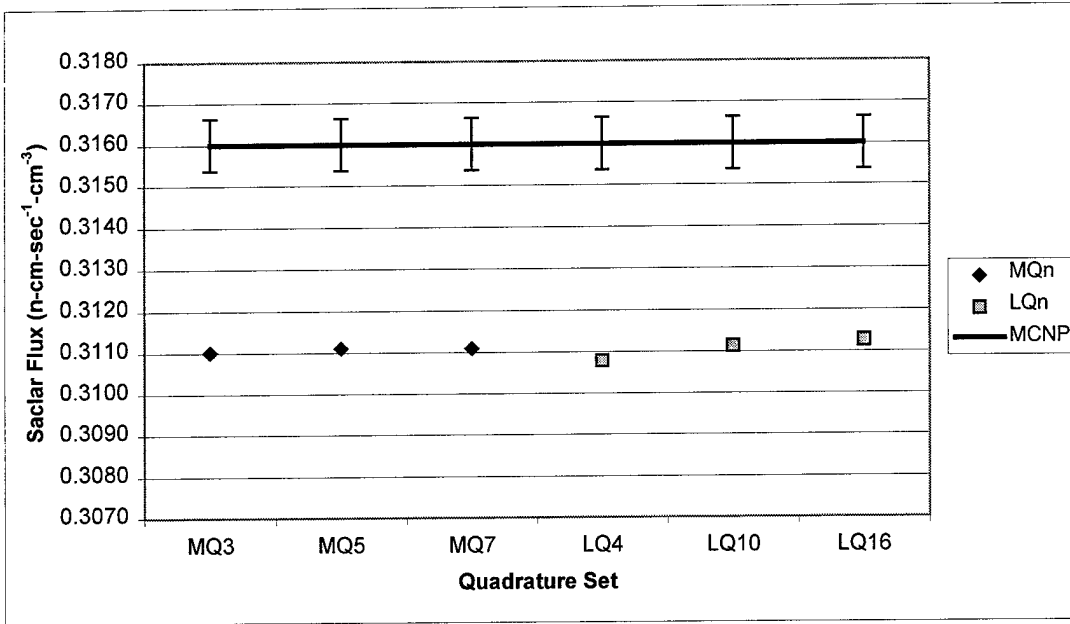


Figure IV-40 : Volume Average Scalar Flux, Sphere Problem, Parallelepiped Mesh

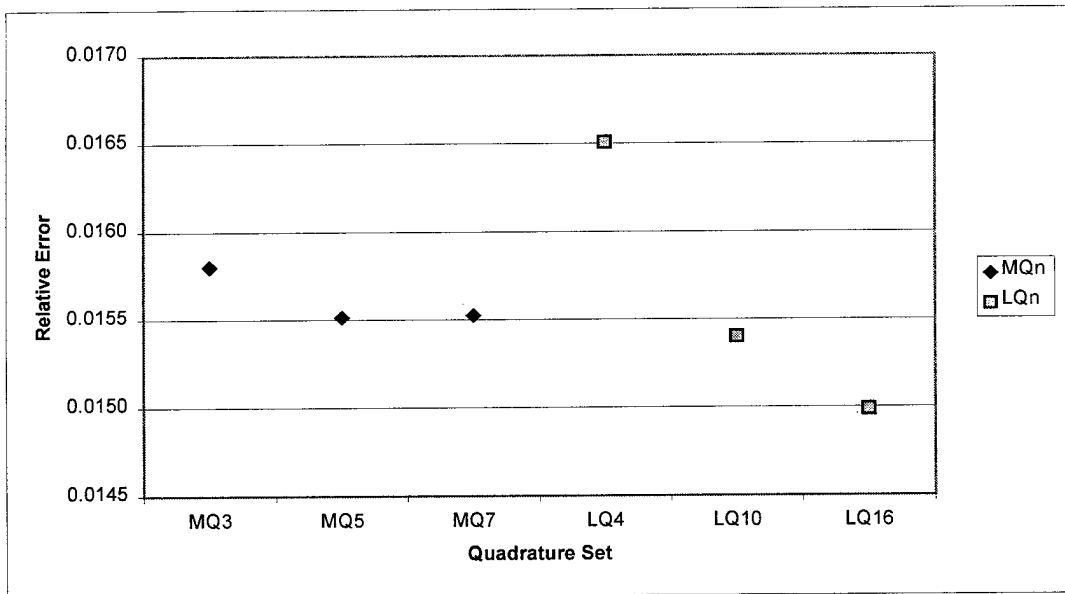


Figure IV-41: Relative Error, Volume Average Scalar Flux, Sphere Problem, Parallelepiped Mesh

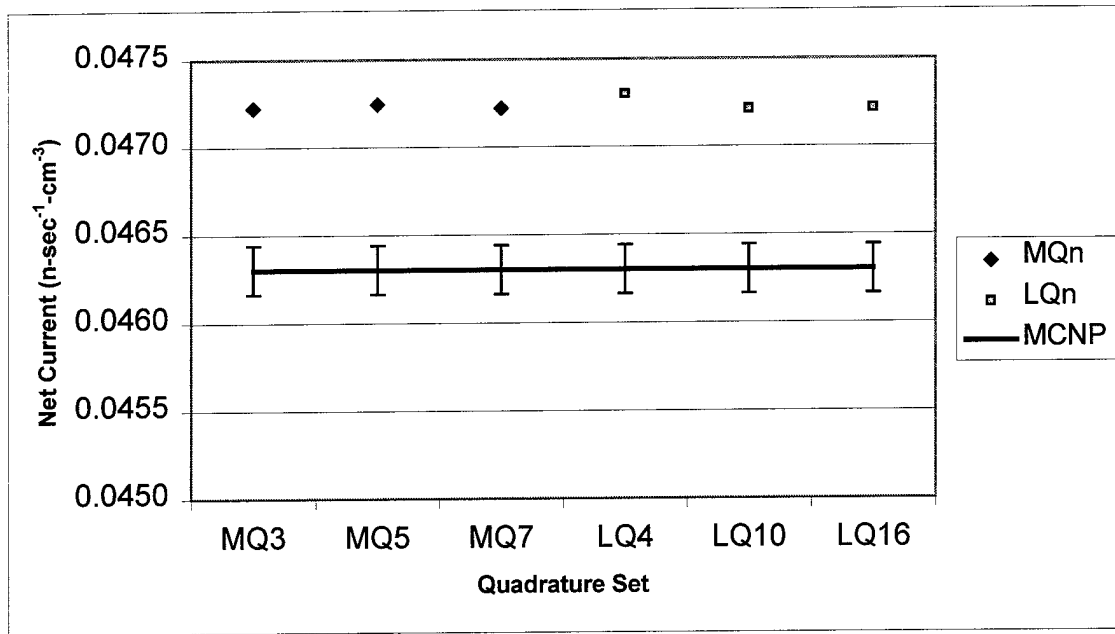


Figure IV-42: Net Current, Sphere Problem, Parallelepiped Mesh

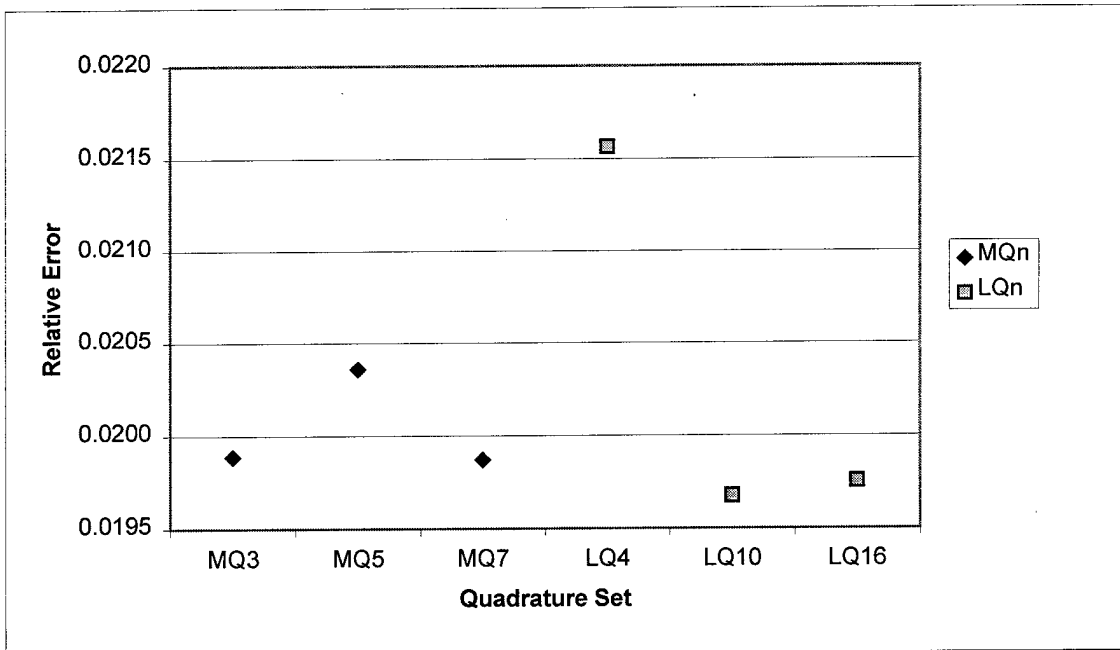


Figure IV-43: Relative Error in Net Current, Sphere Problem, Parallelepiped Mesh

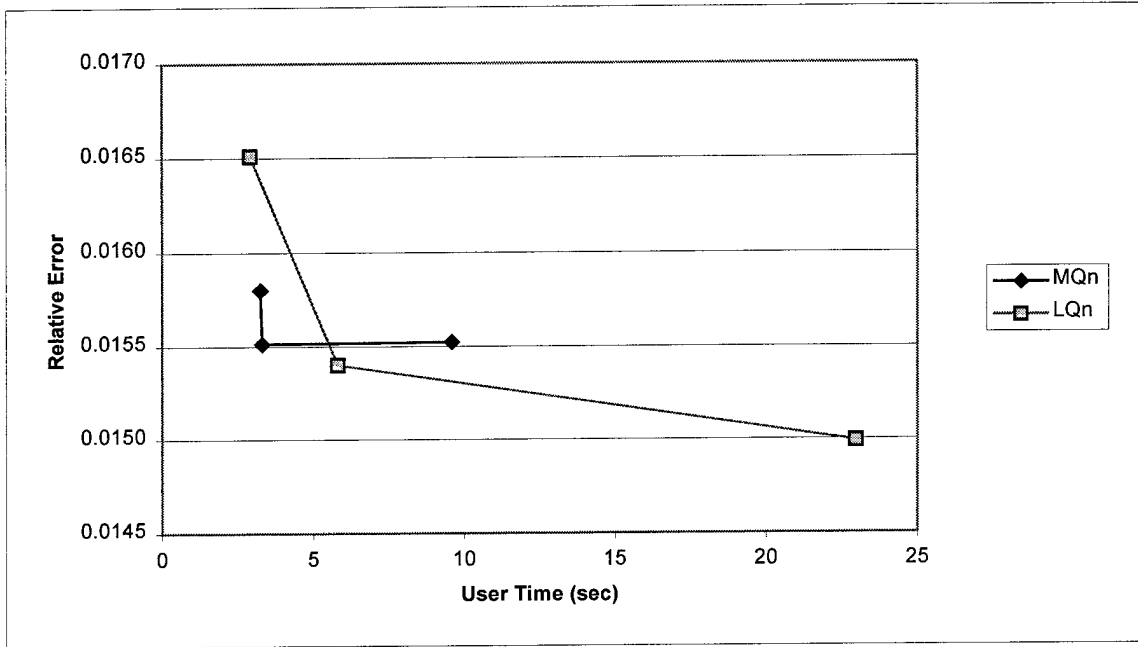


Figure IV-44: Time vs. Error in Flux, Sphere Problem, Parallelepiped Mesh

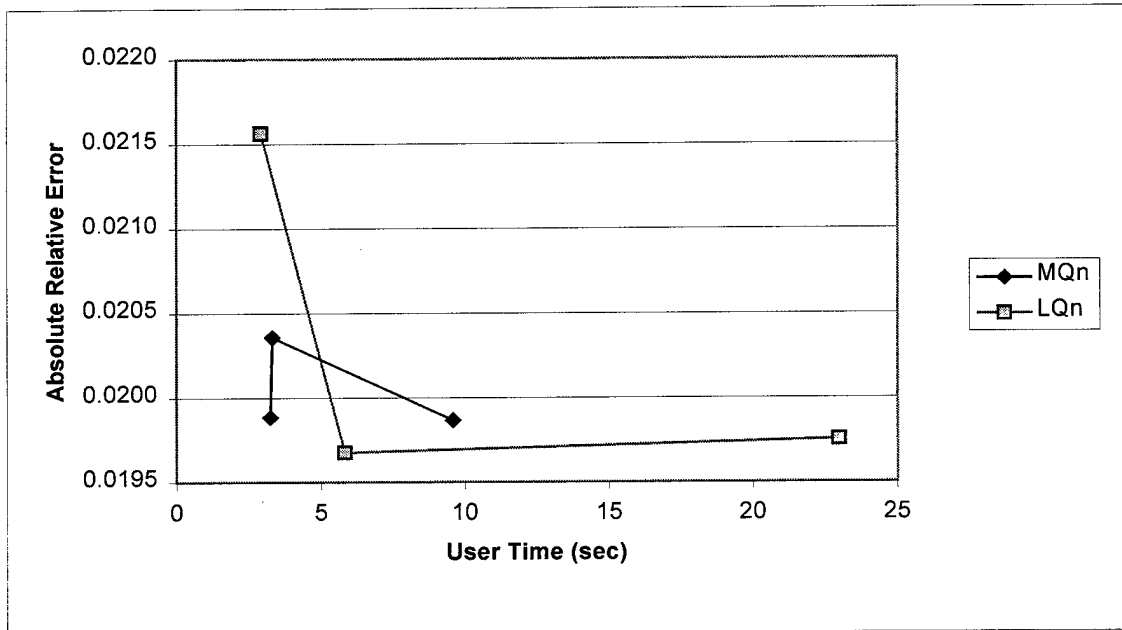


Figure IV-45: Time vs. Error in Current, Sphere Problem, Parallelepiped Mesh

V. Conclusion

The quadratures developed here show the potential for use in discrete ordinates transport calculations. The MQ_n quadratures tested do provide accuracy comparable to traditional methods, and often at a substantial saving in time. However, there is as yet insufficient data to make conclusive statements on the effectiveness of the method.

Decreased computational cost for use on parallelepiped meshes may be obtained by development of new computer codes to take advantage of the one, or two dimensional aspect of the special directions, and by use of more flexible quadrature input modules to allow any number of ordinates.

The MQ_n quadratures seem to perform best in the unstructured mesh. It is difficult to determine the type problem with regard to mesh type and problem geometry that these quadratures will work best with due to the limited amount of data obtained. The sphere in sphere problem did not adequately differentiate performance between quadrature sets. More work is need on a greater variety of problems before significant conclusions on this aspect of performance can be made.

The reduced number of angles in the new quadratures does reduce the computational cost of the problems solved. Using the tetrahedral mesh, these quadratures had comparable accuracy to the LQ_n quadratures with regard to smoothness and global accuracy. Their performance was best when used to find integral results. On the parallelepiped mesh, the MQ_n quadratures

showed substantial ray effects though still did well when calculating integral results.

I recommend using the MQ_n quadratures on problems with little symmetry on an unstructured mesh. For structured meshes and problems with high symmetry, more data is need before a recommendation can be made.

Recommendations for further research

More quadrature sets need to be solved and more data needs to be generated. From an increased database, the optimal quadrature set to use as a function of problem geometry and mesh type may be found. Also, the potential benefits of the higher order of these quadratures as compared to others with the same number of angles needs to be investigated by evaluating them on anisotropic test problems.

Development of code to take advantage of the one- and two-dimensional aspects of the MQ_n quadrature sets may provide an interesting challenge with potentially a great deal of gain. Integrating the new code modules with current programs may allow for easy transition to these new sets where applicable

I have been unable to solve any quadrature above seventh order. I spent many hours on Mathematica, and attempted to write a FORTRAN program using an expansion method, but was unsuccessful. More time in

developing a method of solving the high order polynomials may yield higher order quadratures.

VI. Bibliography

1. Lewis, E. E., and Miller, W. F., Jr. *Computational Methods of Neutron Transport*, American Nuclear Society, Inc., La Grange Park, Illinois, 1993.
2. Wing, G., Milton. *An Introduction to Transport Theory*, John Wiley and Sons, Inc., New York, London, 1962.
3. Mathews, K. A. *Discrete Elements Method of Neutral Particle Transport*, Air Force Institute of Technology (AU), Wright-Patterson AFB OH, 1983 (AD-A138080).
4. Lathrop, K. D., and Carlson, B. G. "Discrete Ordinates Angular Quadrature of the Neutron Transport Equation," LA-3186, Los Alamos Scientific Laboratory, 1965.
5. Carlson, B. G. "Tables of Equal Weight Quadrature E_{q_n} Over the Unit Sphere," LA-4734, Los Alamos Scientific Laboratory, 1971.
6. Carlson, B. G. "Transport Theory: Discrete Ordinates Quadrature Over the Unit Sphere," LA-4554, Los Alamos Scientific Laboratory, 1965.
7. Gomes, L. M. and Stevens, P. N. "Use of Monte Carlo Procedures to Estimate First and Second Collision Sources for Discrete Ordinates Transport Codes", Nuclear Science and Engineering, July 1993, Volume 114: pp. 228-237.

8. Briggs, L. L. and others. "Ray Effect Mitigation in Discrete Ordinate-Like Angular Finite Element Approximations in Neutron Transport," Nuclear Science and Engineering, 1975, Volume 57: pp. 205-217.
9. Minor, B. and Mathews, K. A. "Exponential Characteristic Spatial Quadrature for the Discrete Ordinates Radiation Transport with Rectangular Cells," Nuclear Science and Engineering, July 1995, Volume 120: pp. 165-186.
10. Haghghat, A., Hunter, M., Mattis, R. "Iterative Schemes for Parallel S_n Algorithms in a Shared-Memory Computing Environment," Nuclear Science and Engineering, Sept 1995, Volume 121: pp. 103-113.
11. Abu-Shumays, I. K. "Compatible Product Angular Quadrature for Neutron Transport in x-y Geometry," Nuclear Science and Engineering, 1977, Volume 64: pp 299-316.
12. "Spherical Harmonics,"
<http://www.astro.virginia.edu/~eww6n/math/SphericalHarmonic.html>
13. Brennan, C. R. and Miller, R. L. TETRAN, An unstructured tetrahedral mesh code for use with the discrete ordinates method, in development, Air Force Institute of Technology, Air University, 1997.
14. DANTSYS 3.0, One-, Two, Three-Dimensional, Multigroup, Discrete Ordinates Transport Code System, Los Alamos National Laboratory, Los Alamos, NM, March 1997.

15. Briesmeister, J. F. *MCNP – A General Monte Carlo Code for Neutron and Photon Transport*, Los Alamos National Laboratory, Los Alamos, NM, 1991.
16. Brennan, C. R. *Characteristic Spatial Quadratures for Discrete Ordinates Neutral Particle Transport on Arbitrary Tetrahedral Meshes*, Air Force Institute of Technology, (AU), Wright-Patterson AFB OH, June 1996.
17. Miller, R. L. *Characterization of Nuclear Weapon Effects Parameters in Reduced Lithium Hydride Content Test Cassettes for the National Ignition Facility*, MS thesis, AFIT/GIM/LSM/86S-15. School of Engineering, Air Force Institute of Technology (AU), Wright-Patterson AFB OH, December 1993.
18. Tait, J.H. *Neutron Transport Theory*, American Elsevier Publishing Company INC., New York, 1965.
19. Gelbard, E. M. and Davis, J. A., Hageman, L. A. "Solution of the Discrete Ordinates Equations in One and Two Dimensions," *Transport Theory, Symposium in Applied Mathematics*-American Mathematical Society Proceedings, American Mathematical Society, Providence, Rhode Island, 1969.
20. Mathematica 3.0, Wolfram Research Inc., 1988-1996
21. Lathrop, K. D. "Remedies for Ray Effects," *Nuclear Science and Engineering*, 45, 255, 1971.
22. Pro/Engineer 18.0, Parametric Technology Corporation, 1997.

23. MSRC Introductory Guide, Multi-Shared Resource Center, Air Force Institute of Technology, 1997.
24. Tecplot 7, Data Visualization Tool, Amtec Engineering, Inc., Bellevue, Washington, August 1996.
25. Mathews, K. A. Private Communication, March 1997-October 1997.

Appendix A

Each case A, B, C, 1, 2, 3, and 4 included in a quadrature contribute to the summation

$$\sum_{n=1}^N w_n \mu_n^{2k}, \quad k = 1, 2, \dots, L.$$

Because of the symmetry requirements all of the weights for a particular case are required to be the identical and all of the angles for each case are functions of the angles, μ and η , in the base hexant. In some of the cases the angles have restrictions on them so they are not free parameters. The number of degrees of freedom provided by a case is the number of free angles plus one for the weight. Each case below will have a discussion of which parameters are free.

CaseA: This consist of six points over the unit sphere, two on each coordinate axis at ± 1 . All of the angles are restricted in this case and only the weight is free, yielding one degree of freedom. The contribution of caseA to the summation is

$$w[(1)^{2k} + (0)^{2k} + (0)^{2k} + (0)^{2k} + (0)^{2k} + (-1)^{2k}]$$

which simplifies to

$$2w$$

for all $k \neq 0$.

CaseB: This case consist of 12 ordiates over the unit sphere. Each ordinate has one direction cosine equal to zero and the other two equal $\frac{1}{\sqrt{2}}$ in the principal octant. The only free parameter for this case then is the weight for one degree of freedom. The contribution of caseB to the summations is

$$w\left[4\left(\frac{1}{\sqrt{2}}\right)^{2k} + 4(0)^{2k} + 4\left(-\frac{1}{\sqrt{2}}\right)^{2k}\right]$$

which simplifies, for $k \neq 0$, to

$$\frac{8w}{2^k}.$$

CaseC: This case consist of 24 ordiates

over the unit sphere. Each ordinate has one direction cosine equal to zero, one free, and the other is found from $\mu^2 + \eta^2 + \xi^2 = 1$.

This leaves one free angle and the weight for two degrees of freedom. The contribution to the summation is

$$w[4\mu^{2k} + 4(\sqrt{1-\mu^2})^{2k} + 8(0)^{2k} + 4(-\mu)^{2k} + 4(-\sqrt{1-\mu^2})^{2k}].$$

This simplifies to, for $k \neq 0$, to

$$8w[\mu^{2k} + (1-\mu^2)^k].$$

Case1 : This case consist of eight ordinates over the unit sphere . Each direction cosine is equal to $\frac{1}{\sqrt{3}}$ in the principal octant . This leaves only the weight free for one degree of freedom . The contribution is

$$w \left[4 \left(\frac{1}{\sqrt{3}} \right)^{2k} + 4 \left(-\frac{1}{\sqrt{3}} \right)^{2k} \right] .$$

This simplifies to

$$\frac{8w}{3^k} .$$

Case2 : This consist of 24 ordinates over the unit sphere . One angle is free, the other two are equal . This yields two degrees of freedom, one angle and one weight . The contribution is

$$w \left[4 \mu^{2k} + 8 \left(\sqrt{\frac{1-\mu^2}{2}} \right)^{2k} + 4 (-\mu)^{2k} + 8 \left(-\sqrt{\frac{1-\mu^2}{2}} \right)^{2k} \right]$$

which simplifies to

$$8w \left[\mu^{2k} + 2 \left(\frac{1-\mu^2}{2} \right)^k \right] .$$

Case3 : This consist of 24 ordinates over the unit sphere . One angles is free and the other two are equal . This yields two degrees of freedom as for case2 above . There are two way to look at the contribution for case3 . The first is to note that all angles for this case result if when solving for a case2, the angles are less than $\frac{1}{\sqrt{3}}$. This puts the angle out of the base hexant if this angle is μ . But if,

when this results, we consider the angle as η instead, this ordinate will lie in the base hexant and is infact a case3 ordinate . The other method is to proceed as normal resulting in the following contribution equation

$$w \left[8 \mu^{2k} + 4 \left(\sqrt{1-2\mu^2} \right)^{2k} + 8 (-\mu)^{2k} + 4 \left(-\sqrt{1-2\mu^2} \right)^{2k} \right]$$

which simplifies to

$$8w \left[2 \mu^{2k} + (1-2\mu^2)^k \right] .$$

I prefer to use the former method and use a contribution equation in the form

$$8w \left[\eta^{2k} + 2 \left(\frac{1-\eta^2}{2} \right)^k \right] .$$

The two equations are equivalent,

as can be easily verified by substituting $\mu = \sqrt{\frac{1-\eta^2}{2}}$ into the first result .

Case4 : This consist of 48 directions over the unit sphere . Both μ and η are free parameters as is the weight . This is the most expensive case to included and the most difficult to solve . To find the three angles defining this ordinate in the base hextant, we must leave μ and η as free parameters and find ξ using $\xi^2 = 1 - \mu^2 + \eta^2$. The resulting contribution equation is

$$w [8 \mu^{2k} + 8 \eta^{2k} + 8 (\sqrt{1 - \mu^2 - \eta^2})^{2k} + 8 (-\mu)^{2k} + 8 (-\eta)^{2k} + 8 (-\sqrt{1 - \mu^2 - \eta^2})^{2k}]$$

which simplifies to

$$16 w [\mu^{2k} + \eta^{2k} + (1 - \mu^2 - \eta^2)^k] .$$

```

Off[General::spell1]

caseA[w_, k_] := 6 w /; k == 0

caseA[w_, k_] := 2 w /; k != 0

caseB[w_, k_] := 12 w /; k == 0

caseB[w_, k_] := 8  $\frac{w}{2^k}$  /; k != 0

caseC[w_,  $\mu$ _, k_] := 24 w /; k == 0

caseC[w_,  $\mu$ _, k_] := 8 w ( $\mu^{2k} + (1 - \mu^2)^k$ ) /; k != 0

case1[w_, k_] := 8  $\frac{w}{3^k}$ 

case2[w_,  $\mu$ _, k_] := 8 w ( $\mu^{2k} + 2 \left(\frac{1 - \mu^2}{2}\right)^k$ )

(* When a case 3 ordinate is desired,
   use the case 2 equation an substitute  $\eta$  for  $\mu$ . *)

case4[w_,  $\mu$ _,  $\eta$ _, k_] := 16 w ( $\mu^{2k} + (1 - \mu^2 - \eta^2)^k + \eta^{2k}$ )

(* The Filter function below
   searches a list of quadrature output from a Solve function and *)
(* returns null values for elements in the list with negative weights or
   angles or imaginary values. *)

Filter[TL_, vars_] := Table[If[(vars /. TL)[[j]] ==
  Table[Select[Re[(vars /. TL)[[i]]], # > 0 &], {i, Length[TL]}][[j]], TL[[j]]],
  {j, Length[TL]}]

GetQuad[Equations_, vars_] := Filter[NSolve[Equations, vars], vars]

Eqns = Table[Expand[caseA[wA, k] + caseC[wC,  $\mu$ C, k]] ==  $\frac{1}{2k+1}$ , {k, 3}]

{2 wA + 8 wC ==  $\frac{1}{3}$ , 2 wA + 8 wC - 16 wC  $\mu$ C2 + 16 wC  $\mu$ C4 ==  $\frac{1}{5}$ , 2 wA + 8 wC - 24 wC  $\mu$ C2 + 24 wC  $\mu$ C4 ==  $\frac{1}{7}$ }

Solve[Eqns, {wA, wC,  $\mu$ C}]

{}

(* The caseA + caseC combination has no solution *)

Eqns = Table[Expand[caseB[wB, k] + caseC[wC,  $\mu$ C, k]] ==  $\frac{1}{2k+1}$ , {k, 3}]

{4 wB + 8 wC ==  $\frac{1}{3}$ , 2 wB + 8 wC - 16 wC  $\mu$ C2 + 16 wC  $\mu$ C4 ==  $\frac{1}{5}$ , wB + 8 wC - 24 wC  $\mu$ C2 + 24 wC  $\mu$ C4 ==  $\frac{1}{7}$ }

```

Solve[Eqns, {wB, wC, μC}]

{}

(* The BC case combination has no solution *)

Eqns = Table[case1[w1, k] + caseC[wC, μC, k] == $\frac{1}{2k+1}$, {k, 3}]

$\left\{ \frac{8w1}{3} + 8wC == \frac{1}{3}, \frac{8w1}{9} + 8wC(\mu C^4 + (1 - \mu C^2)^2) == \frac{1}{5}, \frac{8w1}{27} + 8wC(\mu C^6 + (1 - \mu C^2)^3) == \frac{1}{7} \right\}$

Solve[Eqns, {w1, wC, μC}]

$\left\{ \left\{ w1 \rightarrow \frac{9}{280}, wC \rightarrow \frac{13}{420}, \mu C \rightarrow -\sqrt{\frac{1}{26}(13 - \sqrt{65})} \right\}, \left\{ w1 \rightarrow \frac{9}{280}, wC \rightarrow \frac{13}{420}, \mu C \rightarrow \sqrt{\frac{1}{26}(13 - \sqrt{65})} \right\}, \left\{ w1 \rightarrow \frac{9}{280}, wC \rightarrow \frac{13}{420}, \mu C \rightarrow -\sqrt{\frac{1}{26}(13 + \sqrt{65})} \right\}, \left\{ w1 \rightarrow \frac{9}{280}, wC \rightarrow \frac{13}{420}, \mu C \rightarrow \sqrt{\frac{1}{26}(13 + \sqrt{65})} \right\} \right\}$

(* The fourth solution above belongs to the base set,
the others coincide with the ordinates
resulting from symmetry operations. *)

(* Numerical

conditioning of the quadrature will be best if the weights are similar, the decimal
values below show this to potentially be a good quadrature *)

N[%21[[4]], 16]

{w1 → 0.03214285714285714, wC → 0.03095238095238095, μC → 0.9000482411921158}

Eqns = Table[caseA[wA, k] + caseB[wB, k] + case1[w1, k] == $\frac{1}{2k+1}$, {k, 3}]

$\left\{ \frac{8w1}{3} + 2wA + 4wB == \frac{1}{3}, \frac{8w1}{9} + 2wA + 2wB == \frac{1}{5}, \frac{8w1}{27} + 2wA + wB == \frac{1}{7} \right\}$

Solve[Eqns, {wA, wB, w1}]

$\left\{ \left\{ wA \rightarrow \frac{1}{21}, wB \rightarrow \frac{4}{105}, w1 \rightarrow \frac{9}{280} \right\} \right\}$

N[%24, 16]

{wA → 0.04761904761904762, wB → 0.0380952380952381, w1 → 0.03214285714285714}

(* The above weights are also similar in magnitude. *)

$$\text{Eqns} = \text{Table}[\text{caseA}[wA, k] + \text{caseB}[wB, k] + \text{caseC}[wC, \mu C, k] + \text{case1}[w1, k] == \frac{1}{2k+1}, \{k, 5\}]$$

$$\left\{ \begin{aligned} \frac{8w1}{3} + 2wA + 4wB + 8wC &== \frac{1}{3}, \quad \frac{8w1}{9} + 2wA + 2wB + 8wC (\mu C^4 + (1 - \mu C^2)^2) == \frac{1}{5}, \\ \frac{8w1}{27} + 2wA + wB + 8wC (\mu C^6 + (1 - \mu C^2)^3) &== \frac{1}{7}, \quad \frac{8w1}{81} + 2wA + \frac{wB}{2} + 8wC (\mu C^8 + (1 - \mu C^2)^4) == \frac{1}{9}, \\ \frac{8w1}{243} + 2wA + \frac{wB}{4} + 8wC (\mu C^{10} + (1 - \mu C^2)^5) &== \frac{1}{11} \end{aligned} \right\}$$

`quadABC1 = Solve[Eqns, {wA, wB, wC, w1, \mu C}]`

`{}`

(* TheABC1 case has no solutions *)

$$\text{Eqns} = \text{Table}[\text{caseA}[wA, k] + \text{caseB}[wB, k] + \text{case1}[w1, k] + \text{case2}[w2, \mu 2, k] == \frac{1}{2k+1}, \{k, 5\}]$$

$$\left\{ \begin{aligned} \frac{8w1}{3} + 8w2 + 2wA + 4wB &== \frac{1}{3}, \quad \frac{8w1}{9} + 2wA + 2wB + 8w2 \left(\mu 2^4 + \frac{1}{2} (1 - \mu 2^2)^2 \right) == \frac{1}{5}, \\ \frac{8w1}{27} + 2wA + wB + 8w2 \left(\mu 2^6 + \frac{1}{4} (1 - \mu 2^2)^3 \right) &== \frac{1}{7}, \\ \frac{8w1}{81} + 2wA + \frac{wB}{2} + 8w2 \left(\mu 2^8 + \frac{1}{8} (1 - \mu 2^2)^4 \right) &== \frac{1}{9}, \\ \frac{8w1}{243} + 2wA + \frac{wB}{4} + 8w2 \left(\mu 2^{10} + \frac{1}{16} (1 - \mu 2^2)^5 \right) &== \frac{1}{11} \end{aligned} \right\}$$

`quadAB12 = Solve[Eqns, {wA, wB, w1, w2, \mu 2}]`

$$\left\{ \left\{ wA \rightarrow \frac{4}{315}, wB \rightarrow \frac{64}{2835}, w1 \rightarrow \frac{27}{1280}, w2 \rightarrow \frac{14641}{725760}, \mu 2 \rightarrow -\frac{3}{\sqrt{11}} \right\}, \right. \\ \left. \left\{ wA \rightarrow \frac{4}{315}, wB \rightarrow \frac{64}{2835}, w1 \rightarrow \frac{27}{1280}, w2 \rightarrow \frac{14641}{725760}, \mu 2 \rightarrow \frac{3}{\sqrt{11}} \right\} \right\}$$

(* The second solution belongs

to the base set. Its numerical value shows it to potentially be a good quadrature *)

`N[quadAB12[[2]], 16]`

$$\{wA \rightarrow 0.0126984126984127, wB \rightarrow 0.02257495590828924, w1 \rightarrow 0.02109375, \\ w2 \rightarrow 0.02017333553791887, \mu 2 \rightarrow 0.904534033733291\}$$

Eqns = Table[caseA[wA, k] + caseC[wC, μC, k] + case2[w2, μ2, k] == $\frac{1}{2k+1}$, {k, 5}]

$$\left\{ \begin{aligned} 8 w_2 + 2 w_A + 8 w_C &= \frac{1}{3}, \quad 2 w_A + 8 w_2 \left(\mu_2^4 + \frac{1}{2} (1 - \mu_2^2)^2 \right) + 8 w_C (\mu_C^4 + (1 - \mu_C^2)^2) = \frac{1}{5}, \\ 2 w_A + 8 w_2 \left(\mu_2^6 + \frac{1}{4} (1 - \mu_2^2)^3 \right) + 8 w_C (\mu_C^6 + (1 - \mu_C^2)^3) &= \frac{1}{7}, \\ 2 w_A + 8 w_2 \left(\mu_2^8 + \frac{1}{8} (1 - \mu_2^2)^4 \right) + 8 w_C (\mu_C^8 + (1 - \mu_C^2)^4) &= \frac{1}{9}, \\ 2 w_A + 8 w_2 \left(\mu_2^{10} + \frac{1}{16} (1 - \mu_2^2)^5 \right) + 8 w_C (\mu_C^{10} + (1 - \mu_C^2)^5) &= \frac{1}{11} \end{aligned} \right\}$$

quadAC2 = Solve[Eqns, {wA, wC, w2, μC, μ2}]

(* Large output deleted *)

(* I'll apply the Filter function to better see what I have *)

Filter[quadAC2, {wA, wC, w2, μC, μ2}]

$$\left\{ \begin{aligned} \text{Null, Null, Null, } \{w_A \rightarrow \frac{2(41 - 2\sqrt{22})}{2835}, w_C \rightarrow \frac{44 + 13\sqrt{22}}{5670}, \\ w_2 \rightarrow \frac{11(55 - 4\sqrt{22})}{22680}, \mu_C \rightarrow \sqrt{\frac{1}{66} (33 - \sqrt{33}(-11 + 4\sqrt{22}))}, \mu_2 \rightarrow \sqrt{\frac{1}{33} (11 + 2\sqrt{22})} \}, \\ \text{Null, Null, Null, } \{w_A \rightarrow \frac{2(41 - 2\sqrt{22})}{2835}, w_C \rightarrow \frac{44 + 13\sqrt{22}}{5670}, w_2 \rightarrow \frac{11(55 - 4\sqrt{22})}{22680}, \\ \mu_C \rightarrow \sqrt{\frac{1}{66} (33 + \sqrt{33}(-11 + 4\sqrt{22}))}, \mu_2 \rightarrow \sqrt{\frac{1}{33} (11 + 2\sqrt{22})} \}, \text{Null, Null, Null,} \\ \text{Null, Null, Null, Null, Null} \end{aligned} \right\}$$

(* Let's see what the numerical values are *)

N[%, 16]

{Null, Null, Null, {wA → 0.02230629169689816, wC → 0.01851418075444525,
w2 → 0.01757591298799687, μC → 0.5074563057138757, μ2 → 0.7858759158676477},
Null, Null, Null, {wA → 0.02230629169689816, wC → 0.01851418075444525,
w2 → 0.01757591298799687, μC → 0.8616774905910132, μ2 → 0.7858759158676477},
Null, Null, Null, Null, Null, Null, Null, Null}

(* Since μ2 is greater than $\frac{1}{\sqrt{3}}$ this is a case2 ordinate. The second non null solution is in the base set. *)

$$\text{Eqns} = \text{Table}[\text{caseB}[\text{wB}, \text{k}] + \text{caseC}[\text{wC}, \mu\text{C}, \text{k}] + \text{case2}[\text{w2}, \mu\text{2}, \text{k}] == \frac{1}{2\text{k}+1}, \{\text{k}, 5\}]$$

$$\left\{ \begin{aligned} 8\text{w2} + 4\text{wB} + 8\text{wC} &== \frac{1}{3}, \quad 2\text{wB} + 8\text{w2} \left(\mu\text{2}^4 + \frac{1}{2} (1 - \mu\text{2}^2)^2 \right) + 8\text{wC} (\mu\text{C}^4 + (1 - \mu\text{C}^2)^2) == \frac{1}{5}, \\ \text{wB} + 8\text{w2} \left(\mu\text{2}^6 + \frac{1}{4} (1 - \mu\text{2}^2)^3 \right) + 8\text{wC} (\mu\text{C}^6 + (1 - \mu\text{C}^2)^3) &== \frac{1}{7}, \\ \frac{\text{wB}}{2} + 8\text{w2} \left(\mu\text{2}^8 + \frac{1}{8} (1 - \mu\text{2}^2)^4 \right) + 8\text{wC} (\mu\text{C}^8 + (1 - \mu\text{C}^2)^4) &== \frac{1}{9}, \\ \frac{\text{wB}}{4} + 8\text{w2} \left(\mu\text{2}^{10} + \frac{1}{16} (1 - \mu\text{2}^2)^5 \right) + 8\text{wC} (\mu\text{C}^{10} + (1 - \mu\text{C}^2)^5) &== \frac{1}{11} \end{aligned} \right\}$$

`quadBC2 = Solve[Eqns, {wB, wC, w2, μC, μ2}]`

(* Large output deleted *)

`Filter[quadBC2, {wB, wC, w2, μC, μ2}]`

$$\left\{ \begin{aligned} &\{\text{Null}, \text{Null}, \text{Null}, \text{Null}, \text{Null}, \text{Null}, \text{Null}, \text{Null}, \text{Null}, \text{Null}, \text{Null}, \\ &\left\{ \text{wB} \rightarrow \frac{16(-190 + 169\sqrt{22})}{526995}, \text{wC} \rightarrow \frac{169565 - 5933\sqrt{22}}{9485910}, \text{w2} \rightarrow \frac{11(55 - 4\sqrt{22})}{22680}, \right. \\ &\left. \mu\text{C} \rightarrow \sqrt{\frac{4521 - \sqrt{4521(2761 + 52\sqrt{22})}}{9042}}, \mu\text{2} \rightarrow \sqrt{\frac{1}{33}(11 + 2\sqrt{22})} \right\}, \text{Null}, \text{Null}, \\ &\text{Null}, \left\{ \text{wB} \rightarrow \frac{16(-190 + 169\sqrt{22})}{526995}, \text{wC} \rightarrow \frac{169565 - 5933\sqrt{22}}{9485910}, \text{w2} \rightarrow \frac{11(55 - 4\sqrt{22})}{22680}, \right. \\ &\left. \mu\text{C} \rightarrow \sqrt{\frac{4521 + \sqrt{4521(2761 + 52\sqrt{22})}}{9042}}, \mu\text{2} \rightarrow \sqrt{\frac{1}{33}(11 + 2\sqrt{22})} \right\} \end{aligned} \right\}$$

`N[%, 16]`

$$\left\{ \begin{aligned} &\{\text{Null}, \text{Null}, \text{Null}, \text{Null}, \text{Null}, \text{Null}, \text{Null}, \text{Null}, \text{Null}, \text{Null}, \text{Null}, \\ &\left\{ \text{wB} \rightarrow 0.01829786661080761, \text{wC} \rightarrow 0.01494182037326599, \text{w2} \rightarrow 0.01757591298799687, \right. \\ &\left. \mu\text{C} \rightarrow 0.3039216446504884, \mu\text{2} \rightarrow 0.7858759158676477 \right\}, \text{Null}, \text{Null}, \text{Null}, \\ &\left\{ \text{wB} \rightarrow 0.01829786661080761, \text{wC} \rightarrow 0.01494182037326599, \text{w2} \rightarrow 0.01757591298799687, \right. \\ &\left. \mu\text{C} \rightarrow 0.9526970315441012, \mu\text{2} \rightarrow 0.7858759158676477 \right\} \end{aligned} \right\}$$

(* This quadrature also has promising weights,
the last solution is in the base set. *)

$$\text{Eqns} = \text{Table}[\text{caseC}[\text{wC}, \mu\text{C}, \text{k}] + \text{case4}[\text{w4}, \mu4, \eta4, \text{k}] == \frac{1}{2\text{k}+1}, \{\text{k}, 5\}]$$

$$\left\{ 16\text{w4} + 8\text{wC} == \frac{1}{3}, 16\text{w4} (\eta4^4 + \mu4^4 + (1 - \eta4^2 - \mu4^2)^2) + 8\text{wC} (\mu\text{C}^4 + (1 - \mu\text{C}^2)^2) == \frac{1}{5}, \right.$$

$$16\text{w4} (\eta4^6 + \mu4^6 + (1 - \eta4^2 - \mu4^2)^3) + 8\text{wC} (\mu\text{C}^6 + (1 - \mu\text{C}^2)^3) == \frac{1}{7},$$

$$16\text{w4} (\eta4^8 + \mu4^8 + (1 - \eta4^2 - \mu4^2)^4) + 8\text{wC} (\mu\text{C}^8 + (1 - \mu\text{C}^2)^4) == \frac{1}{9},$$

$$\left. 16\text{w4} (\eta4^{10} + \mu4^{10} + (1 - \eta4^2 - \mu4^2)^5) + 8\text{wC} (\mu\text{C}^{10} + (1 - \mu\text{C}^2)^5) == \frac{1}{11} \right\}$$

quadC4 = Solve[Eqns, {wC, w4, μC, μ4, η4}]

(* Large output deleted *)

(* The decimal equivalent after filtering is shown below *)

N[quadC4, 25]

Eqns = Table[case1[w1, k] + caseC[wC, μC, k] + case2[w2, μ2, k] == $\frac{1}{2k+1}$, {k, 5}]

$$\left\{ \begin{aligned} \frac{8w1}{3} + 8w2 + 8wC &== \frac{1}{3}, \quad \frac{8w1}{9} + 8w2 \left(\mu2^4 + \frac{1}{2} (1 - \mu2^2)^2 \right) + 8wC (\mu C^4 + (1 - \mu C^2)^2) == \frac{1}{5}, \\ \frac{8w1}{27} + 8w2 \left(\mu2^6 + \frac{1}{4} (1 - \mu2^2)^3 \right) + 8wC (\mu C^6 + (1 - \mu C^2)^3) &== \frac{1}{7}, \\ \frac{8w1}{81} + 8w2 \left(\mu2^8 + \frac{1}{8} (1 - \mu2^2)^4 \right) + 8wC (\mu C^8 + (1 - \mu C^2)^4) &== \frac{1}{9}, \\ \frac{8w1}{243} + 8w2 \left(\mu2^{10} + \frac{1}{16} (1 - \mu2^2)^5 \right) + 8wC (\mu C^{10} + (1 - \mu C^2)^5) &== \frac{1}{11} \end{aligned} \right\}$$

quad1C2 = Solve[Eqns, {w1, wC, w2, μC, μ2}]

(* Large output deleted *)

N[quad1C2, 40]

Filter[%, {w1, wC, w2, μC, μ2}]

{Null, Null, Null, {w1 → 0.03139662070471866287073752871645825335788 + 0. × 10⁻⁵² I,
wC → 0.03118946912313230360638905694603843725377 + 0. × 10⁻⁵³ I,
w2 → 0.00001165730862814210336510014847547829359805 + 0. × 10⁻⁵³ I,
μC → 0.440124599527176955730943844695059472227 + -0. × 10⁻⁶⁸ I,
μ2 → 1.482898731354957472518351725181578455870 + -0. × 10⁻⁶⁸ I}, Null,
Null, Null, {w1 → 0.03139662070471866287073752871645825335788 + 0. × 10⁻⁵² I,
wC → 0.03118946912313230360638905694603843725377 + 0. × 10⁻⁵³ I,
w2 → 0.00001165730862814210336510014847547829359805 + 0. × 10⁻⁵³ I,
μC → 0.897936710960768162219787279180959387596 + -0. × 10⁻⁶⁸ I,
μ2 → 1.482898731354957472518351725181578455870 + -0. × 10⁻⁶⁸ I}, Null, Null,
Null, Null, Null, Null, Null, Null, Null, Null, Null, Null, Null, Null, Null}

(* From the above two sets of output,

we see that there are no acceptable 1C2 quadratures. The filtered output shows quadratures with cosines greater than one and from the unfiltered solutions we see there are quadratures with valid angles but negative weights. *)

Eqns = Table[caseA[wA, k] + caseB[wB, k] + case4[w4, μ4, η4, k] == $\frac{1}{2k+1}$, {k, 5}]

$$\left\{ \begin{aligned} 16w4 + 2wA + 4wB &== \frac{1}{3}, \quad 2wA + 2wB + 16w4 (\eta4^4 + \mu4^4 + (1 - \eta4^2 - \mu4^2)^2) == \frac{1}{5}, \\ 2wA + wB + 16w4 (\eta4^6 + \mu4^6 + (1 - \eta4^2 - \mu4^2)^3) &== \frac{1}{7}, \\ 2wA + \frac{wB}{2} + 16w4 (\eta4^8 + \mu4^8 + (1 - \eta4^2 - \mu4^2)^4) &== \frac{1}{9}, \\ 2wA + \frac{wB}{4} + 16w4 (\eta4^{10} + \mu4^{10} + (1 - \eta4^2 - \mu4^2)^5) &== \frac{1}{11} \end{aligned} \right\}$$

quadBC2 = Solve[Eqns, {wA, wB, w4, μ4, η4}]

(* Large output deleted *)

N[%, 40]

Filter[%, {wA, wB, w4, μ 4, η 4}]

{Null, Null, Null, Null, Null, Null, Null, Null, Null, Null, Null, Null, Null,
Null, Null, Null, Null, Null, Null, Null, Null, Null, Null, Null}

(* there are no valid AB4 quadratures *)

(* The next series of quadratures are of order 7 *)

Eqns = Table[

$$\text{caseA}[wA, k] + \text{caseB}[wB, k] + \text{caseC}[wC, \mu C, k] + \text{case1}[w1, k] + \text{case2}[w2, \mu 2, k] == \frac{1}{2k+1},$$

{k, 7}]

$$\left\{ \frac{8 w1}{3} + 8 w2 + 2 wA + 4 wB + 8 wC == \frac{1}{3}, \right.$$

$$\frac{8 w1}{9} + 2 wA + 2 wB + 8 w2 \left(\mu 2^4 + \frac{1}{2} (1 - \mu 2^2)^2 \right) + 8 wC (\mu C^4 + (1 - \mu C^2)^2) == \frac{1}{5},$$

$$\frac{8 w1}{27} + 2 wA + wB + 8 w2 \left(\mu 2^6 + \frac{1}{4} (1 - \mu 2^2)^3 \right) + 8 wC (\mu C^6 + (1 - \mu C^2)^3) == \frac{1}{7},$$

$$\frac{8 w1}{81} + 2 wA + \frac{wB}{2} + 8 w2 \left(\mu 2^8 + \frac{1}{8} (1 - \mu 2^2)^4 \right) + 8 wC (\mu C^8 + (1 - \mu C^2)^4) == \frac{1}{9},$$

$$\frac{8 w1}{243} + 2 wA + \frac{wB}{4} + 8 w2 \left(\mu 2^{10} + \frac{1}{16} (1 - \mu 2^2)^5 \right) + 8 wC (\mu C^{10} + (1 - \mu C^2)^5) == \frac{1}{11},$$

$$\frac{8 w1}{729} + 2 wA + \frac{wB}{8} + 8 w2 \left(\mu 2^{12} + \frac{1}{32} (1 - \mu 2^2)^6 \right) + 8 wC (\mu C^{12} + (1 - \mu C^2)^6) == \frac{1}{13},$$

$$\frac{8 w1}{2187} + 2 wA + \frac{wB}{16} + 8 w2 \left(\mu 2^{14} + \frac{1}{64} (1 - \mu 2^2)^7 \right) + 8 wC (\mu C^{14} + (1 - \mu C^2)^7) == \frac{1}{15} \}$$

quadABC12 = Solve[Eqns, {wA, wB, wC, w1, w2, μ C, μ 2}]

(* Large output deleted *)

N[quadABC12, 16]

Filter[%, {wA, wB, w1, wC, w2, μ C, μ 2}]

{Null, Null, Null, {wA \rightarrow 0.009048188830155413,
wB \rightarrow 0.02103246043742795, w1 \rightarrow 0.01827941392341811, wC \rightarrow 0.006451491538566835,
w2 \rightarrow 0.0163437597273743, μ C \rightarrow 0.2979519566503113, μ 2 \rightarrow 0.8753170875981718},
Null, Null, Null, {wA \rightarrow 0.009048188830155413, wB \rightarrow 0.02103246043742795,
w1 \rightarrow 0.01827941392341811, wC \rightarrow 0.006451491538566835, w2 \rightarrow 0.0163437597273743,
 μ C \rightarrow 0.9545808669401723, μ 2 \rightarrow 0.8753170875981718}, Null, Null, Null, Null,
Null, Null, Null, Null}

(* The second of the above valid quadratures is in the base set,
the other is a reflection. *)

Eqns = Table[caseA[wA, k] + caseC[wC, μC, k] + case2[w2, μ2, k] + case2[w3, μ3, k] == $\frac{1}{2k+1}$,
{k, 7}]

$$\{8 w_2 + 8 w_3 + 2 w_A + 8 w_C == \frac{1}{3},$$

$$2 w_A + 8 w_2 \left(\mu_2^4 + \frac{1}{2} (1 - \mu_2^2)^2 \right) + 8 w_3 \left(\mu_3^4 + \frac{1}{2} (1 - \mu_3^2)^2 \right) + 8 w_C (\mu_C^4 + (1 - \mu_C^2)^2) == \frac{1}{5},$$

$$2 w_A + 8 w_2 \left(\mu_2^6 + \frac{1}{4} (1 - \mu_2^2)^3 \right) + 8 w_3 \left(\mu_3^6 + \frac{1}{4} (1 - \mu_3^2)^3 \right) + 8 w_C (\mu_C^6 + (1 - \mu_C^2)^3) == \frac{1}{7},$$

$$2 w_A + 8 w_2 \left(\mu_2^8 + \frac{1}{8} (1 - \mu_2^2)^4 \right) + 8 w_3 \left(\mu_3^8 + \frac{1}{8} (1 - \mu_3^2)^4 \right) + 8 w_C (\mu_C^8 + (1 - \mu_C^2)^4) == \frac{1}{9},$$

$$2 w_A + 8 w_2 \left(\mu_2^{10} + \frac{1}{16} (1 - \mu_2^2)^5 \right) + 8 w_3 \left(\mu_3^{10} + \frac{1}{16} (1 - \mu_3^2)^5 \right) + 8 w_C (\mu_C^{10} + (1 - \mu_C^2)^5) == \frac{1}{11},$$

$$2 w_A + 8 w_2 \left(\mu_2^{12} + \frac{1}{32} (1 - \mu_2^2)^6 \right) + 8 w_3 \left(\mu_3^{12} + \frac{1}{32} (1 - \mu_3^2)^6 \right) + 8 w_C (\mu_C^{12} + (1 - \mu_C^2)^6) == \frac{1}{13},$$

$$2 w_A + 8 w_2 \left(\mu_2^{14} + \frac{1}{64} (1 - \mu_2^2)^7 \right) + 8 w_3 \left(\mu_3^{14} + \frac{1}{64} (1 - \mu_3^2)^7 \right) + 8 w_C (\mu_C^{14} + (1 - \mu_C^2)^7) == \frac{1}{15} \}$$

quadAC23 = Solve[Eqns, {wA, wC, w2, w3, μC, μ2, μ3}]

\$Aborted

(* The computer was not able to solve this exactly,
I will now try the numerical function *)

quadAC23 = NSolve[Eqns, {wA, wC, w2, w3, μC, μ2, μ3}]

\$Aborted

(* The computer was not able to find this solution directly either. I
will lend some assistance *)

Eqns14 = Table[

$$\text{caseA}[w_A, k] + \text{caseC}[w_C, \mu_C, k] + \text{case2}[w_2, \mu_2, k] + \text{case2}[w_3, \mu_3, k] == \frac{1}{2k+1}, \{k, 4\}]$$

$$\{8 w_2 + 8 w_3 + 2 w_A + 8 w_C == \frac{1}{3},$$

$$2 w_A + 8 w_2 \left(\mu_2^4 + \frac{1}{2} (1 - \mu_2^2)^2 \right) + 8 w_3 \left(\mu_3^4 + \frac{1}{2} (1 - \mu_3^2)^2 \right) + 8 w_C (\mu_C^4 + (1 - \mu_C^2)^2) == \frac{1}{5},$$

$$2 w_A + 8 w_2 \left(\mu_2^6 + \frac{1}{4} (1 - \mu_2^2)^3 \right) + 8 w_3 \left(\mu_3^6 + \frac{1}{4} (1 - \mu_3^2)^3 \right) + 8 w_C (\mu_C^6 + (1 - \mu_C^2)^3) == \frac{1}{7},$$

$$2 w_A + 8 w_2 \left(\mu_2^8 + \frac{1}{8} (1 - \mu_2^2)^4 \right) + 8 w_3 \left(\mu_3^8 + \frac{1}{8} (1 - \mu_3^2)^4 \right) + 8 w_C (\mu_C^8 + (1 - \mu_C^2)^4) == \frac{1}{9} \}$$

Solve[Eqns14, {wA, wC, w2, w3}]

{wA, wC, w2, w3} = {wA, wC, w2, w3} /. %%[[1]];

Expand[wA];

Together[%];

Cancel[%];

PowerExpand[%];

Simplify[%]

$$\begin{aligned} & (- (1 - 2 \mu C^2)^2 (3 + 9 \mu 3^6 - 29 \mu C^2 + 29 \mu C^4 + \mu 3^2 (-1 + 54 \mu C^2 - 54 \mu C^4) + \mu 3^4 (-11 - 21 \mu C^2 + 21 \mu C^4)) + \\ & 9 \mu 2^6 (- (1 - 2 \mu C^2)^2 + \\ & \mu 3^4 (-39 + 210 \mu C^2 - 210 \mu C^4) + 21 \mu 3^6 (1 - 5 \mu C^2 + 5 \mu C^4) + \mu 3^2 (19 - 105 \mu C^2 + 105 \mu C^4)) + \\ & \mu 2^2 ((1 - 2 \mu C^2)^2 (1 - 54 \mu C^2 + 54 \mu C^4) + \\ & 9 \mu 3^6 (19 - 105 \mu C^2 + 105 \mu C^4) + \mu 3^4 (-281 + 1716 \mu C^2 - 2556 \mu C^4 + 1680 \mu C^6 - 840 \mu C^8) + \\ & \mu 3^2 (109 - 653 \mu C^2 + 989 \mu C^4 - 672 \mu C^6 + 336 \mu C^8)) - \\ & \mu 2^4 ((1 - 2 \mu C^2)^2 (-11 - 21 \mu C^2 + 21 \mu C^4) + \\ & 27 \mu 3^6 (13 - 70 \mu C^2 + 70 \mu C^4) - 3 \mu 3^4 (207 - 1225 \mu C^2 + 1645 \mu C^4 - 840 \mu C^6 + 420 \mu C^8) + \\ & \mu 3^2 (281 - 1716 \mu C^2 + 2556 \mu C^4 - 1680 \mu C^6 + 840 \mu C^8)) / \\ & (630 (-1 + \mu 2^2) (-1 + \mu 3^2) \mu C^2 (-1 + \mu C^2) (9 \mu 2^4 \mu 3^2 (-1 + \mu 3^2) + (-1 + \mu 3^2) (1 - 2 \mu C^2)^2 + \\ & \mu 2^2 (-9 \mu 3^4 + (1 - 2 \mu C^2)^2 + 4 \mu 3^2 (2 - 3 \mu C^2 + 3 \mu C^4)))) \end{aligned}$$

wA = %27;

Expand[wC];

Together[%];

Cancel[%];

PowerExpand[%];

Simplify[%]

$$\begin{aligned} & (3 + 2 \mu 3^2 - 9 \mu 3^4 - 9 \mu 2^4 (1 - 18 \mu 3^2 + 21 \mu 3^4) + 2 \mu 2^2 (1 - 54 \mu 3^2 + 81 \mu 3^4)) / \\ & (2520 \mu C^2 (-1 + \mu C^2) (9 \mu 2^4 \mu 3^2 (-1 + \mu 3^2) + (-1 + \mu 3^2) (1 - 2 \mu C^2)^2 + \\ & \mu 2^2 (-9 \mu 3^4 + (1 - 2 \mu C^2)^2 + 4 \mu 3^2 (2 - 3 \mu C^2 + 3 \mu C^4)))) \end{aligned}$$

wC = %33;

Expand[w2];

Together[%];

Cancel[%38];

PowerExpand[%];

Simplify[%]

$$\frac{(-9 \mu^3 + (1 - 2 \mu^2)^2 - 3 \mu^3 (5 - 24 \mu^2 + 24 \mu^4) + \mu^3 (23 - 84 \mu^2 + 84 \mu^4))}{(630 (-1 + \mu^2) (\mu^2 - \mu^3) (9 \mu^4 \mu^3 (-1 + \mu^3) + (-1 + \mu^3) (1 - 2 \mu^2)^2 + \mu^2 (-9 \mu^3 + (1 - 2 \mu^2)^2 + 4 \mu^3 (2 - 3 \mu^2 + 3 \mu^4)))}$$

w2 = %;

Expand[w3];

Together[%];

Cancel[%];

PowerExpand[%];

Simplify[%]

$$\frac{(9 \mu^6 - (1 - 2 \mu^2)^2 + \mu^4 (-23 + 84 \mu^2 - 84 \mu^4) + 3 \mu^2 (5 - 24 \mu^2 + 24 \mu^4))}{(630 (\mu^2 - \mu^3) (-1 + \mu^3) (9 \mu^4 \mu^3 (-1 + \mu^3) + (-1 + \mu^3) (1 - 2 \mu^2)^2 + \mu^2 (-9 \mu^3 + (1 - 2 \mu^2)^2 + 4 \mu^3 (2 - 3 \mu^2 + 3 \mu^4)))}$$

w3 = %;

lhs5 = caseA[wA, 5] + caseC[wC, \mu C, 5] + case2[w2, \mu 2, 5] + case2[w3, \mu 3, 5];

Expand[%];

Together[%];

Cancel[%];

PowerExpand[%];

Simplify[%]

$$\left((-23 + 25 \mu^3 - 5 \mu^4 + 3 \mu^6) (1 - 2 \mu^2)^2 - 3 \mu^6 (9 \mu^3 - (1 - 2 \mu^2)^2 + \mu^4 (-23 + 84 \mu^2 - 84 \mu^4) + 3 \mu^3 (5 - 24 \mu^2 + 24 \mu^4)) + \mu^4 (-5 (1 - 2 \mu^2)^2 + \mu^4 (65 + 636 \mu^2 - 636 \mu^4) + 3 \mu^3 (23 - 84 \mu^2 + 84 \mu^4) + 3 \mu^3 (-43 - 124 \mu^2 + 124 \mu^4)) + \mu^2 (25 (1 - 2 \mu^2)^2 - 9 \mu^3 (5 - 24 \mu^2 + 24 \mu^4) + \mu^3 (149 - 112 \mu^2 + 112 \mu^4) + 3 \mu^4 (-43 - 124 \mu^2 + 124 \mu^4)) \right) / \left(252 (9 \mu^2 \mu^3 (-1 + \mu^3) + (-1 + \mu^3) (1 - 2 \mu^2)^2 + \mu^2 (-9 \mu^4 + (1 - 2 \mu^2)^2 + 4 \mu^3 (2 - 3 \mu^2 + 3 \mu^4))) \right)$$

lhs5 = %;

lhs6 = caseA[wA, 6] + caseC[wC, μC, 6] + case2[w2, μ2, 6] + case2[w3, μ3, 6];

Expand[%];

Together[%];

Cancel[%];

PowerExpand[%];

Simplify[%]

$$\left((1 - 2 \mu^2)^2 (27 \mu^3 + 33 \mu^8 + 2 (-97 - 6 \mu^2 + 6 \mu^4) + \mu^3 (245 - 8 \mu^2 + 8 \mu^4) - 3 \mu^4 (37 - 12 \mu^2 + 12 \mu^4)) - 33 \mu^8 (9 \mu^3 - (1 - 2 \mu^2)^2 + \mu^4 (-23 + 84 \mu^2 - 84 \mu^4) + 3 \mu^3 (5 - 24 \mu^2 + 24 \mu^4)) - 3 \mu^6 (9 + 11 \mu^3) (9 \mu^3 - (1 - 2 \mu^2)^2 + \mu^4 (-23 + 84 \mu^2 - 84 \mu^4) + 3 \mu^3 (5 - 24 \mu^2 + 24 \mu^4)) + \mu^2 ((1 - 2 \mu^2)^2 (245 - 8 \mu^2 + 8 \mu^4) - 99 \mu^3 (5 - 24 \mu^2 + 24 \mu^4) - 12 \mu^6 (31 - 151 \mu^2 + 151 \mu^4) + \mu^3 (676 + 2220 \mu^2 - 3948 \mu^4 + 3456 \mu^6 - 1728 \mu^8) + 54 \mu^4 (-1 - 162 \mu^2 + 210 \mu^4 - 96 \mu^6 + 48 \mu^8)) + 3 \mu^4 (-6 \mu^3 (-7 - 6 \mu^2 + 6 \mu^4) - (1 - 2 \mu^2)^2 (37 - 12 \mu^2 + 12 \mu^4) + 11 \mu^3 (23 - 84 \mu^2 + 84 \mu^4) + 18 \mu^3 (-1 - 162 \mu^2 + 210 \mu^4 - 96 \mu^6 + 48 \mu^8) - 4 \mu^4 (60 - 991 \mu^2 + 1243 \mu^4 - 504 \mu^6 + 252 \mu^8)) \right) / \left(2520 (9 \mu^2 \mu^3 (-1 + \mu^3) + (-1 + \mu^3) (1 - 2 \mu^2)^2 + \mu^2 (-9 \mu^4 + (1 - 2 \mu^2)^2 + 4 \mu^3 (2 - 3 \mu^2 + 3 \mu^4))) \right)$$

lhs7 = %;

lhs7 = caseA[wA, 7] + caseC[wC, μC, 7] + case2[w2, μ2, 7] + case2[w3, μ3, 7];

Expand[%];

Together[%];

Cancel[%];

PowerExpand[%];

Simplify[%]

$$\begin{aligned} & - \left(9 \mu 2^{10} \left(9 \mu 3^6 - (1 - 2 \mu C^2)^2 + \mu 3^4 (-23 + 84 \mu C^2 - 84 \mu C^4) + 3 \mu 3^2 (5 - 24 \mu C^2 + 24 \mu C^4) \right) + \right. \\ & \quad \mu 2^8 (10 + 9 \mu 3^2) \left(9 \mu 3^6 - (1 - 2 \mu C^2)^2 + \mu 3^4 (-23 + 84 \mu C^2 - 84 \mu C^4) + 3 \mu 3^2 (5 - 24 \mu C^2 + 24 \mu C^4) \right) + \\ & \quad \mu 2^6 (7 + 10 \mu 3^2 + 9 \mu 3^4) \\ & \quad \left(9 \mu 3^6 - (1 - 2 \mu C^2)^2 + \mu 3^4 (-23 + 84 \mu C^2 - 84 \mu C^4) + 3 \mu 3^2 (5 - 24 \mu C^2 + 24 \mu C^4) \right) + (1 - 2 \mu C^2)^2 \\ & \quad (47 - 7 \mu 3^6 - 10 \mu 3^8 - 9 \mu 3^{10} + 12 \mu C^2 - 12 \mu C^4 - 8 \mu 3^2 (9 - \mu C^2 + \mu C^4) + \mu 3^4 (51 - 36 \mu C^2 + 36 \mu C^4)) + \\ & \quad \mu 2^2 (-8 (1 - 2 \mu C^2)^2 (9 - \mu C^2 + \mu C^4) + 27 \mu 3^{10} (5 - 24 \mu C^2 + 24 \mu C^4) + 3 \mu 3^8 (47 - 228 \mu C^2 + 228 \mu C^4) + \\ & \quad \mu 3^6 (95 - 464 \mu C^2 + 464 \mu C^4) + \mu 3^4 (-349 + 4348 \mu C^2 - 6940 \mu C^4 + 5184 \mu C^6 - 2592 \mu C^8) + \\ & \quad \mu 3^2 (50 - 1872 \mu C^2 + 3600 \mu C^4 - 3456 \mu C^6 + 1728 \mu C^8)) - \\ & \quad \mu 2^4 (-3 (1 - 2 \mu C^2)^2 (17 - 12 \mu C^2 + 12 \mu C^4) - \\ & \quad 4 \mu 3^6 (-5 - 24 \mu C^2 + 24 \mu C^4) + 9 \mu 3^{10} (23 - 84 \mu C^2 + 84 \mu C^4) + \\ & \quad \mu 3^8 (95 - 192 \mu C^2 + 192 \mu C^4) - 4 \mu 3^4 (155 - 1376 \mu C^2 + 2132 \mu C^4 - 1512 \mu C^6 + 756 \mu C^8) + \\ & \quad \mu 3^2 (349 - 4348 \mu C^2 + 6940 \mu C^4 - 5184 \mu C^6 + 2592 \mu C^8)) \Big) / \\ & \left(720 \left(9 \mu 2^4 \mu 3^2 (-1 + \mu 3^2) + (-1 + \mu 3^2) (1 - 2 \mu C^2)^2 + \right. \right. \\ & \quad \left. \left. \mu 2^2 (-9 \mu 3^4 + (1 - 2 \mu C^2)^2 + 4 \mu 3^2 (2 - 3 \mu C^2 + 3 \mu C^4)) \right) \right) \end{aligned}$$

lhs7 = %;

$$\text{NSolve}\left[\left\{\text{lhs5} == \frac{1}{11}, \text{lhs6} == \frac{1}{13}, \text{lhs7} == \frac{1}{15}\right\}, \{\mu C, \mu 2, \mu 3\}\right]$$

\$Aborted

$$\text{Solve}\left[\text{lhs5} == \frac{1}{11}, \{\mu C\}\right]$$

(* Large output deleted *)

Length[%]

4

(* The four solutions above correspond to the base angle and its reflections,
I will continue only using the last solution above *)

$$\mu C = \mu C /. \%78[[4]]$$

Expand[%];

Together[%];

PowerExpand[%];

Simplify[%]

$$\left(\sqrt{(-1 + 23\mu^3 - 55\mu^4 + 33\mu^6 + 33\mu^2(1 - 18\mu^3 + 21\mu^4) + \mu^2(23 - 448\mu^3 + 1023\mu^4 - 594\mu^6) + 11\mu^4(-5 + 93\mu^3 - 159\mu^4 + 63\mu^6) - \mu^2\mu^3\sqrt{(71 - 1807\mu^3 + 8006\mu^4 - 14190\mu^6 + 11187\mu^8 - 3267\mu^{10} + 1089\mu^{12}(-3 + 52\mu^3 - 18\mu^4 - 204\mu^6 + 189\mu^8) + 33\mu^8(339 - 6287\mu^3 + 9822\mu^4 + 7698\mu^6 - 18513\mu^8 + 6237\mu^{10}) - 2\mu^4(-4003 + 83437\mu^3 - 287774\mu^4 + 360954\mu^6 - 162063\mu^8 + 9801\mu^{10}) - 22\mu^6(645 - 12706\mu^3 + 32814\mu^4 - 19704\mu^6 - 11547\mu^8 + 10098\mu^{10}) + \mu^2(-1807 + 40008\mu^3 - 166874\mu^4 + 279532\mu^6 - 207471\mu^8 + 56628\mu^{10}))})} \right) / \left(\sqrt{2} \sqrt{(-1 + 23\mu^3 - 55\mu^4 + 33\mu^6 + 33\mu^2(1 - 18\mu^3 + 21\mu^4) + \mu^2(23 - 448\mu^3 + 1023\mu^4 - 594\mu^6) + 11\mu^4(-5 + 93\mu^3 - 159\mu^4 + 63\mu^6))} \right)$$

$\mu C = %$;

Expand[lhs6];

Together[%];

PowerExpand[%];

Together[%];

Cancel[%];

PowerExpand[%92];

Simplify[%]

(* Large ugly equation deleted *)

lhs6 = %;

Expand[lhs7];

Together[%];

Cancel[%];

PowerExpand[%];

Simplify[%];

lhs7 = %

(* Large ugly equation deleted *)

NSolve[{lhs6 == $\frac{1}{13}$, lhs7 == $\frac{1}{15}$ }, { μ_2 , μ_3 }]

Out of memory. Exiting.

```
quadAC23 = FindRoot[Eqns, {wA, .0130608}, {wC, .0154866},  
  {w2, .00673874}, {w3, .0161761}, {μC, .410254}, {μ2, .848421}, {μ3, .300144},  
  AccuracyGoal → 24, WorkingPrecision → 34]  
  
{wA → 0.01306075218457543404037831995817255, wC → 0.01548662322913343575994122509932307,  
  w2 → 0.00673874365125243712696660016440459, w3 → 0.01617611174013693526966426141339587,  
  μC → 0.410253515086337171560174981725413, μ2 → 0.848421498634701466179649259967932,  
  μ3 → 0.3001438436359286871701637504638956}
```

(* The FindRoot function is a root solving function. The initial guesses used are from a previous effort on a slower computer. This is one possible solution to the system of equations. *)

Appendix C: Valid Quadrature Base Sets

N = 3

Cases	weight	mu	eta	xi
AB				
A	0.0476190476190476	1	0	0
B	0.0380952380952381	0.7071067811865475	0	0.7071067811865475
1	0.0321428571428571	0.5773502691896258	0.5773502691896258	0.5773502691896258
C1				
C	0.0309523809523810	0.9000482411921158	0	0.4357902747044488
1	0.0321428571428571	0.5773502691896258	0.5773502691896258	0.5773502691896258

N = 5

Cases	weight	mu	eta	xi
AB12				
A	0.0126984126984127	1	0	0
B	0.0225749559082892	0.7071067811865475	0	0.7071067811865475
1	0.0210937500000000	0.5773502691896258	0.5773502691896258	0.5773502691896258
2	0.0201733355379189	0.9045340337332910	0.3015113445777637	0.3015113445777637
AC2				
A	0.0223062916968982	1	0	0
C	0.0185141807544452	0.8616774905910132	0	0.5074563057138757
2	0.0175759129879969	0.7858759158676477	0.4372636760921183	0.4372636760921183
BC2				
B	0.0182978666108076	0.7071067811865475	0	0.7071067811865475
C	0.0149418203732660	0.9526970315441012	0	0.3039216446504885
2	0.0175759129879969	0.7858759158676477	0.4372636760921183	0.4372636760921183
C4				
C	0.0170731707317073	0.9451972790030246	0	0.3264997760570111
4	.01229674796747967	0.7573160195117944	0.5872843412419646	0.2856038324721905

N = 7

Cases	weight	mu	eta	xi
ABC12				
A	0.0090481888301554	1	0	0
C	0.0064514915385668	0.9545808669401723	0	0.2979519566503114
B	0.0210324604374280	0.7071067811865475	0	0.7071067811865475
1	0.0182794139234181	0.5773502691896258	0.5773502691896258	0.5773502691896258
2	0.0163437597273743	0.8753170875981718	0.7854361833270270	0.7854361833270270
AC23				
A	0.0130607521845754	1	0	0
C	0.0154866232291334	0.911971520037388	0	0.4102535150863372
2	0.0067387436512524	0.8484214986347015	0.374286628571238	0.374286628571238
3	0.0161761117401369	0.3001438436359287	0.674504882535127	0.674504882535127


```

* 42. 0.0032257457692834124 0.010516230218714844 0.0032257457692834124 *
* 43. 0.0022620472075388518 0 0 0 0 *
* 44. mu=0.00000000000000000 0.297951956650311267 0.34192104071 *
* 45. 0.0000000000000000000 0.707106781188 0.57735026919 *
* 46. 0.0000000000000000000 0.954580866940172434 0.875317087598171994 *
* 47. 0.34192104071 0.00000000000000000 1.00000000000000000 *
* 48. 0.9545808669401724 0.70710678118655 0.29795195665031112 *
* 49. 0.00000000000000000 0.1 0.1 0.1 *
* 50. eta=0.00000000000000000 0.00000000000000000 0.3419210407 *
* 51. 0.297951956650311267 0.00000000000000000 0.57735026919 *
* 52. 0.707106781188 0.00000000000000000 0.3419210407 *
* 53. 0.875317087598171994 0.954580866940172434 0.00000000000000000 *
* 54. 0.29795195665031107 0.707106781186545 0.95458086694017243 *
* 55. 1.00000000000000000 0.1 0.1 0.1 *
* 56. t *
* 57. *
* 58. *
* 59. /***** B L O C K V I *****/ *
* 60. pted=1 *
* 61. edoutf=2 *
* 62. t *
* *
*****

```

1 --- DETAIL OUTPUT DELETED ---

```

*****
* *
* ...flux and eigenvalue convergence as monitored by threedant...
* *
*****
*Key start iteration monitor *
*****
* *
* cpu time outer diffusion max ptwise max ptwise inners
* (sec) no. inners sub-outers sourc multip lambda-1 flux change fiss change converged
* .87 0
* -----
* *
* -- inner iteration summary for outer iteration no. 1 --
* *
* iter per max flux at
* group group change mesh
* 1 8 .54E-06 1, 8, 16
* *
* *
* cpu time outer diffusion max ptwise max ptwise inners

```



```

1 *****
*
* Multigrd work units... Total= 75.54 WU.
* By group...
* 1 75.54
*
* Multigrd average convergence rate by group...
* 1 .5720
*
* timing info...tswep,tdsa,trelx,tput3,tintrp= 10.24 .34 .09 .08 .04 seconds.
*
integral summary information
summary eigenvalue not used
integral-source-i neutron 1.2500000E-01
integral-fission-i neutron 0.0000000E+00
integral-absorption-i neutron 6.5240937E-02
integral-in-scak-i neutron 0.0000000E+00
integral-self-scak-i neutron 1.3048187E-01
integral-out-scak-i neutron 8.3266727E-16
integral-net lkage-i neutron 5.9759067E-02
integral-right lkage-i neutron 1.9919689E-02
integral-horizontal lkage-i neutron 1.9919689E-02
integral-top lkage-i neutron 1.9919689E-02
integral-vertical lkage-i neutron 1.9919689E-02
integral-back lkage-i neutron 1.9919689E-02
integral-fr-back lkage-i neutron 1.9919689E-02
integral-particle bal-i neutron -3.5202419E-08
1 *****
*
* flux components for group, 1 and plane 1
*
*****
*
* ...interface file rtflux written..
*
*
*
1 threedant iteration time, mins 1.9200E-01
*****
*

```


Vita

Joseph M. Oder was born on [REDACTED] in [REDACTED]. He attended the United States Air Force Academy in Colorado Springs, Colorado where he majored in High Energy Physics. Upon receipt of a Bachelor of Science on 31 May 1989, he received a regular commission as a second lieutenant in the United States Air Force. He was assigned to duty as a Minuteman II Missile Combat Crewmember, at Ellsworth AFB, South Dakota. While at Ellsworth, he was selected as the Missile Combat Crew Flight Commander, ACP responsible for the field operations of the 44th Missile Wing. He received a Master of Science in Engineering Management from West Coast University while stationed at Vandenberg AFB, California. He entered the Air Force Institute of Technology School of Engineering in May 1996.

Permanent Address: [REDACTED]
[REDACTED]

REPORT DOCUMENTATION PAGE			Form Approved OMB No. 0704-0188	
Public reporting burden for this collection of information is estimated to average 1 hour per response, including the time for reviewing instructions, searching existing data sources, gathering and maintaining the data needed, and completing and reviewing the collection of information. Send comments regarding this burden estimate or any other aspect of this collection of information, including suggestions for reducing this burden, to Washington Headquarters Services, Directorate for Information Operations and Reports, 1215 Jefferson Davis Highway, Suite 1204, Arlington, VA 22202-4302, and to the Office of Management and Budget, Paperwork Reduction Project (0704-0188), Washington, DC 20503.				
1. AGENCY USE ONLY (Leave blank)	2. REPORT DATE December 1997	3. REPORT TYPE AND DATES COVERED Master's Thesis		
4. TITLE AND SUBTITLE Reduced Computational Cost, Totally Symmetric Angular Quadrature Sets for Discrete Ordinates Radiation Transport			5. FUNDING NUMBERS	
6. AUTHOR(S) Joseph M. Oder, Captain, USAF				
7. PERFORMING ORGANIZATION NAME(S) AND ADDRESS(ES) Air Force Institute of Technology 2750 P Street WPAFB, OH 45433-7765			8. PERFORMING ORGANIZATION REPORT NUMBER AFIT/GAP/ENP/97D-07	
9. SPONSORING/MONITORING AGENCY NAME(S) AND ADDRESS(ES) MR MIKE MARTINEZ SA-ALC/NWIC 1651 FIRST STREET SE, B-20360 KIRTLAND AFB NM 87117-5617			10. SPONSORING/MONITORING AGENCY REPORT NUMBER	
11. SUPPLEMENTARY NOTES				
12a. DISTRIBUTION AVAILABILITY STATEMENT Approved for public release; distribution unlimited			12b. DISTRIBUTION CODE	
13. ABSTRACT (Maximum 200 words) Several new quadrature sets for use in the discrete ordinates method of solving the Boltzmann neutral particle transport equation are derived. These symmetric quadratures extend the traditional symmetric quadratures by allowing ordinates perpendicular to one or two of the coordinate axes. Comparable accuracy with fewer required ordinates is obtained. Quadratures up to seventh order are presented. The validity and efficiency of the quadratures is then tested and compared with the Sn level symmetric quadratures relative to a Monte Carlo benchmark solution. The criteria for comparison include current through the surface, scalar flux at the surface, volume average scalar flux, and time required for convergence. Appreciable computational cost was saved when used in an unstructured tetrahedral cell code using highly accurate characteristic methods. However, no appreciable savings in computation time was found using the new quadratures compared with traditional Sn methods on a regular Cartesian mesh using the standard diamond difference method. These quadratures are recommended for use in three-dimensional calculations on an unstructured mesh.				
14. SUBJECT TERMS Neutron Transport Theory, Boltzmann Equation, Numerical Quadrature, Numerical Analysis			15. NUMBER OF PAGES 140	
			16. PRICE CODE	
17. SECURITY CLASSIFICATION OF REPORT Unclassified	18. SECURITY CLASSIFICATION OF THIS PAGE Unclassified	19. SECURITY CLASSIFICATION OF ABSTRACT Unclassified	20. LIMITATION OF ABSTRACT UL	